Algorithms for In-situ Efficiency Determination of Induction Machines

Mahmud Ghasemi Bijan

A Thesis

In the Department

of

Electrical and Computer Engineering

Presented in Partial Fulfillment of the Requirements
For the Degree of
Doctor of Philosophy (Electrical and Computer Engineering) at
Concordia University
Montreal, Quebec, Canada

April 2019

CONCORDIA UNIVERSITY

SCHOOL OF GRADUATE STUDIES

This is to certify that the thesis prepared

By: Mahmud Ghasemi Bijan

Entitled: Algorithms for In-Situ Efficiency Determination of Induction Machines

and submitted in partial fulfillment of the requirements for the degree of

Doctor of Philosophy (Electrical and Computer Engineering)

complies with the regulations of the University and meets the accepted standards with respect to originality and quality.

Signed by the final examining committee:

Dr. Mehdi Hojjati	Chair
Dr. Joseph Olorunfemi Ojo	External Examiner
Dr. Ashutosh Bagchi	External to Program
Dr. Chunyan Lai	Examiner
Dr. Luiz A.C. Lopes	Examiner
Dr. Pragasen Pillay	Thesis Supervisor

Approved by

Dr. Rastko K. Selmic, Graduate Program Director

June 20, 2019

Dr. Amir Asif, Dean
Gina Cody School of Engineering & Computer Science

ABSTRACT

Algorithms for In-situ Efficiency Determination of Induction Machines

Mahmud Ghasemi Bijan, Ph.D.

Concordia University, 2019

Robust structure, high reliability and low maintenance costs allow induction motors to be widely-used in various industrial applications. In recent decades, due to the increased concerns on global warming, and the effort to enhance the efficiency of tools, equipment, and systems, efficiency of induction machines (IMs) has received a lot of attention. The rated efficiency of an IM can be found on the nameplate. However, it is affected by aging, ambient temperature, load, supplied voltage and other technical reasons. Furthermore, based on NEMA MG 1 standard, the actual efficiency of an IM may vary from the nameplate value. As a result, efficiency estimation of IMs is essential to evaluate the efficiency of the whole system and energy cost.

Applying available international standards to in-situ machines needs load decoupling and in some cases, the no-load/locked-rotor test is required. This is not allowed with in-situ machines. Therefore, having a non-intrusive method which is capable of estimating the efficiency of the machine by using only available data such as the input voltages, currents, active power and nameplate data is necessary.

This thesis investigates in-situ methods to determine the efficiency of IMs and three related subjects are addressed. First, an optimization based algorithm is proposed to determine the efficiency of the IM at different loads. This algorithm is proven to have minimum intrusiveness and only uses the data of one operating point of the machine. Assumptions and techniques to increase the accuracy of the algorithm are addressed. The proposed algorithm is then applied to two conditions. In the first condition, the required input data are recorded when the machine reaches its thermal stability and final temperature rise of the machine is used as an input. In the second condition, the required input data are recorded 30 minutes after start of the machine and

then the machine final temperature rise is predicted. Two approaches are proposed to predict final temperature rise and are based on machine insulation class and temperature rise of the machine in the first 30 minutes of operation of the machine after start.

Moreover, a method is proposed to determine the range of IM equivalent circuit parameters and improve the probability of converging to the correct answer. The method is based on the nameplate data of the machine and empirical results provided by Hydro-Québec. The method is also improved by using the operating data of the machine. The proposed range determination is very helpful for in-situ applications where the output power of the machine is not available.

Second, two dimensional finite element analysis (FEA) is used to predict the efficiency of the IMs at different loads. Two methodologies are adopted. In the first methodology, the losses are calculated directly using FEA while in the second one, the equivalent circuit parameters are first estimated using FEA and then the efficiency at different loads are estimated using the equivalent circuit parameters. To improve the results, a simple formula based on the rated power of the machine is proposed to evaluate the friction and windage losses also known as the mechanical loss of the machine. The proposed formula is applicable for 4-pole 60 Hz IMs and was achieved after study of more than 100 IMs of this type.

Third, the effects of the adjustable-speed drives on the losses and efficiency of the IMs are addressed. The direct torque control and scalar control schemes implemented by an industrial drive are employed to control two types of IMs. Two IMs designed for direct-fed application and two other IMs designed for PWM applications are studied while method B of IEEE Std-112 is applied to segregate the losses. Variations of different losses at drive-fed and direct-fed conditions are compared and results are discussed.

ACKNOWLEDGEMENTS

Foremost, I would like to express my sincere gratitude to my advisor *Professor Pragasen Pillay* for his continuous support of my Ph.D study and research, for his patience, motivation, enthusiasm, and immense knowledge. His guidance helped me during all times of my research and writing of this thesis. I could not have imagined having a better advisor and mentor for my Ph.D study.

Besides my advisor, I would like to thank the rest of my thesis committee: *Professor Luiz A.C. Lopes*, *Professor Joseph Olorunfemi Ojo*, *Professor Ashutosh Bagchi, Dr. Chunyan Lai*, and *Dr. Akshay Kumar Rathore* for their encouragement, insightful comments, and hard questions.

My sincere thanks also goes to *Dr. Maher Al-Badri* for all his comments and advices during my research and *Dr. Mohammad Masadeh*, for all the comments and advices for writing this thesis.

I thank my fellow labmates in Power Electronics and Energy Research (PEER) Group: *Dr. Amir Masoud Takbash*, *Dr. Chirag Desai*, *Amit Kumar*, Rajendra Thike, and *Dr. Mohammad Hosssein Ashourianjozdani*, for the stimulating discussions, for the days and nights we were working together, and for all the fun we have had in the last four years.

I would like to extend my many thanks to *Mr. Pierre Angers* of Hydro-Québec on his generous contribution to this research work by providing priceless data that has significantly improved the outcome of this research.

Last but not the least, I would like to thank my parents *Valiollah Ghasemi Bijan* and *Zahra Nejati*, who taught me that you cannot be happy unless you do your best to achieve what you want and thanks to my beloved family to encourage and support me throughout all difficulties and challenges during my life.

I would like to thank and acknowledge the support of the Natural Sciences & Engineering Research Council of Canada and Hydro-Québec for this work.

This work was supported in part by the R&D program of the NSERC Chair entitled "*Design and Performance of Special Electrical Machines*" occupied by *Professor Pragasen Pillay* at Concordia University.

Table of Contents

List of Figures

List of Tables

List of Symbols

Symbol	Unit	Definition
R_1	Ω	Stator resistance
X_1	Ω	Stator reactance
R_2	Ω	Rotor resistance
X_2	Ω	Rotor reactance
R_{fe}	Ω	Core loss resistance
X_m	Ω	Magnetizing reactance
R_{th}	Ω	Thevenin equivalent resistance of the stator
X_{th}	Ω	Thevenin equivalent reactance of the stator
T	°C	Machine temperature
T_{fl}	°C	Full load Machine temperature
ΔT	°C	Temperature rise
s	-	slip
N_r	rpm	Rotor speed
N_s	rpm	Synchronous Speed
ω_s	rad/s	Angular synchronous Speed
P_{out}	W	Rated output power
P_2	W	Output power
P_{in}	W	Input power
$P_{in,fl}$	W	Full load input power
P_{mec}	W	Mechanical power
P_{gap}	W	Airgap power
P_{FW}	W	Friction and windage losses
P_{SLL}	W	Stray load loss
P_{fe}	W	Core loss
P_{rcl}	W	Rotor resistance loss
P_{scl}	W	Stator resistance loss
ΔP	W	Total loss
Q_{in}	VAR	Input reactive power
V_1	V	Stator voltage or input voltage
V_2	V	Voltage across the parallel branch of equivalent circuit
V_{LL}	V	Rated line voltage
V_{th}	V	Thevenin equivalent voltage of the stator
v_{CA}	V	Instantaneous line voltage between phase C and A
v_{BA}	V	Instantaneous line voltage between phase B and A
I_1	A	Stator current or input current

I_0	A	No load current
I_2	A	Rotor current
I_{LL}	A	Rated line current
i_A	A	Instantaneous line A current
i_C	A	Instantaneous line C current
η	%	Efficiency
f_{sh}	Hz	Desired harmonic frequency
f_1	Hz	Input frequency
f	Hz	Rated frequency
P	-	Number of pole pairs
τ_{max}	Nm	Maximum torque
τ_{AG}	Nm	Airgap torque
φ	degree	Input power factor angle
φ_0	degree	No-load Input power factor angle
X_i	-	Position vector of particle
V_i	-	Position vector of particle
V_{max}	-	Maximum velocity of particle
c_1 , c_2	-	Accelerating coefficient
r_1 , r_2	-	Random number
w	-	Inertia coefficient
Iter	-	Number of iteration
Pbest	-	Particle best - Best experience of a particle
Gbest	-	Global best - Best experience of all particles
Lbest	-	Local best - Best experience of three neighbor particles

List of Index

Index	Definition
meas	Measured value
est	Estimated value
cold	Cold temperature
hot	Hot temperature
rated	Rated or nameplate value
min	Minimum value
max	Maximum value

List of Abbreviations

IM	Induction Machine
PSO	Particle Swarm Optimization
GA	Genetic Algorithm
IEEE	Institute of Electrical and Electronics Engineers
IEC	International Electrotechnical Commission
NEMA	National Electrical Manufacturers Association
DTC	Direct Torque Control
TEFC	Totally Enclosed-Fan Cooled
ASD	Adjustable-Speed Drive

Chapter 1: Induction Motor Efficiency

1.1 Introduction

By the incidence of the energy crisis in the 1970s and the rising cost of energy, energy and energy consumption issues are of prominent importance. Because of the continuous rise of the energy cost and demand due to development of the industry, increasing the efficiency of the energy-consuming systems and equipment are becoming crucial and necessary.

Nowadays, electric machines have a very prominent role in the progress and advances of the industry. They consume around two-thirds of the total generated electricity [1]. Induction machines (IMs) are the most widely-used type of electric machines in industry due to robustness, simple structure, high reliability and low maintenance costs. The efficiency of these machines is of a great importance in terms of energy consumption and cost. Replacing lower efficient IMs with high efficiency machines is one of the most effective solutions in this field. The cost of the new machines is paid back by the amount of energy saved in the long run.

To make the right decision and to estimate the amount of future savings, the first step is to measure or estimate the efficiency of the IMs. Several methods have been proposed in this regard and two international standards are developed. To apply these standards, the IM should be decoupled from the load to install new equipment such as torque transducer on the machine's shaft or transfer to workshops for performing the required tests. However, in in-situ applications where the IM is working, decoupling the machine from load results in an interruption of the whole system performance which is not desirable.

This chapter will discuss the available standards and methods to measure or estimate the efficiency of IMs. Their advantages and drawbacks will be discussed and their ability to apply to in-situ applications will be considered. At the end, the objectives of this thesis and thesis outline and contributions will be provided.

1.2 International Standards

A significant amount of research works has resulted in development of international standards. The main two standards are the IEEE Std-112 [2] and IEC 60034-2-1 [3]. In this section, a brief review of these standards is presented.

1.2.1 IEEE Std-112

IEEE Std-112 is developed within the IEEE Societies and the Standards Coordinating Committees of the IEEE Standards Association (IEEE-SA) Standards Board [2]. This standard in association with IEEE Std-43 [4], IEEE Std-118 [5], IEEE Std-119 [6] and IEEE Std-120 [7], provides five methods to measure or estimate IMs efficiency (i.e. methods A, B, C, E and F) [2].

Method A: Efficiency of an IM is generally considered as a ratio of the output power to the input power. Method A is a direct method and proposes to measure the input and output powers directly. The input power can be measured by using input voltages and stator currents and their phase angles. This can be done easily by using a power meter based on the IEEE Std-120 guides. The output power can be measured by using a torque transducer and a speed sensor such as a tachometer. Method A is the most accurate method to measure the efficiency of an IM and can be considered as a reference whereby the accuracy of other methods can be determined. This method requires decoupling of the torque transducer. As a result, using this method in in-situ is not possible. The requirement for a torque transducer, which is an expensive tool, is another disadvantage of Method A.

Method B: This method is based on loss segregation of the IM. In this method, the core loss (P_{fe}) and friction and windage losses (P_{FW}) are measured by performing a no-load test. The stator copper loss (P_{scl}) is calculated using the measured cold stator resistance and its corresponding temperature, as well as the current and temperature at the operating point. Rotor copper loss (P_{rcl}) is based on both the slip (s) and airgap power (P_{gap}) measurement at the operating point.

$$P_{rcl} = sP_{gap} \tag{1-1}$$

Stray load loss (P_{SLL}) is measured by subtracting the sum of stator and rotor resistive loss, core loss and friction and windage loss from the total losses which is the difference between the output and input powers. Because of requirements to decouple the machine and perform several

tests which need a variable voltage and frequency supply, Method B is considered to be too intrusive and expensive and cannot be applied to the working (in-situ) IMs.

Method C: This method is used when two identical machines are available and coupled together using two independent power sources and each machine operates as a generator and motor alternatively. Therefore, Method C also cannot be considered as a suitable solution for a working IM.

Methods E and E1: Method E is similar to Method B, but the output power measurement is not required and the stray load loss is measured by performing the removed-rotor test and the reverse rotation test. This method is also too intrusive. On the other hand, method E1 uses empirical results for stray load loss which decreases the intrusiveness of Method E, but yet, it is intrusive.

Methods F and F1: These method are based on the IM equivalent circuit calculations. Equivalent circuit parameters are estimated by performing the no-load and impedance tests. P_{FW} is measured using the no-load test and P_{SLL} is measured using the removed-rotor and reverse rotation tests. Method F1 uses empirical results to decrease the intrusiveness of the method. However, it is not applicable for in-situ testing.

1.2.2 IEC 60034-2-1

IEC 60034-2-1 which is a part of IEC 60034 is intended to develop methods of determining the efficiency and losses from the described tests. This standard applies to DC machines, AC synchronous and induction machines of all sizes within the scope of IEC 60034-2-1 [3].

The old version of the IEC 60034-2 which was published in 1972 was in use in Europe until 2007 due to its simplicity and required less information in determining the winding temperature and stray load loss. A new version of this standard was published in November 2007 to overcome its high measurement uncertainties and low accuracy specifically in stray load loss determination. Although rotor copper loss and friction and windage loss determination are similar in both standards, there are some differences in determination of the stator copper loss, core loss, and stray load loss. The IEC 60034-2-1 provides more accurate estimation of the core loss values by considering the effects of the load variation and resistive voltage drop in the stator. In terms of the

accuracy of stray load loss, several studies debate the accuracy of the IEC 60034-2-1 compared to the IEEE Std-112 [8, 9].

Since the measured losses by the methods described in these standards are almost similar, the measured efficiency values by utilizing IEEE and IEC standards are approximately the same. In terms of temperature measurement, the IEEE Std-112 needs some sensors to obtain the winding temperature which is intrusive while the IEC 60034-2-1 uses a method which removes the requirement of the sensors but an accurate winding temperature is not guaranteed [10].

1.3 Other Methods

Due to the difficulty of employing the standards and their requirements of performing some intrusive tests, other methods are proposed by researchers which can be categorized in five main groups and are discussed in the followings subsections.

1.3.1 Current Method

This method is based on the input current measurement, rated current and power rating data shown on the nameplate. In the simplest version of this method, a linear relationship between the load power and input current is assumed. It uses the rated power ($P_{2,rated}$), rated current ($I_{1,rated}$) and measured current ($I_{1,meas}$) to calculate the output power (P_2) as follows:

$$P_2 = \frac{I_{1,meas}}{I_{1,rated}} P_{2,rated} \tag{1-2}$$

and the estimated efficiency is given as follows:

$$\eta = \frac{P_2}{P_{in,meas}} \tag{1-3}$$

The method is simple, but it suffers from the low accuracy and other drawbacks. First, the no-load current is not zero, therefore, the method will show some incorrect values of efficiency. As a result, this method suffers from inaccurate results at lower loads. Second, assuming a linear relationship between the output power and input current always overestimates the load and consequently efficiency [11, 12].

In two modified versions of the current method, the accuracy is improved by adding the no-load current (I_0) value to (1-3) as follows [11, 13]:

$$\eta = \frac{P_{2,rated}}{P_{in,meas}}\left(\frac{I_{1,meas} - I_0}{I_{1,rated} - I_0}\right) \tag{1-4}$$

$$\eta = \frac{P_{2,rated}}{P_{in,meas}}\left(\frac{2I_{1,meas} - I_0}{2I_{1,rated} - I_0}\right) \tag{1-5}$$

This reduces the effect of the linear relationship assumption, but causes intrusiveness due to the requirement of the no-load current measurement. Regardless of the assumed relationship between the output power and the input current, the accuracy of the method is still low due to using nameplate data which might have up to 20% deviation from the real values [11, 13].

1.3.2 Slip method

Theoretically, the efficiency of an IM is given by [14]:

$$\eta = \frac{(1 - s)}{(1 + s)} \tag{1-6}$$

where *s* is the slip. This equation is based on the assumption that there is no loss in the machine except rotor resistive loss. Therefore, this method always overestimates the efficiency and has very large error.

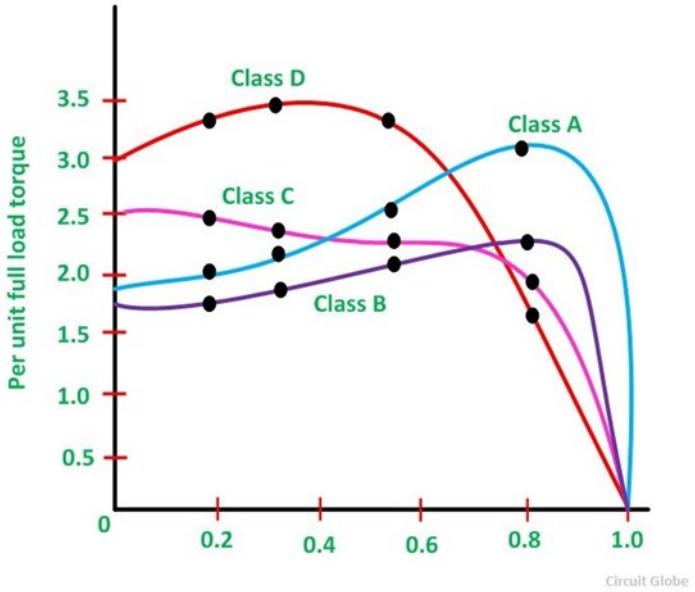

Fig. 1-1: Torque vs slip of the IMs [15].

Fig. 1-1 shows the torque-speed curves of different design classes of IMs. It is clear that the speed changes almost linearly from the no-load to the full load point. Therefore, it can be assumed

that the output power of the machine varies linearly with the load and as a result, the efficiency can be estimated as follows:

$$\eta = \frac{P_{2,rated}}{P_{in,meas}} \times \frac{s_{meas}}{s_{rated}} \tag{1-7}$$

Despite the non-intrusiveness of this method, it suffers from the low accuracy due to the following reasons. First, in reality, slip does not change linearly with the load. Second, using the nameplate data which may have up to 20% of deviation based on the NEMA standard, introduces inaccurate results [11], [13]. Third, the ambient temperature affects the slip [16].

Using the voltage terms in the equation is an option to improve the accuracy to some extent which is presented in [16] and [17]. However, the accuracy is still considered low.

$$= \frac{P_{2,rated}}{P_{in,meas}} \left(\frac{s_{meas}}{s_{rated}}\right) \left(\frac{V_{1,meas}}{V_{1,rated}}\right)^2 \tag{1-8}$$

$$\eta = \frac{P_{2,rated}}{P_{in,meas}} \left(\frac{s_{meas} - s_{meas}^2}{s_{rated} - s_{rated}^2}\right) \left(\frac{V_{1,meas}}{V_{1,rated}}\right)^2 \tag{1-9}$$

where $V_{1,meas}$ and $V_{1,rated}$ are the stator measured and rated voltage.

1.3.3 Equivalent Circuit Method

The IEEE Std-112 method F/F1 is the standard equivalent circuit method. The no-load test at variable voltage and locked rotor test at different frequencies are the requirements of this method. Furthermore, the removed-rotor and reverse-rotation tests are required to measure the stray load loss (P_{SLL}) [2]. Although this method is very accurate, it is too intrusive and cannot be applied to working machines.

Ontario Hydro modified method F (OHMF) eliminates the need for a variable voltage test, but no-load and full load tests at rated voltage are required [18]. Therefore, decoupling the IM from the load is still necessary. The stator voltage and current, input power and stator resistance as well as the rotor speed are the required measured data.

Locked-rotor method and standstill frequency response method are based on an equivalent circuit with two rotor loops. The first method requires two locked-rotor impedance tests or a locked-rotor test plus one no-load test which is highly intrusive [19]. The second method requires

a variable frequency source in the range of 0.01 to 500 Hz to measure the impedance of the motor with its rotor stationary over this range [20].

ORMEL96 is another equivalent circuit method which uses the nameplate data to keep the method non-intrusive [21], [12]. Although this method is non-intrusive, its accuracy is low because it relies completely on the nameplate data in which this data may have up to 20% inaccuracies according to NEMA MG 1 [22]. Even with typical nameplate data, its average accuracy is low (within 4% error).

The rockwell motor-efficiency wizard (RMEW) method uses data from two different load operating points to find the IM equivalent circuit parameters [23]. The stator resistance, speed and temperature of the machine must also be recorded. However, it is not mentioned how the authors solved the nonlinear equations used to calculate the input impedance.

In [24], a method is proposed to estimate the equivalent circuit parameters from the no-load acceleration–deceleration tests. In addition to the requirement of performing the no-load test and recording 5 samples of data in each second, the proposed method can only be applied to medium and large machines which have longer acceleration periods. The necessity of instruments which are required to record the transient values of current, voltage or speed is the main problems of these techniques that require the transient start-up data [25, 26].

1.3.4 Air-Gap Torque Method

The air-gap torque is a result of interaction of the flux linkages and currents in both the stator and rotor. It can be calculated using the following formula [27, 28]:

$$\tau_{AG} = \frac{P}{2\sqrt{3}}\Big\{(2i_A + i_C).\int[v_{CA} - R_1(i_C - i_A)]dt - (i_C - i_A).\int[-v_{BA} - R_1(2i_A + i_C)]dt\Big\} \quad (1\text{-}10)$$

where P is the number of poles and R_1 is the stator resistance. According to (1-10), to calculate the air-gap torque, only two line-to-line voltages (v_{CA} and v_{BA}) and two line currents (i_A and i_C) should be measured as well as the stator resistance. This method requires data logging devices to record the instantaneous values of the voltages and currents for at least 5 cycles instead of the RMS values [28]. The effect of unbalanced voltages on the air-gap torque is taken into account.

The efficiency of the machine can be estimated as follows:

$$\eta = \frac{1}{P_{in,meas}}\left[\tau_{AG}.2\pi.\frac{N_{r,meas}}{60} - P_{FW} - P_{SLL}\right] \quad (1\text{-}11)$$

where $N_{r,meas}$ and $P_{in,meas}$ are the measured rotor speed and input power. To maintain a high accuracy, P_{FW} and P_{SLL} values are necessary. This requires to decouple the machine and perform tests such as no load test, reversed rotation and removed rotor tests. This makes the method to be highly intrusive. In the modified version of the air-gap method, empirical values are used which decrease the level of intrusiveness but also lessen the accuracy [29]. The main drawback of the air-gap method is its inability to provide information about other operating points of the machine. This means that to evaluate the efficiency at each load, the machine should be run under that particular load before the measurements can be taken which is another undesirable requirement in the in-situ applications.

1.3.5 Optimization Based Methods

Optimization-based methods are mostly based on the extraction of the equivalent circuit parameters of the IM using the input and the nameplate data. These method can consequently help to estimate the efficiency at different conditions by solving the equivalent circuit.

Bacterial foraging algorithm [25], simulated annealing method, particle swarm optimization (PSO) [26] and genetic algorithm (GA) [27] are examples of the optimization algorithms which have been employed in the field of efficiency estimation. These methods will be discussed and criticized in the next chapter in detail. Although, the optimization-based techniques are proven to have the least intrusiveness, their accuracy and repeatability are still to be improved.

1.4 Objectives

The main objective of this work is to develop efficiency estimation techniques which can be applied to different operating conditions and various types of IMs with different number of poles, rated powers and voltages, NEMA designs and etc. The proposed method has the capability to be applied to working machines (in-situ applications) with minimum intrusiveness and high accuracy. For this purpose, two cases are going to be considered.

In the first case, it is assumed that the machine design data are not available and only the nameplate data plus the input data for only one operating point such as the stator voltage, current and input power are available. Therefore, an optimization based method will be used and all challenges and difficulties of this method will be described.

In the second case, it is assumed that the machine design data are available. In this case, the finite element analysis is used and the points and tips are provided to overcome the challenges of this method and improve the results.

The use of adjustable speed drives (ASDs) to control the speed of electrical machine has been increased in the last decades. Although the ASDs provide some advantages, they affect the performance of IMs. As a sub objective of this thesis, the effect of the ASDs on the efficiency of IMs will be investigated.

In the following sections, the outline of this thesis will be provided and the achievements of each chapter will be examined separately.

1.5 Thesis Outline

This thesis is organized as follows:

Chapter 2

This chapter focuses on the optimization-based algorithms to estimate the efficiency of a working IM. The previous works in this area are discussed and criticized in detail. The parameters of the equivalent circuit which are considered as a variables in this method, are discussed. The techniques and assumptions are presented to decrease the number of the variables as much as possible while the method remains non-intrusive. For the remaining parameters which are defined as variables (unknowns) of the problem, a technique is introduced to determine their range before using the optimization-based method. The proposed technique relies on the machine nameplate data and benefits from a database provided by Hydro-Quebec. The proposed technique helps narrow the search space and increase the possibility of convergence of the method to the correct answer. Then, an efficiency estimation algorithm utilizing the genetic algorithm (GA) as a search tool will be proposed. The assumptions and flowchart of the efficiency estimation algorithm are discussed in detail. The proposed parameter range determination technique is utilized in the

algorithm. Finally, the proposed algorithm is applied to four IMs and the accuracy of the results is investigated. Three cases are investigated. In the first case, the stator current, input power, and phase angle between the stator voltage and current as well as output power are used in the objective function but the range of parameters is chosen to be wide. In the second case, the motor rated power is removed from the objective function and the proposed range determination is applied in the algorithm. In the last case, both the range determination method and the rated power are utilized in the algorithm. The results of the three cases are compared with each other and also with the measured values.

Chapter 3

This chapter proposes a particle swarm optimization (PSO) based algorithm to determine the efficiency of IMs under different loads. In addition to using PSO instead of GA, there are some other differences in the proposed method compared with previous method. First, the rapid test data rather than thermally stable condition data are used as inputs for the proposed method. In the previous method, it was necessary to record the input data of the machine at thermally stable condition. This procedure normally requires several running hours to make sure that the machine's temperature is at steady state condition. The input data of the machine at 30 minutes after start are recorded and two techniques are proposed to predict the temperature of the machine at a thermally stable condition. The first technique is based on the machine insulation class, while the second technique is based on the temperature rise of the machine at the first 30 minutes of machine operation after start. Furthermore, to force PSO to converge to the correct answer, the range determination method proposed in the second chapter is improved by using the operating data of the machine. Three IMs are tested and all results are validated by the experimental results.

Chapter 4

This chapter deals with the challenges and difficulties of using the finite element analysis (FEA) to predict and estimate the efficiency of an induction machine. Two methodologies are adopted to determine the efficiency. In the first one, the FEA results are used to directly estimate the losses of the machine, and then the efficiency is calculated. All the losses are estimated at different loads. In the second methodology, the equivalent circuit parameters are estimated using the FEA and then method F1 of IEEE Std-112 is applied to the parameters of the machine to calculate the efficiency. The parameters are estimated by implementing the no-load and locked

rotor tests by FEA. Difficulties and challenges are discussed in this chapter to improve the results. Furthermore, since the mechanical loss is not included in FEA, more than 100 IMs with four poles are investigated. A new formula is proposed to estimate the mechanical loss based on the rated power of the machine. The experimental results are utilized to validate the proposed formula and approaches.

Chapter 5

In this chapter, the effects of using adjustable speed drives (ASDs) on the efficiency of IMs are studied. The efficiency of the IM is discussed and compared in this chapter for both the direct-fed and drive-fed machine operation conditions. In other words, this chapter tries to answer the question whether it is possible to predict the efficiency of an IM in a drive-fed condition using the efficiency results of the machine at a direct-fed condition. For this purpose, an industrial drive is used to implement the direct torque control (DTC) and scalar control schemes as the two common types of control schemes in industry. Moreover, the efficiency variation of the two types of squirrel cage IMs are studied. First, the machines which are designed for direct-fed applications and second, the machines designed for drive-fed applications. The no-load and load tests are conducted on four different IMs with and without ASDs. Method B of IEEE Std-112 is used for loss segregation and the variation of each losses are studied.

Chapter 6

The conclusion of this research work are presented in this chapter. Other topics are provided as possible future research works.

1.6 Thesis Contributions

The contributions that achieved in this Ph.D. work are as follows:

In chapter 2, a GA based efficiency estimation algorithm is presented which benefits from the proposed parameter range determination method. The proposed parameter range determination method is based on the nameplate data and empirical results for no-load current of the machine. It is proven that the proposed efficiency estimation algorithm is very effective for in-situ application where there is no access to output power of the machine. The proposed efficiency estimation algorithm and parameter range determination method were presented in International Electric

Machines & Drive Conference 2017 (IEMDC) in Miami, Florida, USA. The extended version of paper was also published in IEEE Transactions on Industry Applications.

M. Ghasemi Bijan, M. Al-Badri, P. Pillay and P. Angers, "Induction machine parameter range constraints in genetic algorithm based efficiency estimation techniques," *2017 IEEE International Electric Machines and Drives Conference (IEMDC)*, Miami, FL, USA, 2017, pp. 1-6.

M. Ghasemi Bijan, M. Al-Badri, P. Pillay and P. Angers, "Induction Machine Parameter Range Constraints in Genetic Algorithm Based Efficiency Estimation Techniques," in *IEEE Transactions on Industry Applications*, vol. 54, no. 5, pp. 4186-4197, Sept.-Oct. 2018.

In chapter 3, a PSO based efficiency estimation algorithm is proposed to estimate the efficiency of induction machines using the rapid test data. Two techniques are proposed to predict the temperature of the machine at thermally stable condition. The first technique is based on the insulation class of the machine and the second techniques uses the temperature rise of the machine during the first 30 min running of the machine after start. Moreover, the previous parameter range determination method is improved by using the operating data of the machine. This research work was accepted and published in IEEE Transaction on industrial Electronics.

M. Ghasemi Bijan and P. Pillay, "Efficiency Estimation of the Induction Machine by Particle Swarm Optimization Using Rapid Test Data With Range Constraints," *IEEE Transactions on Industrial Electronics*, vol. 66, no. 8, pp. 5883-5894, Aug. 2019.

In chapter 4, efficiency of induction machine is evaluated using FEA as an acceptable method for performance analysis of the electrical machines. Two methodologies are adopted. The first methodology is based on the direct calculation of the losses using FEA and the second one is based on the estimated equivalent circuit parameters of an IM from FEA. Moreover, a simple and novel formula is proposed to estimate the mechanical loss of 4-pole 60 Hz IMs. The research work was accepted in the International Electric Machines & Drive Conference 2019 (IEMDC) in San Diego, California, USA and will be presented in May 2019.

M. Ghasemi Bijan and P. Pillay, "Induction Machine Efficiency Evaluation Using the Finite Element Analysis Software and a New Mechanical Loss Formula", *IEEE International Electric Machines and Drives Conference (IEMDC)*, San Diego, CA, USA, 2019.

In chapter 5, the effects of an industrial drive on efficiency of squirrel cage IMs designed for drive-fed and direct-fed applications are studied through the experiment. The industrial drive can

work with direct torque control and scalar control. Method B of IEEE Std-112 is utilized for loss segregation. The research work has been submitted to the 11th annual IEEE Energy Conversion Congress and Exposition (ECCE 2019) and is waiting for the reviewers' decision.

M. Ghasemi Bijan and P. Pillay, "Prediction of Drive-Fed Induction Machine Efficiency Using The Direct-Fed Efficiency Results*" accepted to IEEE Energy Conversion Conference & Congress (ECCE),* Baltimore, Maryland, USA, 2019.

Chapter 2: Induction Machine Parameter Range Constraints in Genetic Algorithm (GA) Based Efficiency Estimation Techniques

2.1 Introduction

Evolutionary algorithms are employed in many different fields. They are used as optimization tools and search algorithms. The general procedure of these techniques are shown in Fig. 2-1.

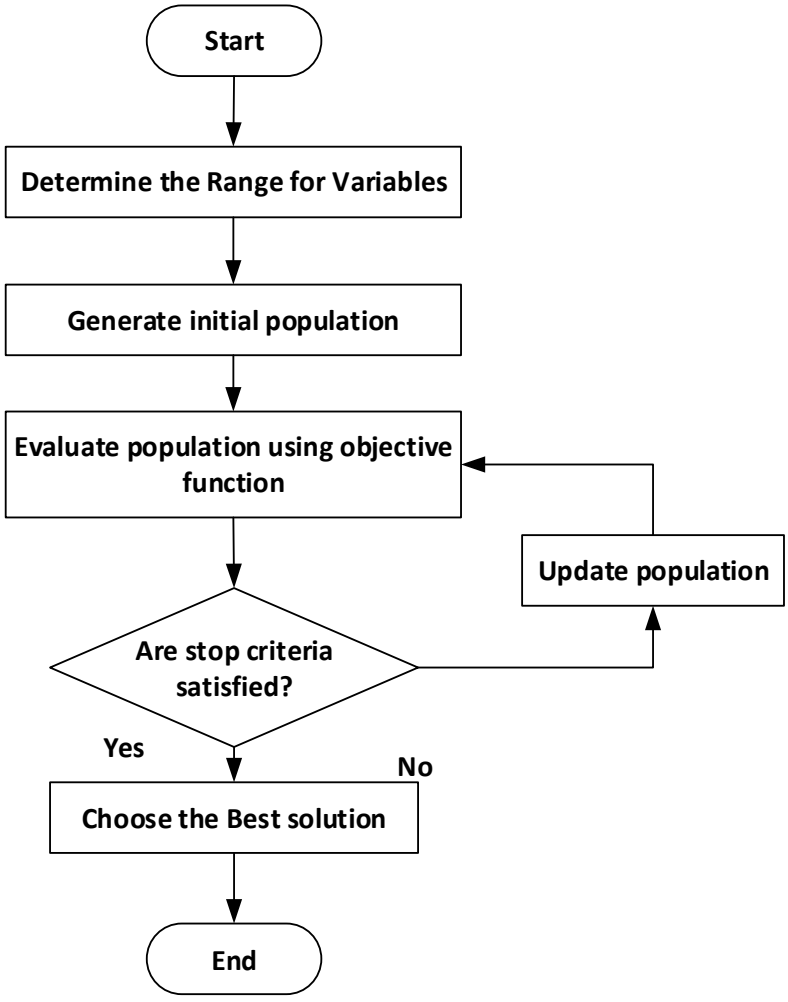

Fig. 2-1: Typical optimization algorithm procedure

When a problem is defined and variables are determined, a range for each variable is to be selected. Then, an initial population is generated. The initial population is evaluated by an objective function which is defined based on the problem. According to the rules of the applied evolutionary algorithm and the evaluation results, the initial population is updated towards the best answer and again the new generation is evaluated. This process iterates until results converge to the desired values. Sometimes, two or three layers of evolutionary algorithm are used to improve the results. In case of efficiency estimation, evolutionary algorithms can be used to estimate the equivalent circuit parameters, and then the efficiency is determined by applying Form F2 Method F1 of IEEE Std-112 [2]. This method is known in the literature as the optimization based efficiency estimation method.

In this chapter, an in-situ induction machine (IM) efficiency estimation algorithm is presented and all challenges and difficulties are discussed. The Genetic Algorithm (GA) is utilized as a search tool in the algorithm. One of the difficulties of using evolutionary algorithms for efficiency estimation is the determination of variable (parameter) constraints (ranges). A technique based on the nameplate information and a large database of tested IMs provided by the testing laboratory of Hydro-Québec are proposed to determine reasonable induction motor parameter ranges. The proposed range determination technique is utilized in a GA based efficiency estimation method and this method is applied to three different cases. In the first case, the stator current, input power and phase angle between the stator voltage and current as well as output power are used in an objective function but the range of parameters is chosen to be wide. In the second case, the motor rated power is removed from the objective function and the proposed range determination is applied in the algorithm. In the last case, both the range determination method and rated power are utilized in the algorithm. The results of the three cases are compared with each other and also with the measured values.

2.2 Optimization Based Method

The optimization based method is one of the promising method for in-situ efficiency estimation which is based on equivalent circuit parameter estimation. When this method is used in the field of IMs efficiency analysis, the variables of the problem are the equivalent circuit parameters. To estimate efficiency of an IM at any loading point, there are seven unknowns related to the equivalent circuit and two additional unknowns to be estimated or calculated (see section

2.3). Before applying the optimization method, the number of unknowns, which are discussed in detail in the following sections, should be minimized. Then, random values are assigned to those variables in the initial population. Each set of these variables is considered as a solution. Error functions are designed to compare the calculated and the measured values. The error functions establish the objective function and are generally built based on the input current or impedance, input power and input power factor or corresponding phase angle. These solutions are updated according to the governing rules of the optimization method and are again targeted by the objective function in the evaluation process. Finally, after meeting a stopping criteria, the best solution is selected as the final answer. The answer is a set of parameters of the IM equivalent circuit.

The genetic algorithm application in efficiency estimation of IM is studied in [30] and some conditions are investigated. The results showed that using data of two loading points can improve the accuracy of the results. Also, using more constraints in the objective function results in better solutions. The input power, current, and power factor are the general terms used in the objective function. It is shown that using the nameplate power in the objective function can be useful to reduce the errors if the output power dose not vary too much from the nameplate power.

In [31, 32, 33], the GA is used to estimate the efficiency under unbalanced supply condition. The input power and stator current as well as the full load temperature of the machine establish the objective function terms. To improve the accuracy, data of several loading points (three or five points) are used as inputs. The number of the required loading point data and determination of the full load temperature based on the insulation class of the machine are the main drawbacks of the proposed algorithm which reduce the accuracy.

In [34] and [35], three layers of the GA are applied to improve the accuracy. The full load operating data are used as inputs and a large database is used to determine the friction and windage losses, the stray load loss (P_{SLL}), and the full load temperature. In addition to the input power, the stator current, the phase angle between the stator current and voltage, and the output power are used in the objective function. Although the results show good accuracy, using the output power in the objective function is a drawback, because for most in-situ applications, there is no information about the output power. Moreover, it is mentioned in [30] that the error in the measured value of the output power can result in a large error in the estimated efficiency.

In [36, 37], three methods are used to estimate the machine parameters: the Newton-Raphson method, simulated annealing method, and particle swarm optimization (PSO) method. Apart from the Newton-Raphson method, two methods are optimization algorithms. The real and imaginary parts of input impedance were used to define the objective function. The inputs of algorithm are the phasor data of the input voltage and current at two operating points. The two points must be chosen carefully because too close conditions result in ill-conditioned equations, while too spread conditions result in additional errors caused by the parameter variations due to temperature change, flux saturation, etc. Considering the P_{SLL} by adding an equivalent resistor in series with the rotor circuit is one of the drawbacks of the model which reduces the accuracy. The error within the results is 2-3% for different loads indicating low accuracy. Disregarding the impact of the load variation on the rotor resistance is another disadvantage of this approach.

Bacterial foraging based algorithm for the efficiency estimation is used in [38, 39]. Besides the stator voltage, stator current, and input power, the stator resistance and operation speed of the rotor are also inputs of the algorithm. A modified equivalent circuit is used to include the P_{SLL} by using a series resistor in the rotor circuit based on IEEE Std. 112. This algorithm is applied to two cases; the first case uses only the full load condition data as inputs and the second case uses data of 25, 50, 75, and 100% load. The objective function includes the input power and current. The results of the second case are better than the first one. However, the error of the results with some loads, especially at low loads, are more than 3%. The same algorithm is used to estimate the efficiency with unbalanced voltages in [40]. The positive and negative sequence equivalent circuits are employed and it is assumed that the magnetizing reactance X_m and core loss resistance R_{fe} are connected in series. In addition, it is assumed that R_1, X_1, X_m, and R_{fe} are of the same values in the positive and negative sequence equivalent circuits, as well as R_2 and X_2 have different values.

So far, the literature work focuses only on the objective function and inputs as the two main parts of the optimization algorithm. None of them have studied the impact of the parameters range (constraints). The determination of the parameter range has a significant effect on the convergence of the optimization algorithm. Since the parameters of a machine depend on the machine rated power, number of poles, insulation class and so on, choosing a fixed parameter range for all machines is not reasonable. Also, choosing a wide range for parameters can cause the optimization algorithm to converge to different answers in each run.

Techniques to estimate five parameters non-intrusively are explained in detail in the next sections. For the remaining four parameters, simple and straightforward methods and relationships are presented to determine the range which can be employed to help improve the accuracy.

2.3 Equivalent Circuit Parameters

Fig. 2-2 shows the conventional per phase equivalent circuit of an IM. R_1 and X_1 are the stator resistance and leakage reactance, R_2 and X_2 are the rotor resistance and leakage reactance, X_m is the magnetizing reactance, R_{fe} is the core loss resistance; s is the slip, P_{in} and P_2 are the input and output power, P_{SLL} is the stray load loss, and P_{FW} is the friction and windage losses.

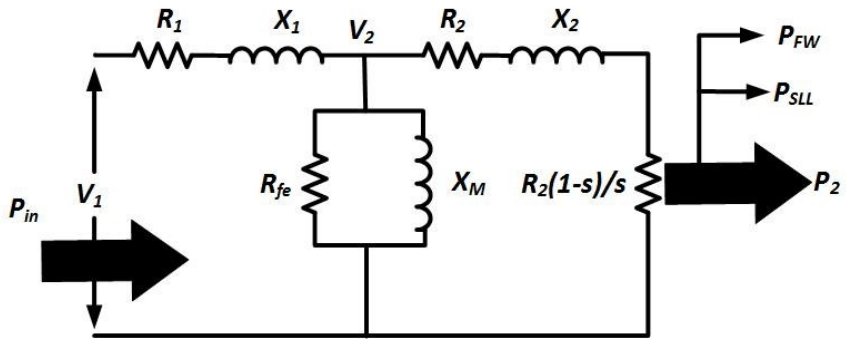

Fig. 2-2: An IM equivalent circuit [33]

According to Fig. 2-2, to estimate the efficiency at any loading point, there are seven unknowns (R_1, X_1, X_m, R_{fe}, R_2, X_2, and s). The additional unknowns are P_{SLL} and P_{FW}. In the following sections, techniques are described to decrease the number of unknowns to four (i.e. X_1, X_m, R_{fe}, and R_2).

2.3.1 Stator Resistance (R_1) and Temperature

The stator copper loss is proportional to the amount of current passing through the stator windings. The losses include the heat loss due to current flow through the winding as well as the skin effect due to the frequency of current [41, 42]. The stator copper loss accounts for 25-40% of the total losses in the machine and are considered load dependent [42]. Therefore, a precise estimation of R_1 is of great importance in determining a precise efficiency of the machine.

R_1 affects the shape of the torque-speed curve, and the speed at which the pull-out torque occurs [43]. A common way to measure R_1 is to perform a DC test. Loading the motor heats the IM and increases the value of R_1. Therefore, in-situ temperature measurement is necessary to

determine the R_1 at different loading conditions. Based on the IEEE Std-112, R_1 can be calculated at different loads as follows [2]:

$$R_1 = \frac{R_{1,cold}(T_{hot} + K)}{T_{cold} + K} \tag{2-1}$$

where T_{hot} is operating point temperature of the machine and T_{cold} is cold temperature measured when the machine is cold at standstill which can also be considered as ambient temperature. $R_{1,cold}$ is the stator resistance at T_{cold}. K is 234.5 for 100% IACS conductivity copper and 225 for aluminum. By having the stator resistance at T_{cold} as a reference, T_{hot} can be estimated instead of measuring R_1 directly. T_{hot} can also be used to correct the rotor resistance. It is possible to find a relationship between the machine temperature and machine load, and this relationship can be used to estimate the temperature at different loading conditions.

Determination of the full load temperature according to the machine insulation class is also a solution to decrease the number of unknown variables in the optimization algorithm [32]. The temperature can be assumed as per Table 2-1. The analysis conducted in [34] showed that this assumption causes significant error in the estimated efficiency. This is because the stator resistive loss (P_{scl}) and rotor resistive loss (P_{rcl}) are significant portions of the total machine losses. An incorrect temperature estimation would result in a large error in the estimated copper losses and consequently the efficiency.

Table 2-1: Rated temperature for efficiency calculations

Class of insulation system	T_{fl} (°C) including 25 °C reference ambient
A	75
B	95
F	115
H	130

Although the aim is to reduce the number of unknowns, it is recommended to measure the stator resistance or the temperature (T_{hot}) using a non-intrusive tool. The intermittently injection of a low level DC current into the stator winding is a cost effective technique which is commercially available to determine the temperature of the machine online [44]. It does not cause

unacceptable torque pulsations in the machine. Moreover, the estimated T_{hot} is also used to correct R_2.

2.3.2 Stator and Rotor Leakage Reactance (X_1 and X_2)

X_1 and X_2 are not temperature-dependent and considered constant at all loads. Based on NEMA design, it is possible to determine the ratio X_1/X_2 as shown in Table 2-2 [22]. This also reduces the number of the unknowns.

Table 2-2: Ratio of X_1/X_2 [22]

Design Class	X_1/X_2
A , D and wound rotor	1.00
B	0.67
C	0.43

2.3.3 Rotor Speed or Slip

The slip or the rotor speed can be estimated or measured non-intrusively. A contactless speed sensor can be used to measure the rotor speed. Moreover, various methods are proposed for sensorless estimation of the speed [45]. The results in [34] show that using the technique proposed in [46] led to higher accuracy in the speed estimation (maximum error of 1 rpm). This technique is based on the harmonic spectrum analysis of the stator current. The slip can be determined as

$$f_{sh} = f_1\left(1 \pm \frac{1-s}{P}\right) \tag{2-2}$$

where f_1 is the input frequency, f_{sh} is desired harmonic in the spectrum, and P is the number of pole pairs.

2.3.4 Stray Load Loss (P_{SLL})

According to the IEEE Std-112, "the stray load loss is that portion of the total loss in the electrical machine not accounted for by the sum of the P_{FW}, the stator copper loss, the rotor copper loss, and the core loss" [2]. P_{SLL} is considered as a load dependent loss and consists of:

- Losses introduced by the load in active iron and other metal parts other than the conductors.

- Eddy-current losses in the primary or secondary winding conductors caused by the current dependent flux pulsations [47].

P_{SLL} can be measured either directly or indirectly. In the indirect method, P_{SLL} can be found using:

$$P_{SLL} = \Delta P - \left(P_{scl} + P_{fe} + P_{rcl} + P_{FW}\right) \quad (2\text{-}3)$$

where ΔP is the total loss which can be calculated by subtracting the P_{in} from the P_2. It should be noticed that all the components in (2-3) can be measured directly using the methods presented in section 5 in [2].

In the direct measurement, the fundamental and high frequency components of the P_{SLL} are determined by the removed-rotor and reverse rotation tests and the total P_{SLL} is the sum of these two components (section 5.7.2 of IEEE Std-112 [2]).

Using a double layer winding with low space harmonic contributions reduces the high frequency flux variations in the motor teeth and insulating the rotor bars to limit the interbar leakage currents are some possible solutions which can be useful to decrease P_{SLL} [48]. These small reductions in P_{SLL} can be significant for efficiency improvements.

Due to the difficulty of P_{SLL} measurement either directly or indirectly, the IEEE Std-112 [2] and IEC 60034-2 [3] standards assume the P_{SLL} based on empirical results. IEEE Std-112 standard determines the P_{SLL} based on the nameplate power of the IM as shown in Table 2-3.

Table 2-3: Assumed values for P_{SLL} [2].

Machine Rating (kW)	P_{SLL} Percent of Rated Load
1-90	1.8%
91-375	1.5%
376-1850	1.2%
1851 and greater	0.9%

IEC 60034-2 introduces a formula that can estimate the P_{SLL} based on the full load input power. In the old version of this standard [49], it is recommended to consider P_{SLL} as 0.5% of the full load input power ($P_{in,fl}$).

Several studies are conducted to compare the accuracy of the two standards in terms of P_{SLL} determination. In [47], 817 IMs in the range of 1-500 hp rated for 50 and 60 Hz have been studied. Based on the results, the accuracy of IEC 60034-2 (old version [49]) is less than IEEE Std-112. Moreover, it is shown that by increasing the rated power, the accuracy of IEC 60034-2 increases. Another study compares the estimated efficiency by IEEE Std-112 [4] , IEC 60034-2 [49] and JEC 37 (Japanese Standard). The comparison shows that the accuracy of the IEEE Std-112 is better than other two standards which is mostly due to better estimation of P_{SLL}.

In the new version of IEC 60034-2 [3], the P_{SLL} is determined using

$$P_{SLL} = P_{in,fl}\left[0.025 - 0.005\, log_{10}\left(\frac{P_{out}}{1kW}\right)\right] \tag{2-4}$$

In [8], around 1000 IMs are studied and it recommends that when testing facilities are not available to measure P_{SLL}, assuming 1.2% of P_{in} for P_{SLL} is a better approximation for IMs rated between 1-200 hp. This can keep the efficiency estimation error in the range of ±1%.

It has been stated in [50] and [34] that using IEEE Std-112 [2] for motors rated less than 40 hp and IEC 60034-2 [3] for motors rated above 40 hp would result in higher accuracy in the efficiency estimation algorithms. This threshold has been determined after a thorough analysis conducted on a large test data provided by Hydro-Québec and BC hydro. Since P_{SLL} is considered as a load dependent loss, the following formulas are proposed for partial loads in [34]:

$$P_{SLL,75} = P_{SLL}/1.8 \tag{2-5}$$

$$P_{SLL,50} = P_{SLL}/4 \tag{2-6}$$

$$P_{SLL,25} = P_{SLL}/16 \tag{2-7}$$

where $P_{SLL,75}$, $P_{SLL,50}$ and $P_{SLL,25}$ are the stray load loss at 75%, 50% and 25% load, respectively.

2.3.5 Friction and windage losses (P_{FW})

P_{FW} consists of two different types of losses. The friction loss is due to the friction in the bearing of the machine. The windage loss which is because of the air flow produced by the cooling fan of machine. These losses can account for 5-15% of the total losses of the machine and are considered to be load independent [42]. According to [51], P_{FW} varies with the square of the speed of the machine.

P_{FW} can be determined by performing a no-load test. However, this technique is too intrusive and unacceptable for in-situ applications. P_{FW} is usually considered constant and as a percentage of the rated output power or full load input power. In [34], the P_{FW} is determined by using the database of 182 motors. If the tested motor has no similarity in the database, the P_{FW} can be assumed based on the number of poles as

$$P_{FW} = 2.5\% \times P_{in,fl} \quad for\ 2-pole \tag{2-8}$$

$$P_{FW} = 1.2\% \times P_{in,fl} \quad for\ 4-pole \tag{2-9}$$

$$P_{FW} = 1.0\% \times P_{in,fl} \quad for\ 6-pole \tag{2-10}$$

The above equations are used in the algorithms proposed in Chapters 2 and 3.

2.3.6 Other Parameters

In the previous sections, the non-intrusive techniques to determine the five parameters (R_1, X_2, s, P_{FW}, and P_{SLL}) are explained. Other four parameters (X_1, X_m, R_{fe}, and R_2) can be estimated using an optimization algorithm. However, it is possible to determine the range for these parameters which is useful in the convergence and repeatability of the optimization algorithm.

2.4 Parameter Range

Since the optimization algorithm is used as a search tool, it must be designed to explore a reasonable limited region of the variable space [52]. Sometimes the region is determined by the problem itself, for example, when one is trying to find the maximum point of a specific area. In some problems, the search region is not determined by the problem. In this case, there are two options.

First, choosing a wide range of variables as an initial search region which ensures that the desired answer is in this region and then focusing on the most promising parts of the region. This solution is ineffective when there are several answers which can satisfy the objective function. For the IMs efficiency estimation using only one loading point data is difficult because there are several answers which can satisfy the objective function. This is due to a lower number of inputs compared to the number of unknowns (variables).

The second option is to limit the search region by using some rules, equations and even standards which are related to the problem. When the search space is smaller, it is more likely to reach the correct answer. In the following subsections, a simple and straightforward solution for determining the range of variables is provided by utilizing some equations, assumptions and NEMA MG 1 standard. This method employs only the nameplate data and a database provided by Hydro-Québec.

2.4.1 Rotor Resistance (R_2):

Rotor resistance has a significant role in the behavior of an IM. The IM characteristics in the normal operating range is affected by rotor resistance [41]. The electromagnetic or airgap power (P_{gap}) of the IM is related to R_2 as

$$P_{gap} = 3\frac{R_2}{s}I_2^2 \tag{2-11}$$

where I_2 is rotor current and s is the slip. I_2 can be calculated as follows [2]:

$$I_2 = \sqrt{I_1^2 - I_0^2} \tag{2-12}$$

where I_1 and I_0 are the input current and no-load current respectively. For a specific condition, for instance, the rated condition provided by the nameplate, s and I_1 are known. At the rated condition, P_{gap} can be estimated as

$$P_{gap} = P_{out} + P_{FW} + P_{SLL} + P_{rcl} \tag{2-13}$$

P_{FW} and P_{SLL} are determined based on the machine rated power and number of pole [34] . P_{out} is the machine rated power. The rotor copper loss (P_{rcl}) is related to P_{gap} as follows:

$$P_{rcl} = sP_{gap} \tag{2-14}$$

Finally, P_{gap} can be estimated at full-load as

$$P_{gap} = \frac{P_{out} + P_{FW} + P_{SLL}}{1 - s} \tag{2-15}$$

At the full-load condition, I_1 is the rated current which is known from the nameplate. The no-load current (I_0) is affected by the flux density, number of poles and the rated power of the

machine. By utilizing the database of 129 IMs in the range of 1-500 hp provided by Hydro-Québec, several useful relationships shown in Table 2-4 are extracted.

Table 2-4: Typical expected no-load current for motors with different rated power.

Rated power (hp)	Ratio of no-load current to full-load current (%)
1 – 7.5	35 – 80
10 – 50	20 – 45
60 – 500	15 – 45

For example, for IMs in the range of 1 to 7.5-hp, by considering the minimum and maximum values of I_0 from Table 2-4, and using (2-11) and (2-12), R_2 range can be determined as follows:

$$I_{0,min} = 0.35 \times I_1 \quad \rightarrow \quad R_{2,min} = \frac{sP_{gap}}{3 \times (0.9367 I_1)^2} \tag{2-16}$$

$$I_{0,max} = 0.8 \times I_1 \quad \rightarrow \quad R_{2,max} = \frac{sP_{gap}}{3 \times (0.6 I_1)^2} \tag{2-17}$$

Using this range not only narrows the R_2 range but also guarantees that the desired R_2 is within this range. The range helps the optimization algorithm to search in a narrow range of R_2 which increases the possibility of convergence to the correct answer.

The minimum and maximum values of R_2 should be corrected as per the machine temperature prior to using them as constraints. If the full-load temperature is known, it can be used for R_2 correction, otherwise, the full-load temperature can be determined based on the machine insulation class [2]. When the rated temperature is determined, (2-1) can be used to find the final range of R_2. It is accepted to use the rated temperature based on insulation class instead of the actual full-load temperature since the purpose is to define a range and not to determine the rotor resistance value.

The only reason for using the rated condition data is that they are known and there is no need to perform any additional test to extract them. In addition, using a loading point other than the full load is acceptable. However, the P_{FW} and P_{SLL} are required at that load. Moreover, the speed and temperature at that load should be known.

2.4.2 Core Loss Resistance (R_{fe})

The core losses (P_{fe}) comprise of the hysteresis and eddy current losses in the iron laminations of the machine as a result of the energy required to magnetize the core [41, 42]. The core losses account for 15% of total losses of an IM and are considered to be load independent [42]. The core loss can be calculated as follows:

$$P_{fe} = \Delta P - (P_{FW} + P_{SLL} + P_{rcl} + P_{scl}) \tag{2-18}$$

where ΔP is the total loss.

At rated condition, ΔP can be calculated based on the nameplate data as

$$\Delta P = P_{in} - P_{out} = (1 - \eta)P_{in} = \left(\frac{1 - \eta}{\eta}\right) P_{out} \tag{2-19}$$

where η is the rated efficiency and P_{out} is the rated power of the machine.

As previously mentioned, for the rated condition, P_{SLL} and P_{FW} are determined based on the machine rated power and number of poles respectively [34]. P_{rcl} can be calculated using (2-14). P_{scl} is calculated as follows:

$$P_{scl} = 3R_1 I_1^2 \tag{2-20}$$

where I_1 is the rated current of machine and R_1 is the stator resistance which should be determined by the DC test. Measured R_1 shall be corrected for rated temperature as per (2-1). The rated temperature is the same as that considered for R_2 correction. R_{fe} can be estimated as follows:

$$R_{fe} = \frac{3V_2^2}{P_{fe}} \tag{2-21}$$

where V_2 is the magnitude of voltage across the parallel branch of the equivalent circuit and can be calculated as follows:

$$V_2 = |V_1 - (R_1 + jX_1)(I_1 < \varphi)| \tag{2-22}$$

By neglecting the second term on the right side of the equation, $V_2 = V_1$ and (2-21) can be rewritten as:

$$R_{fe} = \frac{3V_1^2}{P_{fe}} \tag{2-23}$$

An approximated R_{fe} is employed to determine a reasonable range for R_{fe}. The following range can be considered for R_{fe} in the optimization algorithm.

$$R_{fe,min} = 0.6 \; or \; 0.7 \times R_{fe} \tag{2-24}$$

$$R_{fe,max} = 1.1 \times R_{fe} \tag{2-25}$$

The assumption of $V_2 = V_1$ causes an increase in the amount of approximated R_{fe}. Therefore maximum value of R_{fe} is considered 110% of the approximated R_{fe}.

A recent study conducted on 182 motors of different power ratings, speed, insulation class, and NEMA design has shown that the maximum core loss of an IM is 6% of input power at the rated condition [9]. This criteria can also be useful to narrow the R_{fe} range. It can be helpful to determine the minimum value of R_{fe} in the range. For this purpose, by calculating the input power at the rated condition, the maximum P_{fe} is calculated by considering as 6% of the rated input power. Then $R_{fe,min}$ can be achieved by using (2-25).

2.4.3 Stator Leakage Reactance (X_1)

Reactance has two significant effects on the size and performance of IMs. The first one is the limitation on the possible power output for a given speed and frame size, and the other effect is the determination of a specific performance characteristics for a given design [43, 53].

The equation for the maximum torque of an IM is:

$$\tau_{max} = \frac{3V_{th}^2}{2\omega_s \left[R_{th} + \sqrt{R_{th}^2 + (X_{th} + X_2)^2}\right]} \tag{2-26}$$

Where

$$V_{th} = \frac{V_1 X_m}{\sqrt{R_{th}^2 + (X_1 + X_m)^2}} \tag{2-27}$$

$$R_{th} + jX_{th} = \frac{jX_m(R_1 + jX_1)}{R_1 + j(X_1 + X_m)} \tag{2-28}$$

$$(X_1 + X_m)^2 \gg R_1^2 \rightarrow R_{th} \approx \left(\frac{X_m}{(X_1 + X_m)}\right)^2 R_1 \tag{2-29}$$

$$X_m \gg X_1 \rightarrow X_{th} \approx X_1 \tag{2-30}$$

By neglecting the X_m and R_{fe} from the equivalent circuit, (2-26) can be rewritten as follows:

$$\tau_{max} = \frac{3V_1^2}{2\omega_s \left[R_1 + \sqrt{R_1^2 + (X_1 + X_2)^2}\right]} \tag{2-31}$$

In (2-31), V_1, ω_s and R_1 are known, and τ_{max} and (X_1+X_2) are unknown. Based on the NEMA MG 1 Standard, τ_{max} for each motor should not be less than the presented values in Table 2-5 and Table 2-6 which are expressed in percent of the full-load torque [22]. Hence, by considering the values presented in those tables for τ_{max}, (X_1+X_2) can be estimated. Finally, by using X_1/X_2 ratio from NEMA MG 1 standard (Table 2-2), X_1 can be calculated.

Since τ_{max} is the minimum required value, therefore, the calculated X_1 is the maximum value which can be considered as an upper limit of the X_1 range in the optimization algorithm. The minimum value of X_1 can be considered as half of the upper limit.

Table 2-5: Minimum T_{max} as a percentage of full-load torque for IM Design A and B [22].

	Number of Poles						
hp	2	4	6	8	10	12	14
½	…	…	…	200	200	200	200
¾	…	…	275	200	200	200	200
1	…	300	265	200	200	200	200
1-½	250	280	250	200	200	200	200
2	240	270	240	200	200	200	200
3	230	250	230	200	200	200	200
5	215	225	215	200	200	200	200
7-½	200	215	205	200	200	200	200
10-125	200	200	200	200	200	200	200
150	200	200	200	200	200	200	…
200	200	200	200	200	200	…	…
250	175	175	175	175	…	…	…
300-350	175	175	175	…	…	…	…
400-500	175	175	…	…	…	…	…

Table 2-6: Minimum T_{max} as a percentage of full-load torque for IM Design C [22].

	Number of Poles		
hp	4	6	8
1	200	225	200
1-½	200	225	200
2	200	225	200
3	200	225	200
5	200	200	200
7-½ - 10	200	190	190
25-200 inclusive	190	190	190

The assumption used in (2-31) may cause some arguments. To further explore the effect of these assumptions, (2-26) is rewritten as

$$(X_{th} + X_2)^2 = (\mathrm{A}V_{th}^2 - R_{th})^2 - R_{th}^2 \tag{2-32}$$

where

$$A = \frac{3}{2\omega_s T_{max}} \tag{2-33}$$

By substituting (2-25) and (2-27) in (2-30), (2-34) is derived which is rearranged in (2-35)

$$(X_{th} + X_2)^2 = \left(\mathrm{A}\left(\frac{X_m}{X_m + X_1}\right)^2 V_1^2 - \left(\frac{X_m}{X_m + X_1}\right)^2 R_1\right)^2 - \left(\frac{X_m}{X_m + X_1}\right)^4 R_1^2 \tag{2-34}$$

$$(X_{th} + X_2)^2 = \left(\frac{X_m}{X_m + X_1}\right)^4 ((\mathrm{A}V_1^2 + R_1)^2 - R_1^2) \tag{2-35}$$

It is clear that $\frac{X_m}{X_m+X_1} < 1$. As a result by neglecting X_m ($X_m \to \infty$), $\lim_{X_m \to \infty} \frac{X_m}{X_m+X_1} = 1$, it can be seen that the parallel branch of the equivalent circuit and using $V_{th} = V_1$ and $R_{th} = R_1$ results in a higher estimation for X_1. This overestimation can ensure that the desired X_1 value will be within the range. The effect of the assumption in (2-30) can be neglected due to overestimation.

2.4.4 Magnetizing Reactance (X_m)

The magnetizing reactance of a machine is an important parameter and corresponds to the main magnetic flux that links the machine's stator and rotor, passing two times over the air-gap. This reactance is present within the equivalent circuit and can be determined experimentally by the no-load test [43].

The magnetizing reactance has a significant effect on the no-load current and no-load power factor [43]. At no-load, the rotor speed is very close to the synchronous speed and slip is almost zero. As a result, it can be assumed that the no-load current passes through the parallel branch of the equivalent circuit and hence, the rotor part of the equivalent circuit can be neglected. Also, by neglecting R_1 and X_1, the following equation can be written

$$tan(\varphi_0) = \frac{R_{fe}}{X_m} \tag{2-36}$$

where φ_0 is the angle of the no-load power factor. By assuming cos (φ_0) = 0.5 as a maximum possible no-load power factor, the maximum value for X_m can be achieved by using the maximum estimated value of R_{fe}.

$$X_{m,max} = \frac{R_{fe,max}}{\sqrt{3}} \tag{2-37}$$

For a minimum value of X_m, the previous assumption about the no-load current can be useful. If the maximum no-load current is considered as 80% of the rated current (for IMs in the range of 1 to 7.5-hp), and by neglecting R_1, X_1 and R_{fe}, the $X_{m,min}$ can be calculated as follows:

$$X_{m,min} = \frac{V_1}{0.8 \times I_1} \tag{2-38}$$

Neglecting R_1 and X_1 causes overestimation and neglecting R_{fe} causes underestimation. These two effects oppose each other. Hence, the estimated $X_{m,min}$ can be acceptable.

2.4.5 Parameter Range Determination Results

The proposed technique is applied to four different machines: 3, 5, 7.5 and 250 hp IMs. The specifications of those motors are shown in Table 2-7.

Table 2-7: IM's specification

Power (hp)	3	5	7.5	250
V_{LL} (V)	208	220	460	460
I_L (A)	10	16	8.85	284
f (Hz)	60	60	60	60
connection	Y	D	D	D
Rated rpm	1740	1730	1755	1785
NEMA Design	B	B	B	B
Poles	4	4	4	4

The estimated parameter range for these IMs are shown in Table 2-8. According to Table 2-8, the range of X_1 for each motor is different. This means that the determined range helps to avoid searching the areas where the desired value of the variable does not exist. This proves the effectiveness of the proposed method in narrowing the range as much as possible to increase the possibility of convergence to the correct answer.

The technique is very effective to determine the R_2 range which is mostly limited to less than one unit. For example, the range is between 0.24 Ω and 0.59 Ω for 3 hp IM and for 250 hp IM it is between 0.0187 Ω and 0.0456 Ω. The worst case is for 7.5 hp IM and the range is between 1.845 Ω and 4.497 Ω. This range can be considered as an acceptable range.

Table 2-8: Parameter range

Power (hp)	3	5	7.5	250
$X_{1,min}$ (Ω)	0.606	1.4406	4.6299	0.19
$X_{1,max}$ (Ω)	1.2133	2.8812	9.2598	0.38
$X_{m,min}$ (Ω)	14.695	29.6	113.4	3.5085
$X_{m,max}$ (Ω)	168.4856	1787.7	5721.9	184.6664
$R_{fe,min}$ (Ω)	227.49	516.1	1651.8	53.3086
$R_{fe,max}$ (Ω)	291.825	3096.4	9910.7	319.8516
$R_{2,min}$ (Ω)	0.2421	0.5935	1.8451	0.0187
$R_{2,max}$ (Ω)	0.5901	1.4466	4.4974	0.0456

The determined ranges of X_m and R_{fe} are not as narrow as the R_2 and X_1 ranges. However, it is useful to confine the search space for the evolutionary algorithm. Despite the large determined range for X_m and R_{fe}, a limited range of R_2 and X_1 can be useful after the first few iterations of the evolutionary algorithm to lead the initial answers into a correct answer.

These methods and techniques will be applied in the proposed GA based algorithm presented in the following sections and the results will be discussed. Before that, a brief introduction to GA is presented in the next section.

2.5 Genetic Algorithm (GA)

The GA is a metaheuristic technique inspired by the process of natural selection. GAs are commonly used to generate high-quality solutions for optimization and search problems. For this purpose, GAs employ some bio-inspired operators such as mutation, crossover and selection [52].

A GA starts with an initial number of population which consist of several variables. These initial values are generated randomly within a certain range of variables and each set of variables makes up a chromosome which is considered as a solution for the problem. Then, the solutions are evaluated by a fitness function which is defined according to the problem. The highest ranked solutions are selected for the next iteration and others are removed from the initial population. The selected solutions are mutated to generate a new generation which includes the old and new solutions. Once again, the new generation is evaluated by the fitness function and the best solutions are selected to create a new generation. This process iterates until a stop criteria is satisfied. Fig. 2-3 shows an overview of the GA used in this chapter.

The first step in the process is to define an objective function and a chromosome as an array of variables. In the conventional equivalent circuit of an IM, there are 9 parameters, out of which five parameters (R_1, X_2, s, P_{FW} and P_{SLL}) can be determined or measured non-intrusively which were described in the previous sections. The remaining four parameters are unknown and are defined as a chromosome as

$$Chromosome = \left[X_1 , X_m, R_{fe}, R_2\right] \tag{2-39}$$

where X_1 and X_m are the stator leakage and magnetizing reactance, and R_{fe} and R_2 are the core loss and the rotor resistances.

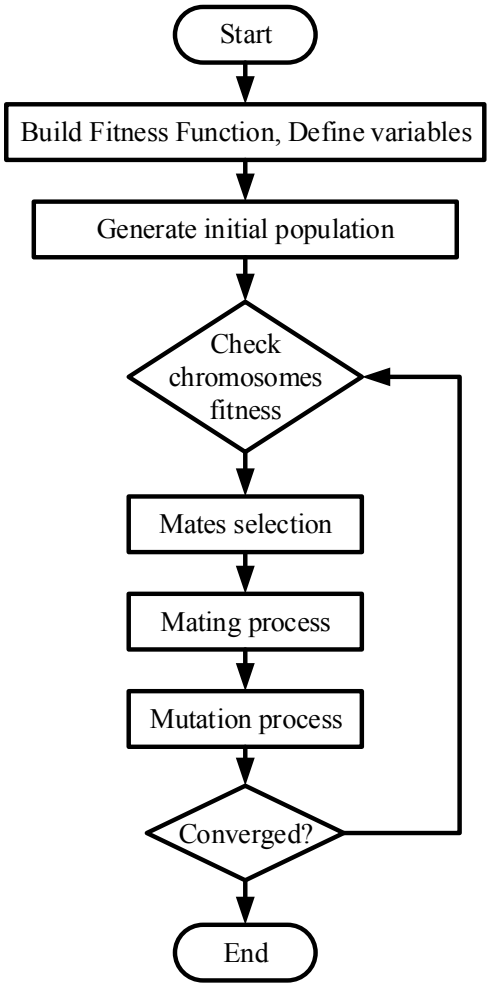

Fig. 2-3: Genetic algorithm flowchart [34].

2.6 Proposed GA Based Efficiency Estimation Algorithm

The proposed algorithm is illustrated as a flowchart in Fig. 2-4. The algorithm starts with the predetermined values of the stator winding cold resistance $R_{1,\text{cold}}$ and cold temperature T_{cold}. The measured input currents, voltages and active power as well as the nameplate data are used as the input of the algorithm. The values of P_{SLL} and P_{FW} are also predetermined.

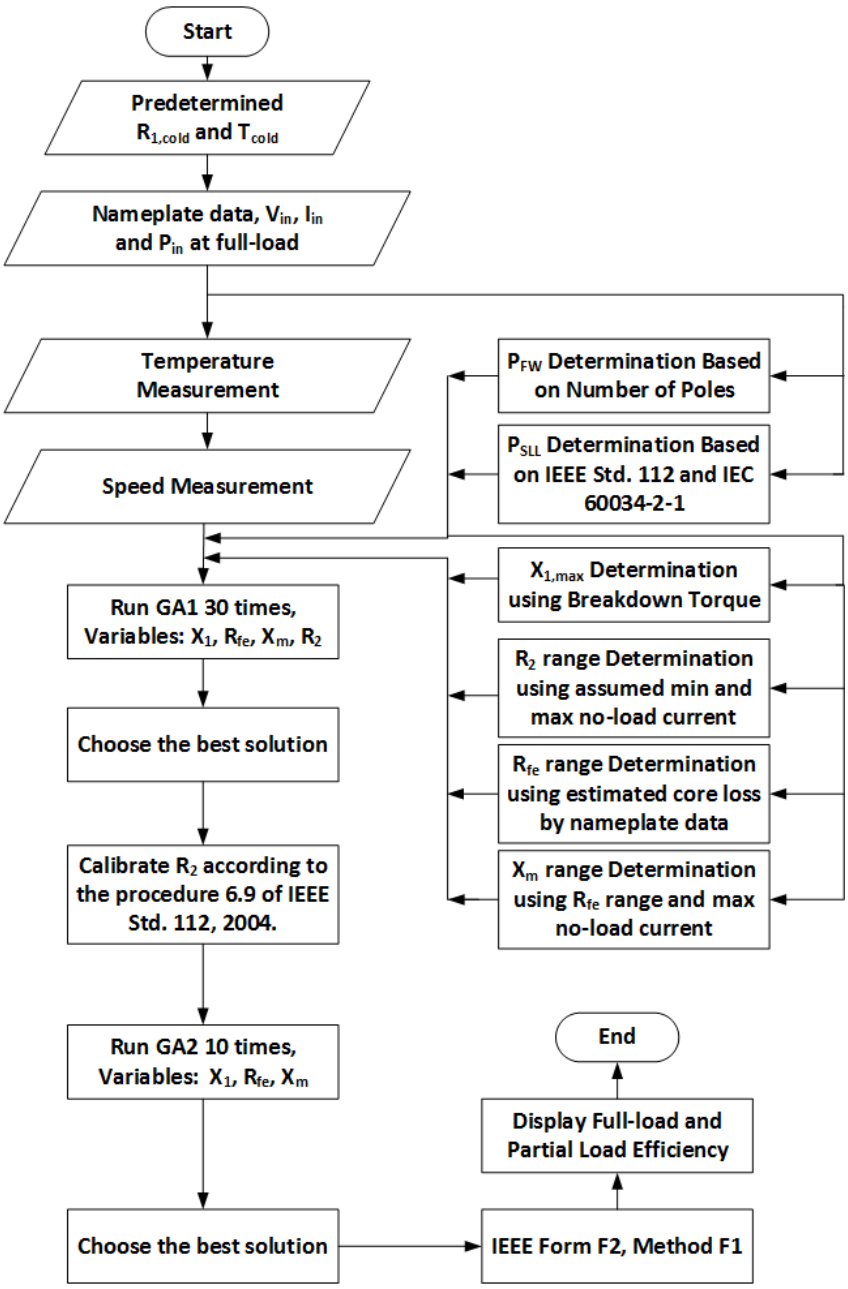

Fig. 2-4: Proposed algorithm flowchart.

P_{SLL} is determined using (2-40) [34]

$$P_{SLL} = \begin{cases} 1.8\%P_{out} & P_{out} < 40\ hp \\ P_{in,fl}\left[0.025 - 0.005\ log_{10}\left(\frac{P_{out}}{1kW}\right)\right] & P_{out} > 40\ hp \end{cases} \quad (2\text{-}40)$$

where P_{out} is the rated output power and $P_{in,fl}$ is the full load input power.

To improve the accuracy at partial loads and by considering the variation in P_{SLL}, (2-5) to (2-7) are utilized to estimate the P_{SLL} at different loads. P_{FW} is determined using (2-8) to (2-10) according to the number of poles. The assumed values of P_{SLL} and P_{FW} as well as the nameplate data are used to determine the parameter range as discussed in the section 2.4. Prior to running the first GA, the rotor speed and temperature are measured or estimated. The first GA is then run for 30 times. At this stage, there are four variables: X_1, X_m, R_{fe}, and R_2.

In the IM equivalent circuit, only R_2/s changes due to load variations. The value of R_2 is calibrated according to IEEE Std-112 described in section 6.9 of the standard. This can be done by increasing the R_2/s in proper steps until the calculated values of the input power and input current match with the measured values with an error of less than 1%. After R_2 calibration, the second GA is run for 10 times with only three variables, X_1, X_m, and R_{fe}. The best solution is chosen for the final step which is used to estimate the full- and partial-load efficiencies of the machine using the IEEE Form F2-Method F1 [2].

The objective of the evolutionary algorithm is to minimize the difference between the measured and estimated value of the input power, stator current and phase shift between the stator current and voltage. For this purpose, each of the chromosomes generated in GA and includes the values for X_1, X_m, R_{fe}, and R_2, are used in the equivalent circuit. Then, the measured voltage is applied to each equivalent circuit and hence, the input power and current are estimated using the following formulas:

$$Z_2 = \frac{R_2}{s} + jX_2 \tag{2-41}$$

$$Y_m = \frac{1}{Z_2} + \frac{1}{R_{fe}} + \frac{1}{jX_m} \tag{2-42}$$

$$Z_t = R_1 + jX_1 + \frac{1}{Y_m} \tag{2-43}$$

$$I_{1,est} = \frac{V_{meas}}{Z_t} \tag{2-44}$$

$$P_{in,est} = real\left(3V_{meas}I_{1,est}^{*}\right) \tag{2-45}$$

where $I_{1,est}^{*}$ is the complex conjugate of the input current. Note that the stator and rotor resistances should be updated by the machine operating temperature. Moreover, the output power is used in the objective function which is estimated using the equivalent circuit as follows:

$$V_2 = V_{meas} - (R_1 + jX_1)I_{1,est} \tag{2-46}$$

$$I_2 = \frac{V_2}{Z_2} \tag{2-47}$$

$$P_{gap} = 3\frac{R_2}{s}I_2^2 \tag{2-48}$$

$$P_{out} = (1-s)P_{gap} - P_{SLL} - P_{FW} \tag{2-49}$$

The single-objective optimization is easier than multi-objective one and therefore the objective function of the proposed algorithm is defined as follows:

$$ff = \frac{1}{1 + \sum_{i=1}^{5} f_i} \tag{2-50}$$

where

$$f_1 = \frac{real(I_{1,meas}) - real(I_{1,est})}{real(I_{1,meas})} \tag{2-51}$$

$$f_2 = \frac{imag(I_{1,meas}) - imag(I_{1,est})}{imag(I_{1,meas})} \tag{2-52}$$

$$f_3 = \frac{P_{in,meas} - P_{in,est}}{P_{in,meas}} \tag{2-53}$$

$$f_4 = \frac{\varphi_{1,meas} - \varphi_{1,est}}{\varphi_{1,meas}} \tag{2-54}$$

$$f_5 = \frac{P_{2,meas} - P_{out}}{P_{2,meas}} \tag{2-55}$$

where φ_1 is the phase difference between the input current and voltage, while P_{out} is the rated output power. The indexes *meas* and *est* refer to the measured and estimated values, respectively.

In other words, the proposed algorithm tries to maximize *ff* rather than minimizing the five functions presented in (2-51) to (2-55).

Moreover, the parameters used to define the objective function may have the values with different order. For example, while the phase angle is in the range of 0 to $\pi/2$ rad, the current can be in the order of a few tens of amperes and power in order of thousands of watts. Therefore, to avoid the complicated determination of the weight of the functions as well as using the weighted sum, f_1 to f_5 are normalized by the measured values.

The algorithm is used to investigate three cases. In the first case, f_5 is included in the objective function without including the proposed parameter range determination. In the second case, f_5 is not considered in the objective function, however the parameter range determination method is applied. In the third case, f_5 is included in the objective function and the parameter range proposed method is also used.

2.7 Results

The proposed algorithm is applied to four different IMs: 3, 5, 7.5 and 250 hp. The specifications of the motors are listed in Table 2-7. To validate the estimated results, an experimental setup is prepared to run the efficiency estimation test based on IEEE Std-112 Method A which are used to determine the accuracy of other methods results. In this method, the output and input power are directly measured. For this purpose, a programmable power supply is connected to the IMs and a digital powermeter is employed to measure the input current, voltage and power at the input terminals of the IM. A 13 kW DC dynamometer is coupled to the IM with a resistor bank as the load. The dynamometer field control is used to control the load. A torque transducer, a multichannel signal conditioner, and a high resolution digital DC voltmeter are employed to measure the shaft torque. The high resolution digital DC voltmeter is used to display the DC analog output of the multichannel signal conditioner that corresponds to the value of the applied torque. The speed is also measured by using a tachometer. Furthermore, the no-load and locked-rotor tests are conducted (except for 250-hp IM) to determine the equivalent circuit parameters and efficiency using method F1 of the IEEE Std-112. Fig. 2-5 shows the experimental set-up for 3, 5 and 7.5 hp IMs. The 250 hp IM is tested at Hydro-Quebec laboratory.

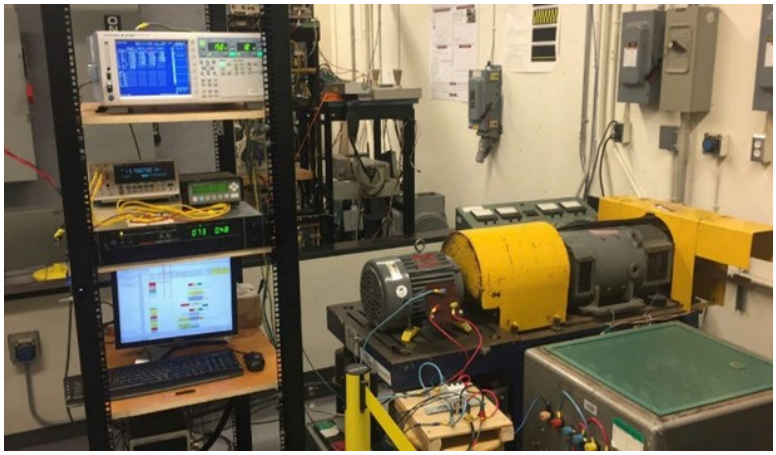

Fig. 2-5: Experimental set-up

Table 2-9 represents the measured efficiencies using methods A and F1 of the IEEE Std-112. Method A of IEEE Std-112 is the result of direct measurement of the output and input power, and method F1 is the result of applying the no-load and locked rotor tests and estimating the parameters of the machine and then using form F2 of IEEE Std-112 to estimate the efficiency.

Table 2-9: Measured efficiency from method A and F1 of IEEE Std-112.

hp	3		5		7.5		250	
Load (%)	A	F1	A	F1	A	F1	A	F1
100	81.79	81.35	88.94	89.32	91.15	91.47	95.01	-
75	81.76	80.79	90.46	89.82	92.21	92.13	95.02	-
50	80.67	79.045	91.33	90.20	92.45	92.40	94.52	-
25	69.1	68.40	88.35	86.84	90.46	90.264	90.96	-

The comparison between the results of method A and method F1 shows some differences. This is due to the intrinsic error of the equivalent circuit. These errors originated from several sources. Using the empirical results to determine the P_{SLL} and approximating the temperature of the machine at different loads are parts of the error sources. Another source is the way the core loss is estimated. By increasing the load, the core loss increases slightly. However, when the equivalent circuit is used, the core loss resistance is considered constant for all loads. The voltage drop across R_1 and X_1 is increased as the load increases. Therefore, the voltage across R_{fe} is decreased and the core loss is decreased. This is one of the main reasons that makes the estimated

efficiencies from the equivalent circuit at lower loads to be lower than the measured values by method A.

In the rest of the chapter, the measured efficiency values of method A are considered as reference values and other estimated values are compared to them. Table 2-10 shows the results of applying the proposed algorithm for each case described in previous section. Fig. 2-6 illustrates the maximum error for 10 runs of the proposed algorithm to prove its repeatability.

According to the results, using the output power in the objective function improves the accuracy especially for higher loads (case 1 and case 2). On the other hand, applying the parameter range determination method to the algorithm improves the accuracy of the results, especially at lower loads (case 3). By comparing case 1 and case 3, it can be seen that a significant improvement is achieved at lower loads due to applying the proposed method. Case 3 shows an accuracy with an error of less than 1%.

Table 2-10: Efficiency estimation results for the proposed algorithm.

hp	Load (%)	Cases						
		#1	Error	#2	Error	#3	Error	Meas.
3	100	81.91	0.12	81.61	-0.18	81.64	-0.15	81.79
	75	81.90	0.14	81.72	-0.04	81.72	-0.04	81.76
	50	81.70	1.03	79.23	-1.44	79.19	-1.48	80.67
	25	71.12	2.02	69.40	0.3	69.29	0.19	69.1
5	100	88.37	-0.57	88.68	-0.26	88.66	-0.28	88.94
	75	89.83	-0.63	91.17	0.71	90.23	-0.23	90.46
	50	90.11	-1.22	91.88	0.55	90.59	-0.74	91.33
	25	86.50	-1.85	89.30	0.95	87.59	-0.76	88.35
7.5	100	90.12	-1.03	91.13	-0.02	90.96	-0.19	91.15
	75	90.95	-1.26	92.58	0.37	92.08	-0.13	92.21
	50	90.74	-1.71	93.09	0.64	92.23	-0.22	92.45
	25	87.31	-3.15	91.46	1	90.28	-0.18	90.46
250	100	94.41	-0.6	95.42	0.41	94.94	-0.07	95.01
	75	94.29	-0.73	95.76	0.74	95.01	-0.01	95.02
	50	93.63	-0.89	95.62	1.1	94.61	0.09	94.52
	25	90.99	0.03	93.64	2.68	92.58	1.62	90.96

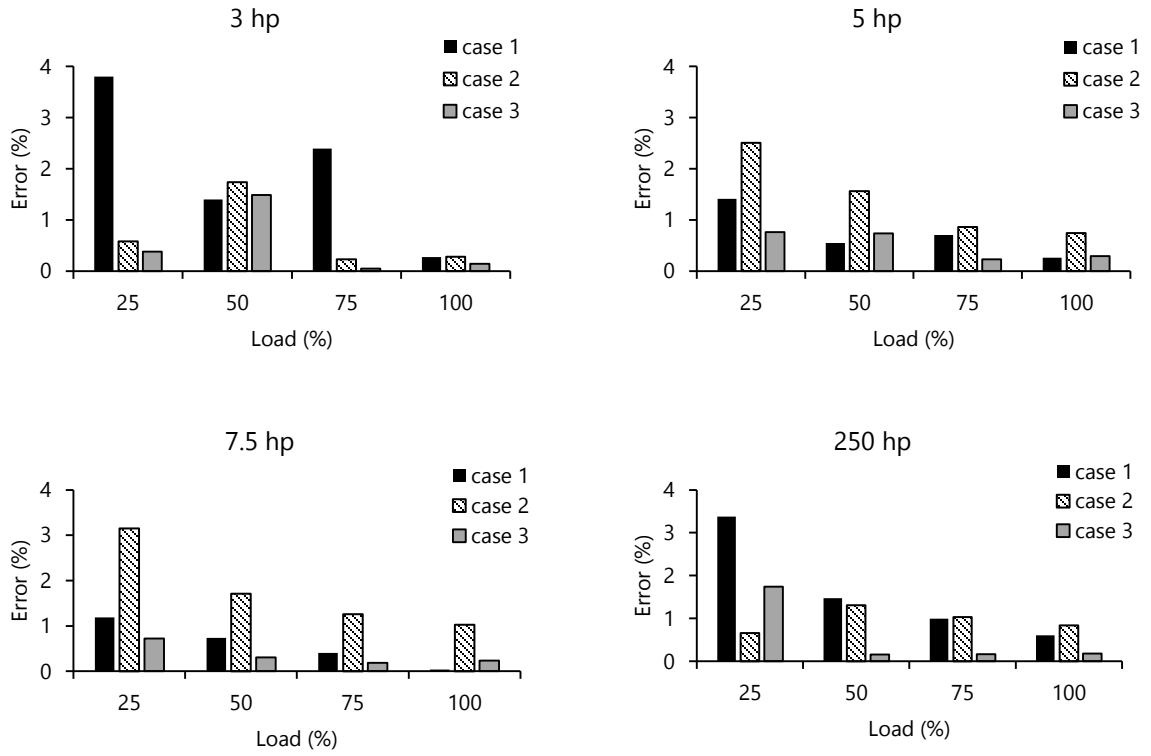

Fig. 2-6: Maximum error of the estimated efficiency for 10 runs.

In case 2, the results are still acceptable. This refers to an important point which is mentioned earlier and stated in [30] that the inclusion of the output power in the objective function is useful if the rated power is known. For in-situ applications, the output power is generally unknown, and also there is no criterion to prove that the machine is working at full load. As a result, despite case 2 is having a lower accuracy compared to case 1 and case 3, it is however more convenient for in-situ applications.

Fig. 2-7 shows the deviation of the estimated parameters for 10 runs for each case. It can be seen from Fig. 2-7 that applying the proposed method to determine the range results in less deviation in the parameters for case 2 and case 3 as compared to case 1. Incorporating the proposed method and the output power in the objective function can reduce the deviation of the parameters significantly (case 3) and maintain the deviation within 1% range.

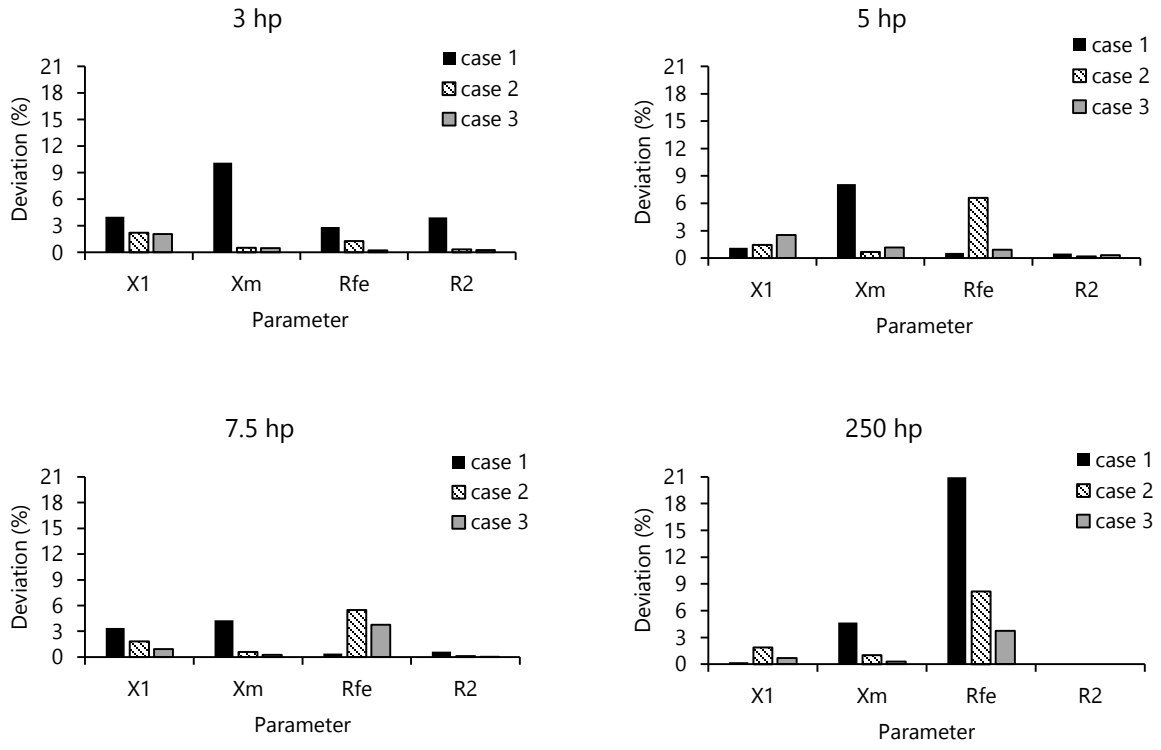

Fig. 2-7: Deviation of the estimated parameters for 10 runs for each case.

Table 2-11 shows the estimated parameters for the three cases and the values extracted from the no-load and locked rotor tests. The interesting part is the difference between case 1 and the other two cases. Cases 2 and 3 which benefit from the proposed range determination method have almost the same results which are close to those extracted by the no-load/locked rotor tests, however, in case 1, the results are quite different. This is one of the difficulties of using just one loading point for parameters and efficiency estimation. It can be seen from Table 2-11 that in case 1, despite the estimated efficiency is within an acceptable error range, the estimated parameters diverge from the data of the no-load/locked rotor tests. Therefore, there are many answers that can satisfy the objective function but only one solution is considered correct.

This comparison demonstrates the functionality of the proposed method which requires only one loading point data. This proves the importance of range determination of the parameters (case 2 and 3). Fig. 2-8 demonstrates the comparison of the estimated parameters for different cases with those extracted by the no-load/locked rotor tests.

Table 2-11: Parameter Estimation Results.

hp	case	Parameters			
		X_1	X_m	R_{fe}	R_2
3	#1	3.0384	183.6136	225.438	0.24443
	#2	0.99715	20.8312	264.85	0.36613
	#3	1.004843	20.8698	265.82	0.36563
	NL/LC	0.953	20.39	238	0.381
5	#1	5.5899	310.4266	3209.42	0.8159
	#2	2.4993	71.3283	2551.196	0.99315
	#3	2.4875	73.3245	3468.328	0.9899
	NL/LC	2.56	78.2	2017	1.09
7.5	#1	10.9751	343.734	8332.715	1.6835
	#2	5.8119	225.556	4855.465	1.8400
	#3	5.3069	219.888	7989.99	1.83438
	NL/LC	5.921	241.94	6452	1.936
250	#1	0.53947	142.9226	533.370	0.015646
	#2	0.23706	8.6120	183.5425	0.18775
	#3	0.21638	8.2343	293.1575	0.018775
	NL/LC	-	-	-	-

By referring to Fig. 2-6 it can be seen that case 1 and case 2 show large errors for the partial loads compared to the full load. One of the reasons is the values assumed for P_{FW} for each motor. P_{FW} is considered constant at all loads. Since all the motors tested here have four poles, based on (2-9), P_{FW} is assumed 1.2% of full load input power. For 25% load, this value becomes approximately 4.8% of the input power. So, if P_{FW} is overestimated, this adds an additional error at 25% loads. Table 2-12 shows the assumed and experimental values of P_{FW} for the motors. It can be seen that using the constant values of P_{FW} for the machines with the same number of poles can cause considerable error especially at low loads.

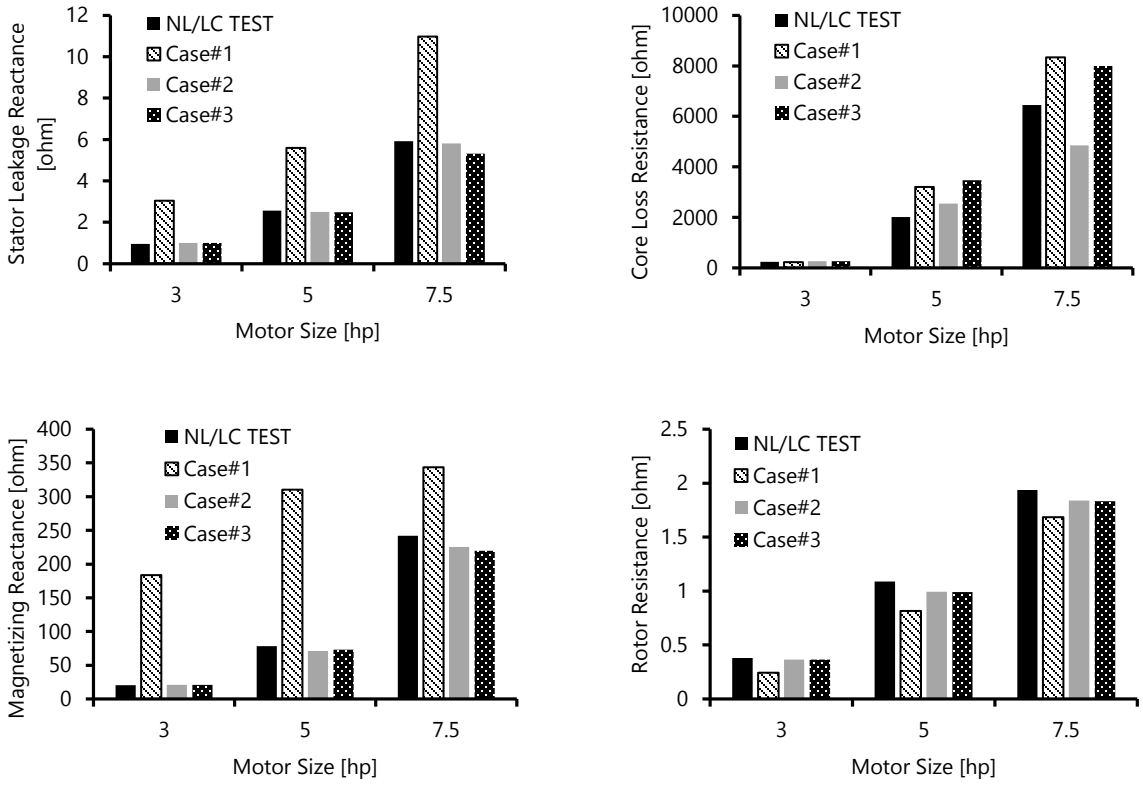

Fig. 2-8: Parameters for different cases compared with the no-load/locked rotor test values.

Table 2-12: Estimated and experimental value of P_{FW}.

hp	3	5	7.5	250
Assumed P_{FW} (W)	33.15	52.04	73.2	2353
Experimental P_{FW} (W)	30.055	34.25	15.24	1062

To show the effect of this error, the experimental values for P_{FW} are used in the proposed algorithm. Table 2-12 shows the measured values of P_{FW} and Table 2-13 shows the estimated values and corresponding errors. Table 2-13 shows a good accuracy for case 3 where errors are less than 0.5% for all loads. Case 2 provides better results for low loads compared to case 1. Also, case 3 shows higher accuracy which proves the effectiveness of the proposed method.

Table 2-13: Efficiency estimation results for the proposed algorithm with measured values of P_{FW}.

hp	Load (%)	Cases						
		#1	Error	#2	Error	#3	Error	Meas.
3	100	81.67	-0.12	81.64	-0.15	81.64	-0.15	81.79
	75	83.50	1.74	81.72	-0.04	81.72	-0.04	81.76
	50	80.69	0.02	79.20	-1.47	79.20	-1.47	80.67
	25	72.05	2.95	69.36	0.26	69.37	0.27	69.1
5	100	88.68	-0.26	88.49	-0.45	88.68	-0.26	88.94
	75	91.08	0.62	89.97	-0.49	90.23	-0.23	90.46
	50	91.69	0.36	90.18	-1.15	90.59	-0.74	91.33
	25	88.94	0.59	86.88	-1.47	87.63	-0.72	88.35
7.5	100	91.13	-0.02	90.48	-0.67	91.06	-0.09	91.15
	75	92.59	0.38	91.43	-0.78	92.23	0.02	92.21
	50	93.16	0.71	91.44	-1.01	92.47	0.02	92.45
	25	91.54	1.08	88.58	-1.88	89.90	-0.56	90.46
250	100	95.47	0.46	94.60	-0.41	95	-0.01	95.01
	75	95.78	0.76	94.54	-0.48	95.08	0.06	95.02
	50	95.61	1.09	93.98	-0.54	94.72	0.2	94.52
	25	93.61	2.65	89.28	-1.68	90.79	-0.17	90.96

2.7.1 Modified Equivalent Circuit

Since determination of P_{FW} and P_{SLL} by performing the tests described in IEEE Std-112 is intrusive, an alternative solution is to include these losses in the IM equivalent circuit. P_{FW} and core loss are constant at different loads and the P_{SLL} varies with load. For this purpose, the following strategy is pursued: R_{fe} is replaced with a resistance (R_{eq}) which represents the core loss and P_{FW}, and a resistance (R_{SLL}) is added to the rotor circuit to represent P_{SLL} as shown in Fig. 2-9.

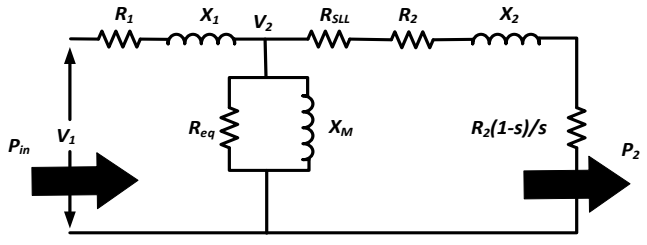

Fig. 2-9: Modified equivalent circuit of an IM.

This strategy increases the number of the unknowns to five: R_{SLL}, R_2, R_{eq}, X_1 and X_m. The flowchart shown in Fig. 2-4 can be used considering the new strategy and the results are shown in Table 2-14. The comparison between the errors in Table 2-14 with errors in Table 2-10 for case 3 shows that a slight improvement can be achieved by using the modified version of the equivalent circuit and five variables. In this case, the proposed parameter range determination method is applied and the output power term is used in the objective function. As shown in Table 2-10, the proposed algorithm with conventional equivalent circuit provides acceptable results when the output power is removed from the objective function (case 2) which makes the method more convenient for in-situ applications.

Table 2-14: Efficiency estimation results for modified equivalent circuit.

hp	Load (%)	Cases				
		#2	Error	#3	Error	Meas.
3	100	83.31	1.52	82.05	0.26	81.79
	75	83.52	1.76	82.11	0.35	81.76
	50	81.21	0.54	79.51	-1.16	80.67
	25	71.54	2.44	70.73	1.63	69.1
5	100	89.53	0.59	88.68	-0.26	88.94
	75	91.39	0.93	90.31	-0.15	90.46
	50	92.13	0.8	90.74	-0.59	91.33
	25	90.32	1.97	87.92	-0.43	88.35
7.5	100	90.47	-0.68	91.14	-0.01	91.15
	75	91.18	-1.03	91.79	-0.42	92.21
	50	90.57	-1.88	91.47	-0.98	92.45
	25	86.55	-3.91	88.11	-2.35	90.46
250	100	95.6	0.59	94.93	-0.08	95.01
	75	95.9	0.88	94.67	-0.35	95.02
	50	95.44	0.92	93.62	-0.9	94.52
	25	93.64	2.68	90.64	-0.32	90.96

As seen in Table 2-14 for case 2, removing the output power from the objective function can results in higher errors. By removing the output power from the objective function, the number of

the known equations is reduced while a new variable (R_{SLL}) is added to the algorithm. Therefore, adding a new variable requires the output power to converge to an acceptable result.

At the end, it can be concluded that modifying the equivalent circuit and defining new variables can improve the results if the output power is available. Otherwise, removing the output power from the objective function can increase error since a new variable is added.

2.8 Summary

In this chapter, the optimization-based efficiency estimation method was discussed and a literature review was presented. The main goal of the chapter is to estimate the parameters of the in-situ IM equivalent circuit by using the input data such as stator voltages and currents as well as input active power. It was shown that for efficiency estimation, there are nine unknowns which should be determined. Seven unknowns correspond to seven equivalent circuit parameters and two unknowns are related to the machine's losses (P_{FW} and P_{SLL}). Some techniques and assumptions were proposed to determine the five unknowns (R_1, X_2, s, P_{FW} and P_{SLL}). The remaining four parameters (X_1, X_m, R_{fe} and R_2) were determined using the proposed GA based efficiency estimation.

Constraints applied on GA variables are decided randomly, which require many iterations and adjustments to obtain reasonable results. In induction machine GA-based efficiency estimation applications, a prior determination of the range of IM parameters reduces the running time and enhances the accuracy of the results. In this chapter, a technique to determine the range of parameters was proposed. Based on the nameplate information and Hydro-Québec database, several useful relationships were generated to determine the range of the four variables (X_1, X_m, R_{fe} and R_2) which comprise one chromosome of the GA. Four different motors were used to investigate three different cases. The results showed that using the output power can give better accuracy, but it results in higher deviation in the estimated parameters. Applying the proposed range determination method without utilizing the output power in the objective function leads to better parameters estimation with the cost of less accuracy. This was useful for in-situ applications where the output power was generally unknown. Using the output power in the objective function plus the proposed range determination shows results with higher accuracy. Also, it was shown that when the friction and windage losses were accurately measured, the proposed technique accuracy could be improved. Furthermore, it was shown that modifying the equivalent circuit to include the

P_{FW} and P_{SLL} could slightly improve the results when the output power was available, otherwise for in-situ applications where the output power was not available it could cause higher error due to the increase in the number of variables.

Chapter 3: Particle Swarm Optimization (PSO) Based Efficiency Estimation Using Rapid Test Data

3.1 General

Temperature rise in an induction machine increases its losses and lowers the efficiency. The temperature rise depends on the machine design. It takes several hours after starting a machine, to reach thermal stability. In most of the in-situ efficiency estimation methods, it is required to obtain the data of the machine at a thermally stable condition which requires the machine to operate for a long time. In this chapter, a method based on Particle Swarm Optimization (PSO) is proposed to estimate the machine efficiency at different loads with thermal stability. The machine operation data at the first 30 minutes after start rather than data at thermal stability condition are used in the method. The proposed algorithm utilizes two approaches to predict the full-load winding temperature at a thermally stable condition. The first approach is based on the insulation class of the machine and uses the equivalent circuit. The second approach is based on the trend of the winding temperature rise in the first 30 minutes of running the machine after start. Furthermore, a method is proposed to narrow the parameters range which helps the PSO to converge to the right answer. All results are validated by the experimental results.

3.2 Introduction

In general, the input voltage, and input power at one or more operating conditions of the machine are used as input data for the most of the efficiency estimation methods, and in particular for the optimization based efficiency estimation method [54], [55]. At the same load power, variation of the machine temperature can change these input data [56]. Therefore, it is necessary for an IM to reach its thermal stability before recording operating data. Increasing the temperature decreases the rotor speed which is another required data point for predicting machine performance.

For efficiency estimation purpose, the temperatures of the stator windings and rotor bars are required. This is due to the dependency of their resistances on the temperature. Since the measurement of the rotor bar temperature is quite difficult for squirrel-cage rotor, therefore, it is

assumed that the rotor bar temperature is equal to the stator winding temperature. Moreover, the effect of the machine temperature does not significantly affect the losses other than the resistive losses, therefore only the stator winding temperature is important for efficiency estimation purpose. As a result, in this chapter, the temperature of the machine's stator windings is measured/estimated and referred as the machine's temperature.

Temperature measurement can be done either directly by using temperature sensors or indirectly by measuring the stator resistance [2]. The temperature affects the IM performance due to change in the stator and rotor resistances. Hence, before recording the operating data, it is necessary to wait until an IM reaches thermal stability. The machine temperature rise is a very complex phenomenon which depends on several factors related to machine design such as external shape, thermal conductivity of materials, cooling system, and the amount of the losses and so on [57], [58]. Developing a thermal model of a machine requires all detailed data of the machine or performing tests which are impossible for most of the in-situ applications. Therefore, predicting the temperature of a machine is difficult. Also after start, it may takes several hours for an IM to reach its thermal stability [59], [60]. The long time requirement for thermal stability is used in several places. In IEEE Std-112, page 21, section 5.8.4.2, it is mentioned that "On continuously-rated machines, when a long time is required to attain steady temperature, reasonable (25% to 50%) overloads during the preliminary heating period are permissible in order to shorten the time of test." This phrase clearly shows that it requires a long time to attain the steady temperature. Thus, even IEEE Std-112 has provided a solution to shorten this process. As a result, having the proper data for the optimization based methods requires a long time.

In this chapter, a PSO based algorithm is proposed to estimate the equivalent circuit parameters of the IM by using the full load operation data, which are obtained only 30 minutes after start. The proposed algorithm is applied to all the IMs working continuously with the rated load or close to the rated load without controlled electric drive. Moreover, the proposed method cannot be applied to applications such as electric blades or cranes which are not working continuously and also have severe transients during their operations. To estimate the efficiency of the IM by solving the equivalent circuit, two approaches are proposed to predict the full load temperature of the IM at the thermally stable condition. The first approach uses the insulation class of the IM and the estimated equivalent circuit parameters. The second approach uses the trend of

the temperature rise in the first 30 minutes after the machine start. The estimated temperature is used to predict the rotor speed and the efficiency of the IM. In addition to the two approaches for full load temperature prediction, two additional techniques are proposed to improve the results. First, before running the PSO, a technique is proposed to narrow the parameter range. This can help the PSO to search in a smaller search space and increase the possibility to converge to the right answer. The second technique is applied to improve the partial load efficiency results. For this purpose, a simple approximation is used to estimate the temperature at partial load which helps to estimate the partial load efficiency. Results are validated by experimental results showing the effectiveness of the proposed approaches and algorithm.

3.3 Thermal Behavior of Induction Machine

The non-idealities in design and materials result in losses during the operation of IMs. These losses convert to heat and increase the temperature of the IM [43]. The increased temperature affects the stator and rotor resistances of the IM, which increases the losses and consequently decreases the rotor speed and efficiency. This is because the machine draws more current and power from the source to compensate the losses at constant power load. The relationship between the resistance and the temperature is described by (3-1) [2] as follows:

$$R_{hot} = \frac{R_{cold}(T_{\text{hot}} + K)}{(T_{\text{cold}} + K)} \tag{3-1}$$

where R_{hot} and R_{cold} are the resistances corresponding to temperature T_{hot} and T_{cold}, respectively. K is 234.5 for 100% IACS conductivity copper, or 225 for aluminum, based on a volume conductivity of 62% [2]. This formula can be applied to both stator and rotor resistances with proper K.

Fig. 3-1 shows the output power of a 7.5 hp IM at different speeds and temperatures, which are estimated from the equivalent circuit. Specifications of a 7.5 hp IM are listed in Table 2-7. To achieve this curve, the equivalent circuit is solved at a certain temperature and the output power of the machine is then calculated at different speed values by using the equations described in section 2-6. By changing the temperature, different curves can be achieved. In the equivalent circuit given in Fig. 2-2, there is no limitation on the output power. Thus, by changing the speed and temperature, it is possible to achieve any output power. However it does not mean that this can happen in the actual performance of the machine. Therefore, different power-speed curves can

be achieved at different temperatures. This is due to the increase of the losses of the machine. It means that by increasing the machine's temperature, the efficiency of the machine decreases as shown in Fig. 3-2.

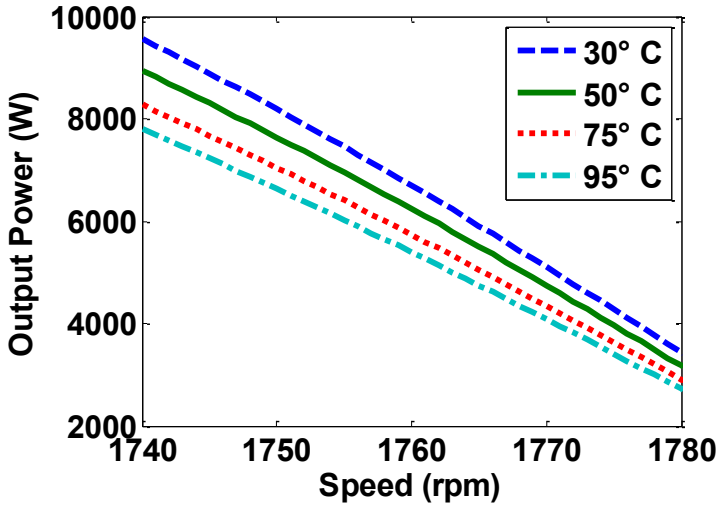

Fig. 3-1: Output power of a 7.5-hp IM vs rotor speed at different temperature.

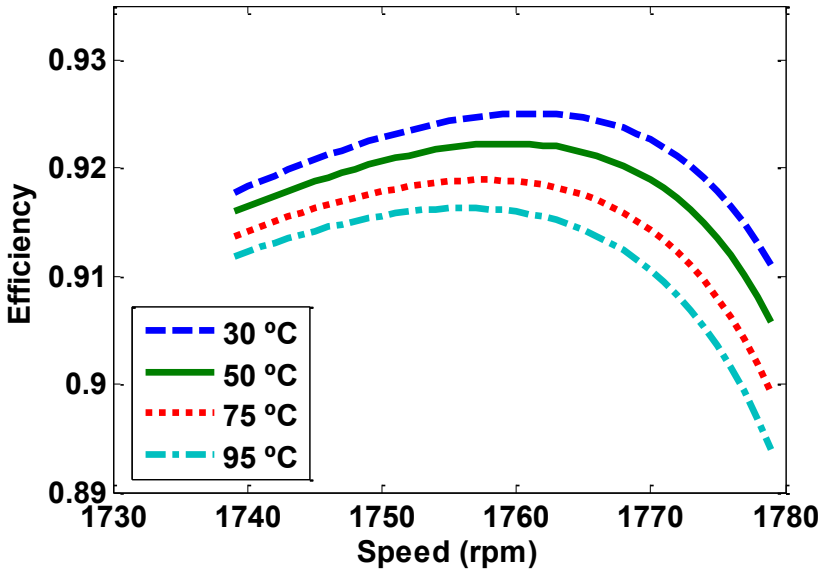

Fig. 3-2: Efficiency of a 7.5-hp IM vs rotor speed at different temperature.

When an IM is started at a certain load, by assuming that it has not been used for an acceptable time, its temperature would be equal to the ambient temperature. After starting, the machine temperature increases gradually until it reaches to a certain point where the heat generated

by the machine losses and the heat removed by the cooling system is equal. This condition is a thermal equilibrium which is also called the point of thermal stability of the machine [57], [58]. In other words, the thermally stable condition refers to a condition that at a constant load and ambient temperature, the temperature of the machine does not vary significantly in time. Fig. 3-3 shows the temperature rise of the 7.5-hp IM during first 60 min after start.

In Fig. 3-3, the temperature rise of the machine is shown regardless of the ambient temperature. It means that machine temperature is the temperature rise of the machine plus the ambient temperature.

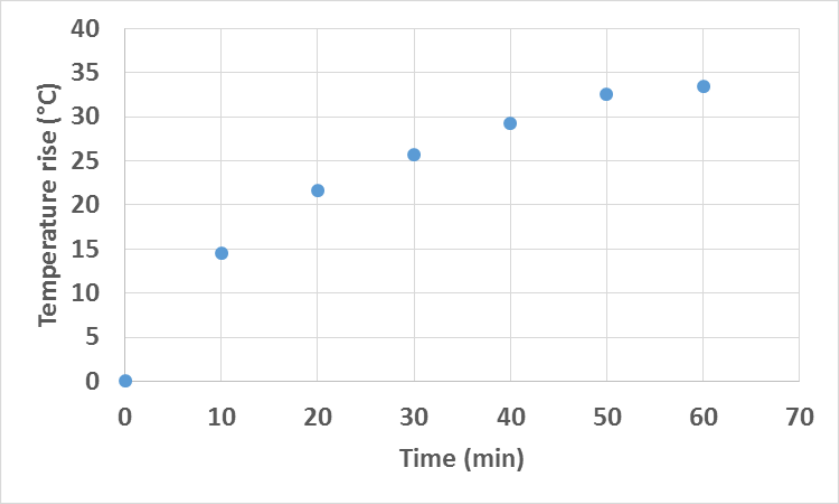

Fig. 3-3: 7.5-hp IM temperature rise at full load.

During the temperature rise of the machine after the start, efficiency decreases as shown in Fig. 3-4. Increasing the temperature of the machine due to the losses increases the stator winding and rotor bar resistances, therefore to maintain the load, the machine draws more power from the source which means the efficiency will decrease. Fig. 3-4 shows that reaching thermal stability is necessary for efficiency estimation which requires several hours running of the machine.

In the next section, two approaches are proposed to predict the full load temperature at a thermally stable condition. These approaches help to avoid the long running time of the machine to achieve the full load temperature at a thermally stable condition. The first approach which is uses the equivalent circuit is based on the insulation class of the machine. The second one is based on the temperature rise of the machine during the first 30 minutes running the machine.

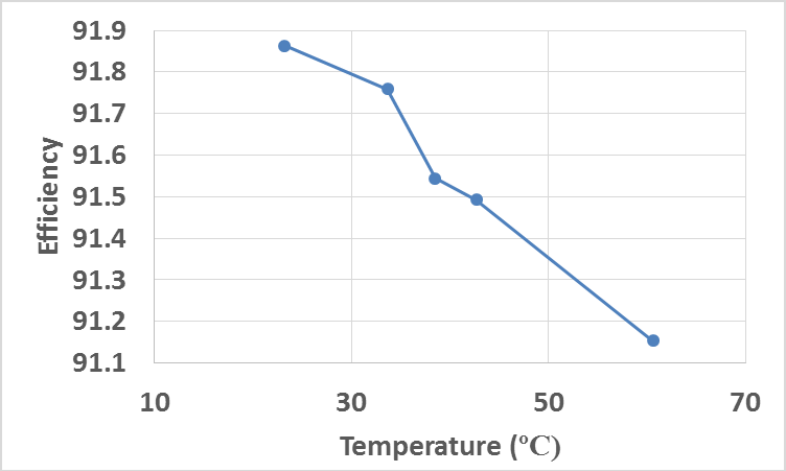

Fig. 3-4: Experimental efficiency variation at different temperatures during temperature rise for 7.5-hp at full load..

3.4 The proposed Approaches to Estimate Temperature at Full Load

In this section two approaches are proposed to predict full-load temperature of the IM at the thermally stable condition.

3.4.1 Approach 1

One way to analyze and predict the performance of an IM is to use the equivalent circuit (Fig. 2-2). The main advantage of using the equivalent circuit method is the capability to predict the performance of the machine at different loads and operating conditions. However, the variation of R_1, R_2 and s with the load and temperature are the main issues of this method. Hence, for the given output power (load), it is necessary to determine both the temperature (for correcting R_1 and R_2) and speed (to calculate s).

Also, for a certain load, it can be seen in Fig. 3-5 that by changing the temperature, the speed changes. Fig. 3-5 (dotted orange line) is extracted by solving the equivalent circuit at a constant load. For this purpose, the output power of the machine is considered equal to full load. Then by applying different temperatures to the equivalent circuit (to correct R_1 and R_2), the speed is calculated by solving the equivalent circuit. This figure is similar to Fig. 3-5 (solid blue line) which has been extracted experimentally. When an IM is started at full load, its temperature is equal to the ambient temperature and the rotor speed at this condition is higher than the final full load speed

and motor draws less power form the source. By heating up the machine due to losses, the rotor speed decreases and drawn power from the source increases.

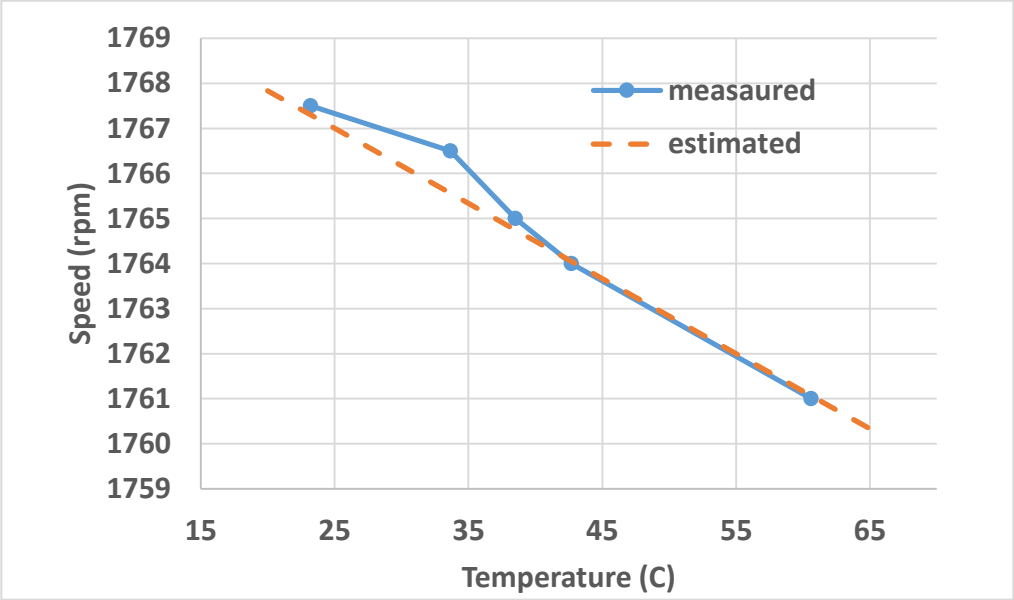

Fig. 3-5: Rotor speed at different temperatures during temperature rise after start for a 7.5 hp IM at full-load extracted from equivalent circuit and experiment.

This is also proved by the experimental results in [56]. Therefore, the effects of the speed and temperature on the output power are obvious due to the relationships between the electromagnetic power, R_2 and s.

Predicting the operating temperature of the machine needs to have some information about the machine structure, materials, cooling system and so on. Here, an approach is presented which uses the nameplate data to estimate the IM's temperature and speed at full load and also at a thermally stable condition. The method is described as follows:

Assuming that $R_{1,cold}$, $R_{2,cold}$, X_1, X_2, X_M and R_{fe} are known which in this case are obtained from PSO based algorithm described in the following sections. P_{FW} and P_{SLL} values are determined using empirical data. The maximum temperature rise of the machine is determined based on the insulation class (Table 3-1) using the following formula:

$$\Delta T_m = Maximum\ allowed\ temperature - 25 \tag{3-2}$$

where ΔT_m is the maximum allowed temperature rise by considering the 25 °C ambient temperature. Now, the full load hot temperature is calculated as follows:

$$T_f = \Delta T_m + T_{amb} \tag{3-3}$$

where T_{amb} is the ambient temperature. If T_{amb} is greater than 25 °C, then T_f would be considered as the value presented in Table 3-1. Then R_1 and R_2 are corrected to the new values corresponding to T_f by using (3-1). For the speed interval between $N_{rated} - 20$ and $N_{rated} + 20$, the output power of the machine is calculated using the estimated equivalent circuit parameters. N_{rated} is the rated speed of the machine and is obtained from the nameplate data. Since there is no limitation on the output power in the equivalent circuit, it is possible to achieve the curve around the rated power and also beyond the rated power by changing the speed.

Table 3-1: Maximum allowed temperature of the machines [2].

Class of insulation system	T_{fl} (°C) including 25 °C reference ambient
A	75
B	95
F	115
H	130

The load power of the machine is assumed to be the rated power and intersection of the load line with output power of the machine at T_f is determined as shown in Fig. 3-6. The speed value at this point is rounded to the higher integer.

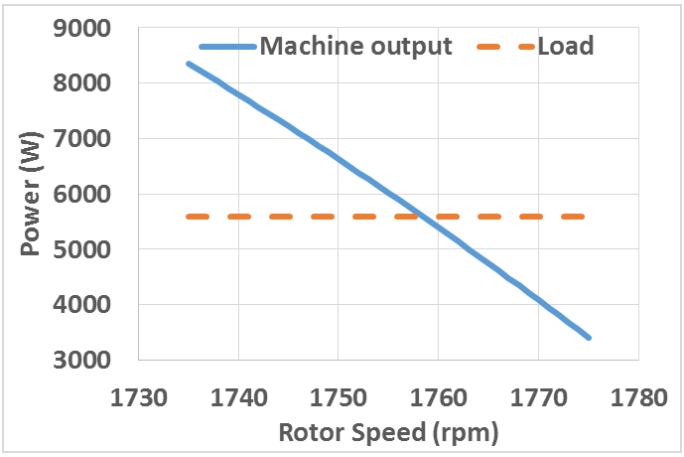

Fig. 3-6: IM output power curve at T_f and load power intersection.

An iterative approach is used to calculate the full load temperature which is described as follows:

1) Assume the speed is equal to the value from previous calculations.
2) Assume the temperature is equal to the ambient temperature
3) Calculate the output power using the equivalent circuit.
4) Compare the calculated output power with the rated power of machine.
5) If the difference between the calculated and the rated power is not less than 1%, increase the temperature by 0.5 °C and go to step 3.
6) If the difference between the calculated and the rated power is less than 1%, compare the calculated input current with the rated current.
7) If the calculated input current exceeds the rated current, increase the speed by 1 rpm and go to step 2.

The estimated speed and temperature can be used to evaluate the machine's performance at full load. The proposed method is used to estimate the efficiency of the machine at partial- and full-loads. This method is described in the next sections.

3.4.2 Approach 2

According to Fig. 3-3, the machine temperature rise (ΔT) curve can be approximated as an exponential curve which reaches its final value after five thermal time-constants (τ). This curve can be formulated as follow:

$$\Delta T = \Delta T_f (1 - \exp(-{}^{t}/_{\tau})) \tag{3-4}$$

where t and τ are expressed in minutes, ΔT_f is the temperature rise at the thermally stable condition. It is possible to estimate ΔT_f and τ by using the temperature of the machine at some points. More data points would result in better and more accurate fitted curve. The objective of this chapter is to estimate the efficiency of the IM using a rapid test data.

For this purpose, the IM is run at full load. The ambient temperature is considered as the starting temperature of the machine. The machine is run for 30 minutes and the temperature of the machine is recorded every 10 minutes. This can be done either by using temperature sensors or by measuring the stator resistance. In this chapter, indirect measurement of winding temperature using

stator resistance measurement based on IEEE Std-112 section 5.8.4.3 is used. For efficiency estimation purposes, the effect of the machine temperature on the winding resistances is the main concern. Therefore, the temperature distribution and hot spots are not necessary for this work.

In an IM, there are four types of losses. The effect of the temperature on the core loss, friction and windage losses and stray load loss is negligible. However, the temperature mainly affects the stator and rotor Joule losses. In terms of the equivalent circuit parameters, the temperature affects the stator winding and rotor bar resistances. Therefore, the resistance variation is of more concern. As a result, measuring the resistance at the operating condition is more desirable than the temperature. This also avoids all the issues related to placing the sensors, thermal distribution of the machine, and hot spots. In other words, the total resistance's change due to temperature variation can be achieved by the indirect method.

Considering the ambient temperature as a starting temperature, there would be four recorded temperatures corresponding to times 0, 10, 20 and 30 minutes. Before using the recorded data, the machine temperature should be transformed into the machine temperature rise. The recorded data is then subtracted from the ambient temperature. Therefore, the starting temperature rise will be zero.

Defining a range for the variables (ΔT_f and τ) helps to get better results of curve fitting. The maximum value for ΔT_f can be determined using Table 3-1 and equation (3-2). The recorded temperature rise for t = 30 min can be considered as the minimum value for ΔT_f. The minimum and maximum values for τ are considered equal to 10 and 95 minutes.

3.5 Range Determination for Induction Machine Parameters

In the previous chapter, it is proven that defining a small range for parameters can definitely improve the estimated efficiency and parameters by confining the optimization algorithm to search in a smaller space. The presented approach is based on the nameplate data and empirical results.

Despite the ability of the proposed approach to confine the range for X_1 and R_2, the determined range for the R_{fe} and X_m seems to be large. Another approach is introduced which can confine the parameter range even further than the previous approach. Narrowing the range may not improve the accuracy of the estimated efficiency results, but it definitely improves the convergence of the evolutionary algorithm and avoids possible divergence.

The approach relies on the available data of the machine at a certain load. Since, one loading point data is going to be used to determine the parameters, the same data can be used for the parameter range. According to the equivalent circuit shown in Fig. 2-2, V_2 can be calculated as:

$$V_2 = \sqrt{(V_1 - R_1 I_1 cos\varphi + X_1 I_1 sin\varphi)^2 + (-R_1 I_1 sin\varphi - X_1 I_1 cos\varphi)^2} \tag{3-5}$$

where, phase angle φ is:

$$\varphi = -cos^{-1}\left(\frac{P_{in}}{3V_1 I_1}\right) \tag{3-6}$$

Also, V_2 can be written in terms of the rotor parameters as follows:

$$V_2 = I_2 \times \sqrt{(R_2/s)^2 + X_2^2} \tag{3-7}$$

where, I_2 is the rotor current.

By determining the ratio $a = X_1/X_2$ which is based on the NEMA design of the machine, X_2 can be replaced by X_1/a [22]. I_2 also can be written in terms of P_{out} as

$$I_2 = \sqrt{\frac{sP_{mec}}{3(1-s)R_2}} \tag{3-8}$$

$$P_{mec} = P_{out} + P_{FW} + P_{SLL} \tag{3-9}$$

By using (3-7) through (3-9), the following equation can be derived:

$$\begin{aligned}(V_1 - R_1 I_1 cos\varphi + X_1 I_1 sin\varphi)^2 + (-R_1 I_1 sin\varphi - X_1 I_1 cos\varphi)^2 \\ = \frac{sP_{mec}}{3(1-s)R_2}\left[\left(\frac{R_2}{s}\right)^2 + \left(\frac{X_1}{a}\right)^2\right]\end{aligned} \tag{3-10}$$

Given the available full load data and R_1 from the DC test, X_1 and R_2 are the unknowns in (3-10). Having one of those two parameters determined, the other one can be calculated by solving a quadratic equation. As this is a real system, there would be two answers, only one of them is true.

In [61], a method based on the nameplate data is presented to determine the X_1 range. This method uses the NEMA design class of the machine to determine the maximum torque (T_{max}) of the machine and then determine the maximum value of X_1 using

$$T_{max} = \frac{3V_1^2}{2\omega_s \left[R_1 + \sqrt{R_1^2 + (X_1 + X_2)^2}\right]} \tag{3-11}$$

In (3-11), V_1 and ω_s are determined using the nameplate data. T_{max} and the ratio of X_1/X_2 are obtained based on NEMA design [22], R_1 is measured using the DC test. At the end, X_1 can be determined using (3-11). Since T_{max} is the minimum required value based on [22], the calculated X_1 value is at its maximum value. A minimum value of X_1 can be considered as half of the maximum value [61].

Given the minimum and maximum values of X_1, the minimum and maximum values of R_2 can be estimated using (3-10). Note that, using the minimum value of X_1 results in the maximum values of R_2 and vice versa.

In the next step, with the given X_1 and R_2, it is possible to determine R_{fe} and X_m. R_{fe} is obtained using

$$R_{fe} = \frac{3V_2^2}{P_{in} - P_{RCL} - P_{SCL} - P_{mec}} \tag{3-12}$$

The stator and rotor copper losses (P_{SCL} and P_{RCL}) are:

$$P_{RCL} = 3R_2 I_2^2 \tag{3-13}$$

$$P_{SCL} = 3R_1 I_1^2 \tag{3-14}$$

V_2 and I_2 can be calculated using (3-7) and (3-8), respectively.

Also, by writing the reactive power flow equation in the machine, X_m can be estimated as

$$X_m = \frac{V_2^2}{(Q_{in}/3) - X_1 I_1^2 - X_2 I_2^2} \tag{3-15}$$

where

$$Q_{in} = |P_{in} \tan \varphi| \tag{3-16}$$

In order to use (3-16), Q_{in} must be positive. Given the minimum and maximum values of X_1, the minimum and maximum values of R_2, R_{fe} and X_m can be determined. Using the minimum value of X_1 results in the maximum values of R_2 and R_{fe}, as well as the minimum value of X_m and vice versa.

Applying the proposed technique limits the parameters to the ranges shown in Table 3-2. The results show that the new proposed technique narrows the parameter range more than the method described in previous chapter and [61]. By a simple review of the values presented in Table 3-2, it is clear that choosing a fixed range of variables for different motors is unreasonable.

Table 3-2: Estimated IM's Parameters range using method described in the previous chapter and the new proposed method.

hp	3		5		7.5	
Method	Pre.	New	Pre.	New	Pre.	New
$X_{1,min}$	0.6201	0.6201	1.4425	1.4425	5.04	5.04
$X_{1,max}$	1.2402	1.2402	2.885	2.885	10.08	10.08
$X_{m,min}$	14.695	18.98	29.6	60.22	113.4	216.62
$X_{m,max}$	168.48	21.58	1787.7	85.15	5721.9	316.81
$R_{fe,min}$	227.49	219.73	516.1	1942.8	1651.8	6784.9
$R_{fe,max}$	291.825	257.81	3096.4	2275.8	9910.7	7107.5
$R_{2,min}$	0.2421	0.3634	0.5935	0.9708	1.8451	1.716
$R_{2,max}$	0.5901	0.3947	1.4466	1.0397	4.4974	2.041

Moreover, according to those values, the effectiveness of the proposed technique is proved. This technique helps narrow the range significantly. Especially, in the case of R_2 which has important effects on the machine performance and output power calculation. The variation of the maximum and minimum values of R_2 around the average value is about 9%. The maximum variation for R_{fe} is around 8% of the of the min and max average values.

3.6 Particle swarm optimization

Particle swarm optimization (PSO) is an evolutionary technique which works based on the behavior of the population. The main idea of the technique was introduced by R. C. Eberhart and J. Kennedy in 1995 [62]. The technique is inspired by a group of fish or birds looking for food. In

a group of birds or fish which do not know where the food is, it is better to use other group members' experience to get to the food as fast as possible.

Unlike other optimization methods, PSO implementation in a computer is simple and needs a small program [63, 64]. The PSO algorithm has a continuous nature and has shown its effectiveness in various applications. In PSO, each solution of the problem is like a bird in a group and is called a particle. The particles are evaluated by an objective function. Particles with high scores from the objective function, are more qualified to be a correct answer to the problem. PSO starts by generating a number of random answers (N, which are called particles) and continues by updating the position of particles looking for the correct answer. Each particle is defined by two vectors; a position vector (X_i) and a velocity vector (V_i). The length of the vector is defined by the number of variables (unknowns) in the problem. Considering each variable as a dimension of the problem, each particle has a position (X_{id}) and a corresponding velocity (V_{id}) in that dimension.

At every step, the position and the velocity of the particle is updated by using its own best experience (*Pbest*) and best experience of all the particles (*Gbest*) which are determined by the objective function. *Pbest* and *Gbest* are called particle best, and global best, respectively. Sometimes, updating is done by local best (*Lbest*). In this version of PSO, particles have information only of their own and their nearest array neighbors' bests (*Lbests*), rather than that of the entire group [63]. In this chapter, the local best model is used. This model has better exploration abilities and its susceptibility to being trapped in local minima is diminished and does not suffer from premature convergence as is the case with the global best [65]. Updating the position is done by [63]:

$$X_{id}(t+1) = X_{id}(t) + V_{id}(t+1) \qquad i = 1, 2, \dots, N \qquad d = 1, 2, \dots, D \tag{3-17}$$

where D is the number of dimensions and $X_{id}(t+1)$ and $V_{id}(t+1)$ are the new position and velocity of the particle in dimension d respectively. $V_{id}(t+1)$ is [63]:

$$V_{id}(t+1) = w \times V_{id}(t) + c_1 \times r_1(Pbest_{id}(t) - X_{id}(t)) + c_2 \times r_2(Lbest_{id}(t) - X_{id}(t)) \tag{3-18}$$

where w is the inertia coefficient and is [0,1]. c_1 and c_2 are accelerating coefficients and are [0, 2]. r_1 and r_2 are random numbers between 0 and 1. To avoid divergence of the algorithm, the velocity of the particles are limited by $-V_{max}$ and V_{max}. V_{max} is considered as 10% of $X_{id,max} - X_{id,min}$.

Choosing a large value for *w* causes the algorithm to search for new areas far from the current position to find the answer. This is good at the start of the (the first iteration of) program which helps to search the whole area. Choosing a small value for *w* forces the algorithm to look for the right answer near to the current position. This is good for the final iterations of the program when the solution is converging to a position which is most likely the right answer. To benefit from both cases, *w* is usually defined as a variable in terms of the number of iterations as follows [63]:

$$w = w_{max} - \frac{w_{max} - w_{min}}{iter_{max}} \times iter \tag{3-19}$$

where w_{max} and w_{min} are the initial and final values of *w* and *iter* is the number of current iteration and $iter_{max}$ is the maximum selected number of iterations for the PSO. The result of the study on the parameter selection shows that the following parameters are appropriate for PSO and are not affected by the problems [66, 67]: w_{max} = 0.9, w_{min} = 0.4, c_1 , c_2 = 2.0 . The values have been applied to power system problems and their appropriateness have been proved [68, 69]. The general flowchart of PSO shown in Fig. 3-7 can be described as follows:

Step 1: Generate initial positions and velocities for particles randomly within the allowable range. The current position of a particle is considered as *Pbest* for that particle. *Lbest* is determined after evaluation of the particles by an objective function.

Step 2: Modify the position and the velocity using (3-17)-(3-19).

Step 3: Evaluate the particles by the objective function. If the evaluated value is better than the current *Pbest* of the particle, the current *Pbest* value is replaced by the evaluated value. The best value among the *Pbest*s of three neighbored particles are compared to *Lbest* and if it is better than *Lbest*, *Lbest* is replaced by the position of the best *Pbest*.

Step 4: check the stop criteria. The current iteration number is $iter_{max}$ then, the iteration is finished and *Gbest* (best experienced among all particles) considered as an answer to the problem. Otherwise go to the step 2.

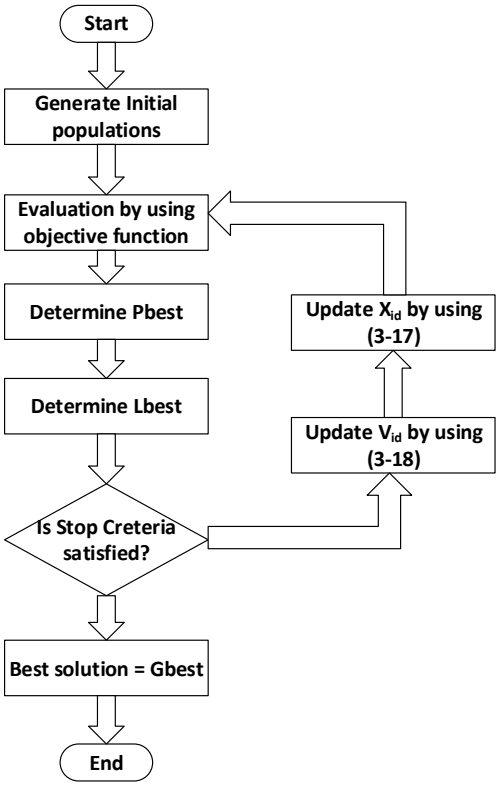

Fig. 3-7: PSO flowchart.

3.7 Proposed PSO based Efficiency Estimation Algorithm

An optimization based algorithm is proposed to estimate the equivalent circuit parameters and to determine the efficiency of the IM at different load conditions. The proposed algorithm of efficiency estimation employs PSO to estimate the parameters and efficiency of the IM. The proposed algorithm helps to avoid the no-load and locked rotor tests.

The proposed algorithm is applied to all IMs working continuously at rated load or close to the rated load without a controlled electric drive. The proposed method cannot be applied to applications such as electric blade and cranes which are not working continuously and have severe transients during their operations. The machines can be connected to the load either by direct or belt coupling.

To estimate the efficiency of an IM using the equivalent circuit, parameters of equivalent circuit and temperature should be known. Two methods described in section 3.3 were proposed to determine the full load temperature. In the equivalent circuit, there are 9 unknown parameters: R_1,

X_1, R_{fe}, X_m, R_2, X_2, s, P_{FW} and P_{SLL}. The parameters, R_1 and s are measured directly and non-intrusively. P_{FW} and P_{SLL} are determined by empirical results, and X_2 is determined by the ratio X_1/X_2 from the NEMA design of the machine. The remaining four parameters (X_1, R_{fe}, X_m and R_2) are determined using PSO by utilizing the full load data of the machine in the first 30 minutes after the start. In order to force PSO to converge to the right answer, the range of these four parameters should be narrowed as much as possible. The proposed approach in section 3.4 is applied to narrow the range of parameters and consequently search space for PSO.

The flowchart of the proposed algorithm is shown in Fig. 3-8. The machine cold temperature (T_{cold}) and the corresponding stator resistance ($R_{1,cold}$) should be predetermined before starting the algorithm. These data in addition to nameplate data are used as a part of inputs for the algorithm. These data are also used to determine the parameter range for PSOs in the future steps according to the method described in section 3.4. In addition, X_1/X_2 ratio is determined based on the machine design class which helps to decrease the number of unknowns [22].

To obtain all the required input data for the proposed algorithm, the stator voltage, stator current, input active power, machine temperature ($T_{30,min}$) and rotor speed ($N_{r30,min}$) at full load, 30 minutes after start of the machine must be recorded and entered to the algorithm.

Having all required input data, the first PSO is run 30 times with 4 variables (X_1, X_m, R_{fe}, R_2). The best solutions which satisfy the following objective function at the full load are selected for future steps.

$$ff = \frac{1}{1 + \sum_{i=1}^{5} f_i} \tag{3-20}$$

where

$$f_1 = \frac{real\left(I_{1,meas}\right) - real\left(I_{1,est}\right)}{real\left(I_{1,meas}\right)} \tag{3-21}$$

$$f_2 = \frac{imag\left(I_{1,meas}\right) - imag\left(I_{1,est}\right)}{imag\left(I_{1,meas}\right)} \tag{3-22}$$

$$f_3 = \frac{P_{in,meas} - P_{in,est}}{P_{in,meas}} \tag{3-23}$$

$$f_4 = \frac{\theta_{1,meas} - \theta_{1,est}}{\theta_{1,meas}} \tag{3-24}$$

$$f_5 = \frac{P_2 - P_{out,est}}{P_2} \tag{3-25}$$

θ_1 is the phase difference between the input current (I_1) and voltage, P_2 is the rated power and P_{out} is the output power. Indexes *meas* and *est* refer to the measured and estimated values, respectively. This objective function is the same as the one used in previous the chapter.

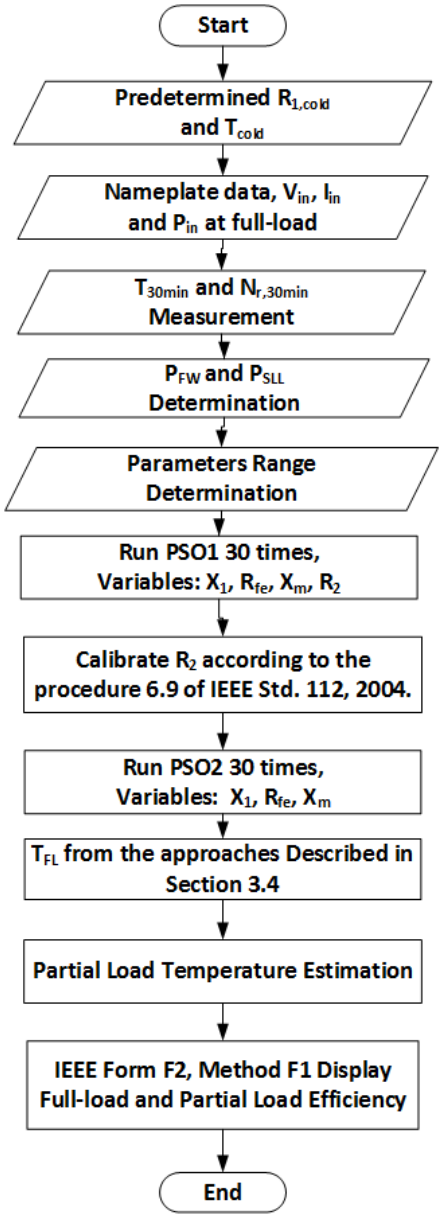

Fig. 3-8: The proposed algorithm flowchart.

The selected solution is used in the next step to calibrate R_2 based on the procedure described in section 6.9 of IEEE Std-112 [2]. After the calibration of R_2, the second PSO is run 30 times with 3 variables (X_1, X_m, R_{fe}) and the best solution is chosen for the next step. Using the estimated parameters and previous data of $R_{1,cold}$, T_{cold}, $T_{30,min}$, $N_{r30,min}$ as well as X_1/X_2, it is possible to estimate the efficiency at full load after 30 minutes running. However, for estimating the efficiency at full load with thermal stability, more information is necessary.

At this point, the approaches described in section 3.3 are employed to determine the speed and temperature of the machine at full load with thermal stability. At the final step, all these data are applied to estimate efficiency at the partial and full load using form F2, method F1 of IEEE Std-112 [2]. The variation of the inductances due to saturation occurs with severe transients such as starting the machine where the machine draws currents more than the rated current. Therefore inductances do not change significantly at different loads and IEEE Std-112 considers all the inductances constant at all loads. Furthermore, additional core loss due to loading is considered as a part of P_{SLL}, therefore core loss resistance is considered constant at all the loads based on IEEE Std-112. For efficiency estimation purpose, the stator and rotor resistances are variable parameters by load due to machine temperature variation by load.

IEEE Std-112 does not explain the method to estimate the temperature for partial loads. To consider the effect of the load on the temperature and to estimate the partial load efficiency, a simple and straightforward approximation is used here. Since the source of the heating of machine is the losses, a direct relationship between the temperature and losses is assumed as follows:

$$\frac{T_{FL}}{T_{NL}} = \frac{P_{Loss,FL}}{P_{Loss,NL}} \tag{3-26}$$

where T_{NL} and T_{FL} are the no-load and full-load temperatures, respectively, $P_{Loss,NL}$ and $P_{Loss,FL}$ are the machine total losses at no-load and full-load conditions. T_{FL} is determined using approaches described in section 3.3. $P_{Loss,FL}$ is estimated using T_{FL} and corresponding rotor speed. To calculate $P_{Loss,NL}$, it is assumed that the temperature is equal to T_{cold} or $T_{ambient}$ and the rotor speed is equal to $N_s - 1$. At no-load, P_{SLL} is neglected. Now T_{NL} can be estimated using (3-26). The temperature at each load is estimated using (3-27).

$$T(x) = \frac{(T_{FL} - T_{NL})}{100} x + T_{NL} \tag{3-27}$$

where x is the load percentage and $T(x)$ is the corresponding temperature. Although (3-26) and (3-27) only provide an approximation, the obtained temperature is more acceptable than considering T_{FL} at all loads.

The last points about the algorithm are about P_{FW} and P_{SLL}. These losses were discussed in the previous chapter and the same methods are used here to determine them. In [70], it is claimed that P_{SLL} is mainly due to the harmonics generated by the winding, slots and airgap. It tends to increase the core loss and high frequency loss in the rotor bars at loaded condition compared to no-load condition. Additional losses due to the skin effect and eddy current in the rotor bars are considered in P_{SLL} which considered as a function of the square of rotor current as mentioned in IEEE Std-112 [2].

3.8 Results

The proposed algorithm and approaches are applied to the motors listed in Table 2-7. Based on [47], more than 75% of the IMs in industry are 4-pole machines, therefore, the proposed method can be applied to a large number of the IMs. Furthermore, the thermal behavior of an IM depends on the machine structure, thermal properties of the materials and cooling system. However, it does not depend on number of poles. The number of poles affects the speed of the cooling fan mounted on the shaft. It can change the effectivity of the cooling fan which has been considered during the machine design. Therefore, the proposed method can be applied to the IMs with different poles.

To validate the estimated results, the experimental setup is prepared to run the rapid test and standard efficiency estimation tests. Both tests have been performed in the laboratory. The laboratory temperature is maintained between 21 and 24 ºC by the central air conditioning system and the pressure is around 101.5 kPa. This means that the air density is around 0.1179 kg/m^3. A programmable power supply is connected to the IMs. A high precision digital power meter is used to measure the input current, voltage and power at the input terminals of the IM. A 13 kW dynamometer is directly coupled to the IM by S-flex coupling and with a resistor bank as the load. Field control is used to control the output load of the dynamometer. Load power is constant during the test and is equal to full load. A torque transducer, a multichannel signal conditioner, and a high resolution digital dc voltmeter are employed to measure the shaft torque. The high resolution

digital dc voltmeter is used to display the dc analog output of the multichannel signal conditioner that corresponds to the value of the applied torque. The speed is also measured by using a tachometer. Fig. 3-9 shows the described experimental setup.

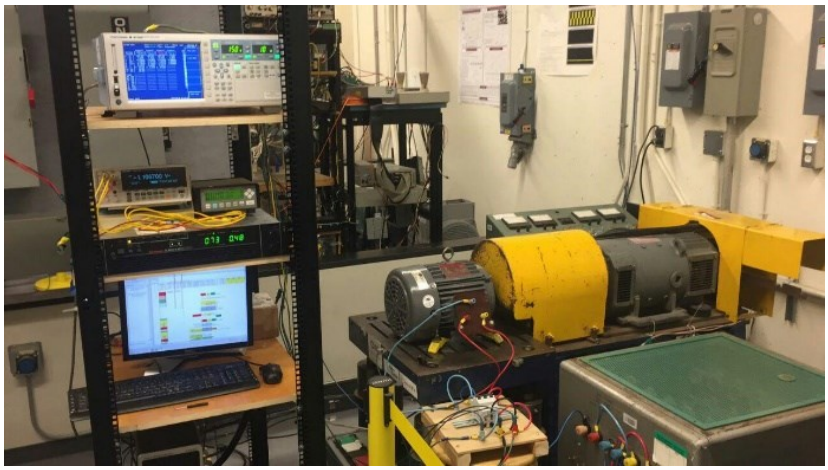

Fig. 3-9: Experimental setup.

Before starting the IM, the stator resistance and ambient temperature are measured. The machine starts at full load and every 10 minutes (t=0, 10, 20, 30 min), the temperature of the machine is recorded. In this chapter, indirect measurement of the temperature using stator resistance based on IEEE Std-112 section 5.8.4.3 is used. At t = 30 min, in addition to the temperature, input current, voltage, active power and rotor speed are measured and recorded. These data plus the nameplate data are the required data for running the proposed algorithm.

For comparison purposes, a torque transducer is installed on the rotor shaft. Then the machine is run at full load for sufficient time to reach thermal stability. For the tested machines, 3 to 5 hours is required to reach this condition. Based on IEEE Std-112, when the machine input power and current do not change for half an hour interval, it can be concluded that machine is in thermally stable condition. Then the shaft torque and speed are measured to obtain the output power. A power analyzer is utilized to record the input power. Based on method A of IEEE Std-112, the ratio of output power to input power can be considered as measured efficiency. Furthermore, the no-load and locked rotor tests are conducted based on IEEE Std-112 to extract the equivalent circuit parameters.

By using the data of the IM in the first 30 minutes of test and applying the proposed algorithm, the equivalent circuit parameters are estimated as listed in Table 3-3. The estimated data are compared with the values extracted from the no-load and locked rotor tests.

Table 3-3: Estimated parameters. (NL: no-load, LC: locked rotor)

hp	case	Parameters			
		X_1	X_m	R_{fe}	R_2
3	#1	0.9809	20.0979	247.07	0.3682
	NL/LC	0.953	20.39	238	0.381
5	#1	2.8005	74.636	2263.9	0.996
	NL/LC	2.56	78.2	2017	1.09
7.5	#1	6.563	234.71	6784.27	1.8727
	NL/LC	5.921	241.94	6452	1.936

Estimating the equivalent circuit parameters with only one operating point is very difficult because the number of unknowns is greater than the number of known variables. There are many answers which can satisfy the objective function with one operating point data. Comparing the results in Table 3-3 proves that the proposed algorithm estimates the results with an acceptable accuracy. This is mainly because the parameter range determination method proposed in section 3.4 can effectively narrow the range of parameters and force the PSO to find the correct answer in a smaller search space.

The predicted temperature at full load for a thermally stable condition by applying the two proposed approaches are compared with experimental results in Fig. 3-10 and Fig. 3-11. The predicted partial load temperature using the described approximation in section 3.6 are also shown in these figures.

The Figures show that the first approach overestimates the temperatures while the second approach provides better approximation of the temperature. Since the partial load temperature estimation is related to the full load temperature estimation, the second approach provides better overall accuracy. Using the predicted temperatures, the estimated partial and full load efficiencies are listed in Table 3-4. The comparison between the estimated efficiencies and the measurements shows the acceptable accuracy of the proposed algorithm and approaches. The second approach

for temperature prediction leads to a lower error in efficiency estimation. The error is less than 0.5% for 75% and 100% of the rated load and less than 1% for other loads.

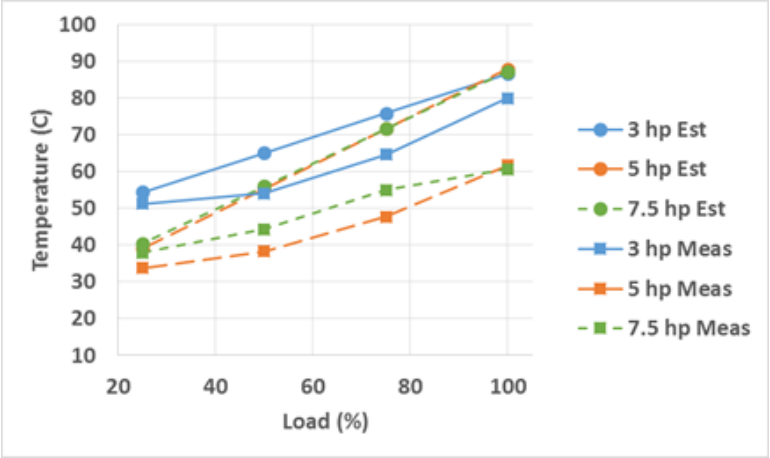

Fig. 3-10: The predicted temperature: Approach 1.

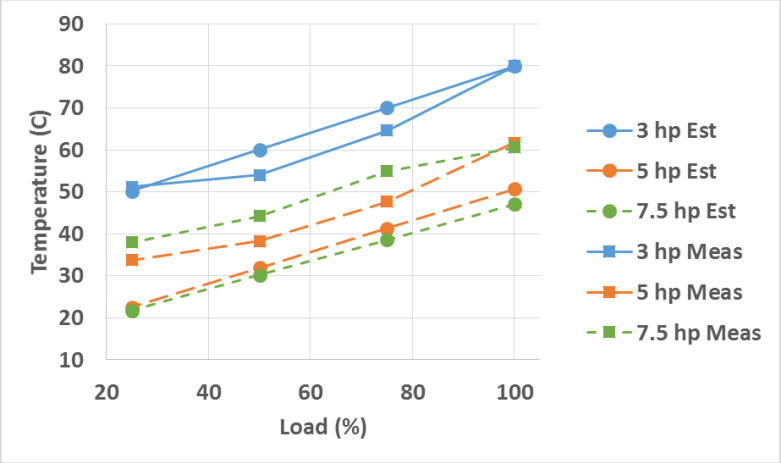

Fig. 3-11: The predicted temperature: Approach 2.

The main error at low loads arises from the error at estimation of P_{FW}. Based on the provided equation for P_{FW} and since all three IMs are 4-pole machines, P_{FW} is considered equal to 1.2% of full load input power. P_{FW} is considered constant at different loads. So at 25% load when the input power reduces to almost 25% of the full load input power, the assumed P_{FW} is around 4.8% of input power. Therefore, the error of P_{FW} estimation has a more significant effect at low loads which was proved in the previous chapter.

Table 3-4: Efficiency estimation results: Approach 1 & 2.

hp	Load (%)	Approaches				
		#1	Error	#2	Error	Meas.
3	100 rapid	81.41	-0.03	81.41	-0.03	81.44
	100 hot	81.07	-0.16	81.29	0.06	81.23
	75	80.87	-0.25	81.14	0.02	81.12
	50	78.24	-0.24	78.08	-0.40	78.48
	25	67.9	-1.07	68.31	-0.66	68.97
5	100 rapid	89.21	-0.08	89.21	-0.08	89.29
	100 hot	88.14	-0.8	89.13	0.19	88.94
	75	89.94	-0.52	90.54	0.08	90.46
	50	90.51	-0.82	90.84	-0.49	91.33
	25	87.89	-0.46	88.09	-0.26	88.35
7.5	100 rapid	91.25	-0.24	91.25	-0.24	91.49
	100 hot	90.39	-0.38	91.16	0.39	90.77
	75	91.72	-0.04	92.20	0.44	91.76
	50	92.00	0.17	92.41	0.58	91.83
	25	89.80	-0.39	89.66	-0.53	90.19

Another source of error originates from the core loss estimation by the equivalent circuit. The proposed PSO based algorithm uses the full load data to extract parameters of the equivalent circuit including the core loss resistance. Core loss is considered constant at all loads, however, when the equivalent circuit is solved to estimate efficiency at lower loads, the estimated core loss increases by reducing the load. Because at lower loads, the current passing through stator (R_1 and X_1) decreases and voltage across the core loss resistance increases and consequently the estimated core loss increases. This results in an intrinsic error in the equivalent circuit which results in errors compared to Method A of IEEE Std-112.

Finally, to prove the repeatability of the proposed algorithm, the maximum errors of 10 times running of the proposed algorithm for each IM are shown in Fig. 3-12. The figure shows the repeatability of the results since errors always remain in an acceptable range. The second approach provides better accuracy when compared to the first approach.

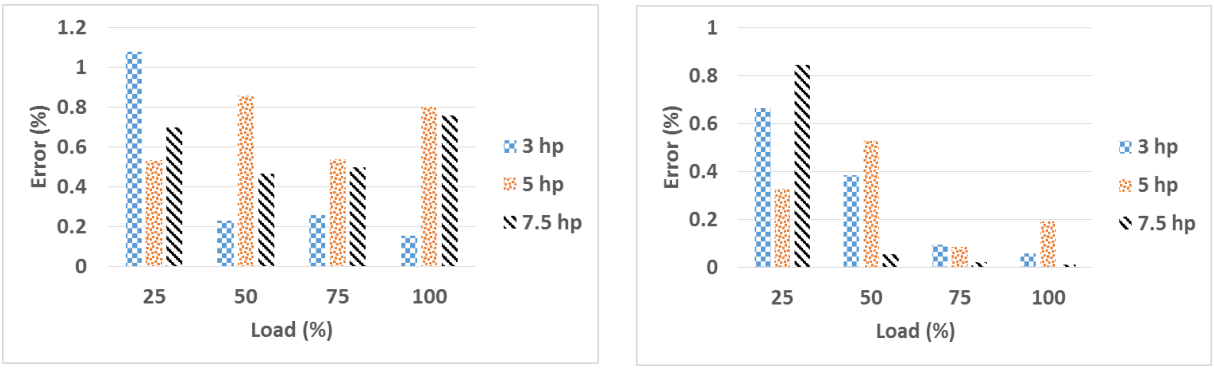

(a) (b)

Fig. 3-12: Maximum error of the estimated efficiency for 10 times running the proposed algorithm: (a) Approach 1 and (a) Approach 2.

3.9 Summary

In this chapter, a PSO based algorithm for parameter and efficiency estimation of IMs was proposed. The proposed algorithm used the nameplate data as well as operating data of the machines in the first 30 minutes after start. To estimate the efficiency by using estimated parameters, two approaches were presented to predict the temperature of the machine at full load with thermal stability. The first approach was based on the insulation class of the IM and the second approach was based on the trend of the temperature rise in the first 30 minutes running the machine and using curve fitting. Furthermore, a technique was introduced to determine the parameter range and to narrow the search space for the PSO which helped to improve the convergence of the algorithm. Also, a very simple and straightforward approximation was used to evaluate the temperature of the machine at partial loads by assuming a direct linear relationship between the machine losses and the temperature. Results of the estimated efficiencies at different loads in comparison to experimental results presented acceptable accuracy of the proposed algorithm and approaches. The second approach showed a higher accuracy when compared to the first approach. It is proved that better prediction of the temperature results in better estimation of the rotor speed and efficiency.

Chapter 4: FEA Based Efficiency Estimation and New Mechanical Loss Formula

4.1 Introduction

The ability to consider saturation of the core magnetic materials, skewed rotor bars, stator winding distribution and leakage fluxes has led to the widespread use of finite element analysis (FEA) in analyzing the performance of different machines. In addition, the ability to analyze new designs has made FEA one of the critical steps in the design process of electrical machines. Despite all of this, due to the inability to consider mechanical losses, stray load loss and core loss in the power flow of the machine, FEA results are not reliable for efficiency estimation. This chapter provides some useful points to evaluate the efficiency of the machine at different loads. For this purpose, two approaches are utilized. In the first approach, losses of the machine are directly calculated using the FEA results and empirical formulas. In the second approach, the method F1 of the IEEE Std-112 is applied to parameters of the equivalent circuit estimated from FEA. Furthermore, by studying more than 100 induction machines (IMs) with 4 poles at different rated power, a new formula based on the rated power of the machine is proposed to estimate the mechanical losses of the IMs. The new formula is used to improve the estimated efficiencies. The experimental results are utilized to validate the proposed formula and approaches.

4.2 FEA Based Efficiency Estimation

Over the decades, several models have been developed for IM analysis. The range of these models varies from the simple models such as the equivalent circuit [71] to more complicated models such as the magnetic equivalent circuit model [72] and the finite element model (FEM) [73]. The application of a particular model for a particular goal depends on the required level of accuracy, the computational time and the complexity of the physical and electrical phenomena should be studied.

FEA is a numerical method based on the geometry and material properties. This method provides accurate information about the effects of the nonlinearities such as saturation of magnetic

materials [74]. In FEA, fine meshes are defined for each element. Then, the field values are calculated by solving the Maxwell equations inside these meshes. A higher number of meshes means finer meshes which results in a better accuracy of results. However, the required time for calculation of the field distribution is directly proportional to the number of defined meshes for each element. Therefore, there has to be a trade-off between defining the finer meshes to obtain the high precision and required processing resources to obtain an acceptable simulation time [75].

Estimating the efficiency of an IM before manufacturing is an essential step. During the design process of the machine, FEA tools can be helpful for this purpose. The IM losses can be classified as follows [42]:

- Stator resistive losses
- Rotor resistive losses
- Core loss
- Mechanical losses (also called friction and windage losses)
- Stray load loss

Stator and rotor resistive losses which are also called Joule losses are due to the resistances of the stator windings, rotor bars and end rings. They are about 25-45% of the IM total losses. Core loss which includes the hysteresis and eddy current losses is up to 15% of the total losses. The mechanical loss originates from the bearing friction and ventilation loss. It comprises up to 15% of the total loss. Stray load loss cannot be categorized under any of the previous losses [42]. FEA is not able to include the mechanical and stray load losses in the power flow of the machine, therefore its results for efficiency estimation cannot be reliable. The FEA solution can be utilized to evaluate the resistive loss and core loss.

This chapter addresses the efficiency estimation of an IM using FEA using two approaches. In the first approach, the FEA solution at different loads and empirical formulas are utilized for direct estimation of the losses and efficiency. The second approach relies on the estimated parameters of the equivalent circuit of the machine using FEA. For this purpose, DC, no-load and locked rotor tests are performed using FEA to extract equivalent circuit parameters. Then the method F1 of IEEE Std-112 is applied to extract the machine's parameters to evaluate the efficiency at different loads. The results of both methods are compared to experimental results to

evaluate their accuracy. To improve the results, a new empirical formula is presented to determine the mechanical loss of the IMs. This formula is a result of studying more than 100 4-pole, the Totally Enclosed, Fan-Cooled (TEFC) IMs operating at 60 Hz.

4.3 Mechanical Loss

IEEE Std-112 [2] and IEC 60034-2 [76] are the two commonly accepted international standards to determine the mechanical loss in rotating machines which is based on performing the no-load test. To perform the no-load test, IEEE Std-112 requires running the machine at the rated voltage and frequency for enough time until the machine's bearing loss is stabilized. This can be monitored by observing the input power change at half-hour intervals. Then, machine input power and stator currents are recorded at proper steps of voltages starting from 125% of the rated voltage down to the voltage that current starts to increase. The rated voltage should be included in the steps. For the 3 or more last points, input power is subtracted from the loss in stator resistance, and then a curve is developed to show these values versus the stator phase voltage. The intercept of the developed curve with the zero voltage axis using the linear extrapolation is the friction and windage loss (P_{FW}) which is known as mechanical loss. Using the squared stator phase voltage rather than the stator phase voltage can result in more accurate value of mechanical loss. This is probably because of the fact that the core loss is proportional with square of the voltage. Fig. 4-1 shows the results of the no-load test for a 5 hp IM.

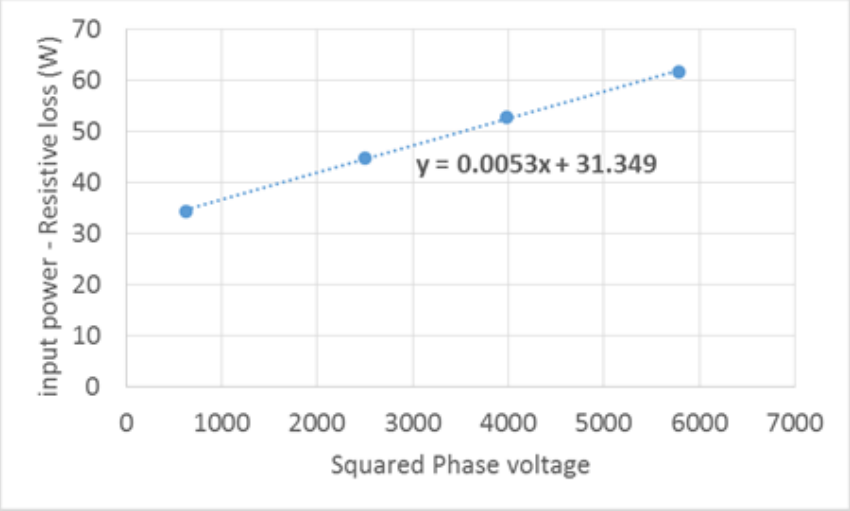

Fig. 4-1: No load loss curve for P_{FW} determination.

Mechanical loss can vary with the speed of the rotor, shape of the machine structure, cooling system, bearing types, lubricant, etc. Fig. 4-2 shows the mechanical loss of the 108 IMs with four poles and TEFC ventilation system. This is the commonly used type of the IM in the industry [77].

Fig. 4-2 shows that even for IMs with the same number of poles and almost the same speed, the mechanical loss varies between 0.21% and 3.25% of the rated power. The variation is reduced by increasing the rated power. In addition, there are only 2 IMs out of 108 IMs which have the mechanical loss greater than 2.5% of the rated power and only 7 IMs with mechanical loss greater than 2%.

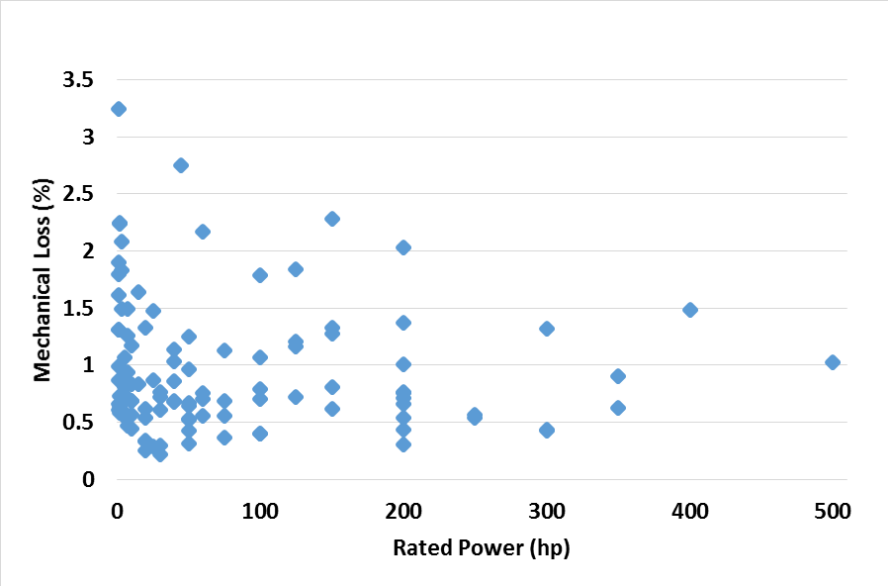

Fig. 4-2: Mechanical loss distribution of IMs.

In the next section, a formula based on these data will be introduced to determine the mechanical loss.

4.3.1 New Formula for Mechanical Loss

During the design process of an IM or for in-situ application where the machine is working and cannot be decoupled from the load, determination of the mechanical loss using the no-load test is not possible. Therefore, formulas and equations should be used to determine the mechanical loss.

The mechanical loss sometimes called as friction and windage losses is usually referred to the sum of the frictional loss in bearings and loss due to friction between cooling air and rotary

parts. In addition, the power consumed for ventilation called ventilator loss is considered as a part of the mechanical loss. This power can be consumed by the fan mounted on the shaft or another motor which drives the fan [78].

Bearing losses depend on the bearing type, shaft speed, lubricant properties and the bearing load [79]. Furthermore, the ventilation method (with or without fan), the cooling medium (air, hydrogen or other gases), and the pressure and velocity of the cooling medium flow can affect the ventilation loss [80]. Due to the number of parameters affecting the mechanical loss, the exact determination of this loss is complicated. Therefore, simple empirical formulas are presented to determine the mechanical loss.

For IMs with a radial ventilation system, the following formula is presented in [80]:

$$P_m = (11 + i)\left(\frac{n_r}{1000}\right)^2 (10D_1)^3 \tag{4-1}$$

where i is the number of radial core ducts (machine with no radial duct $i = 0$), D_1 is the inner stator diameter and n_r is the rotor rotational speed in *rpm*.

In [78], an experimental equation is presented for the sum of windage and ventilation losses which is valid for normal speed IMs:

$$P_m = k_\rho D_r (l_r + 0.6\tau_p) v_r^2 \tag{4-2}$$

where k_ρ is an experimental factor which is determined by Table 4-1, D_r and l_r are the rotor diameter and length respectively, τ_p is the pole pitch in *m* which can be calculated using number of poles (P) as follows:

$$\tau_\rho = \frac{\pi D_r}{P} \tag{4-3}$$

v_r is the surface speed of the rotor in *m/s* and can be calculated as follows:

$$v_r = \frac{n_r \pi D_r}{60} \tag{4-4}$$

where n_r is the rotor rotational speed in *rpm*.

These two formulas require the design data of the machine which are suitable during the design process but they cannot be applied for in-situ applications.

Table 4-1: Experimental factors for mechanical loss [78]

Cooling method	$K\rho$ (W s^2/m^4)
TEFC motors, small and medium-sized machines	15
Open-circuit cooling, small and medium-sized machines	10
Large machines	8
Air-cooled turbogenerators	5

In [81], the mechanical loss is determined as a percentage of the full load input power based on the number of the poles as follows:

$$P_{FW} = 2.5\% \times P_{in,fl} \quad for\ 2-pole \tag{4-5}$$

$$P_{FW} = 1.2\% \times P_{in,fl} \quad for\ 4-pole \tag{4-6}$$

$$P_{FW} = 1.0\% \times P_{in,fl} \quad for\ 6-pole \tag{4-7}$$

Despite presenting a simple formula to determine the mechanical loss, this work does not provide any analysis to show the accuracy of the presented formulas.

Fig. 4-3 presents the mechanical loss of 108 IMs. This data were collected by Hydro Québec by performing the no-load test. All the tested IMs are three-phase, 4-pole with rated frequency of 60 Hz. Their cooling method is TEFC and they vary from 1-hp to 500-hp. These IMs can be easily found in the industry due to their wide range of applications [77].

Using a linear regression, a trend line is fitted to the data and is shown on the figure. Because of the higher number of the small tested motors, the results for motors less than 50 hp (37.3 kW) are shown in the Fig. 4-3(b). Assuming zero mechanical loss for zero hp IM, the trend lines is defined to pass from the zero center. The trend line shown in the figure can be formulated as follows:

$$P_{FW} = 0.0093 \times P_{out} \tag{4-8}$$

where P_{out} is the rated power in W.

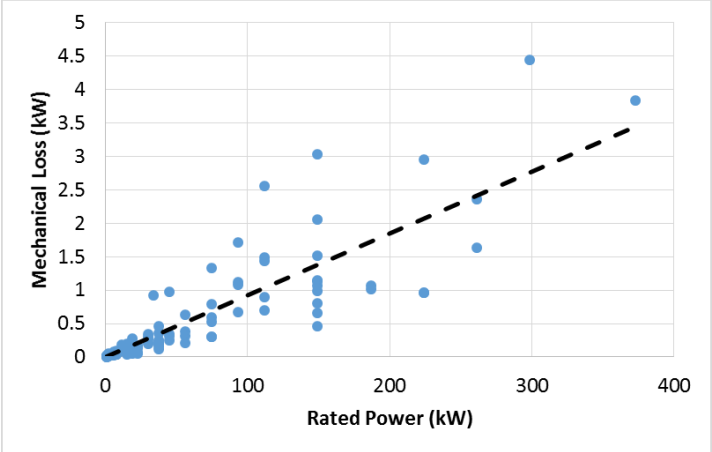

(a)

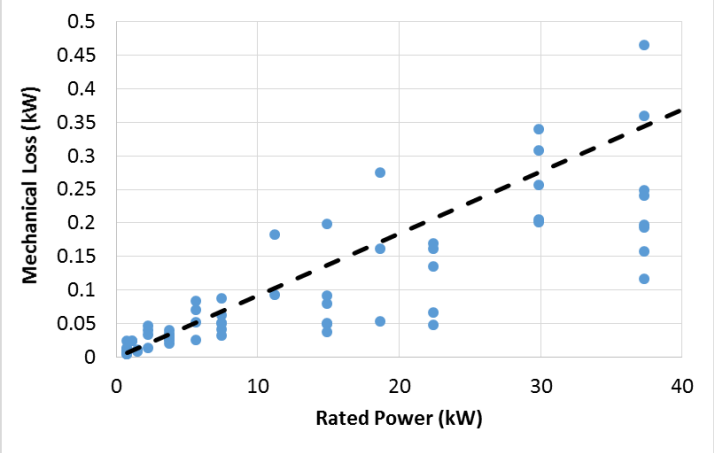

(b)

Fig. 4-3: Mechanical loss formula.

To study the accuracy of the proposed formula, it has been applied to estimate the mechanical loss of the IMs. To show the effect of the formula on the estimated efficiencies, the error of the estimated values are expressed in the percentage of the rated power. Fig. 4-4 shows the number of the motors with their errors in a specific range. For example, the number of IMs where their estimated errors are less than 0.1% is 13. By considering the total number of the IMs which is 108, it means that the proposed formula presents a high accuracy for around 12% of the IMs. For 22 IMs (or around 20%), the error is between 0.3% and 0.4%.

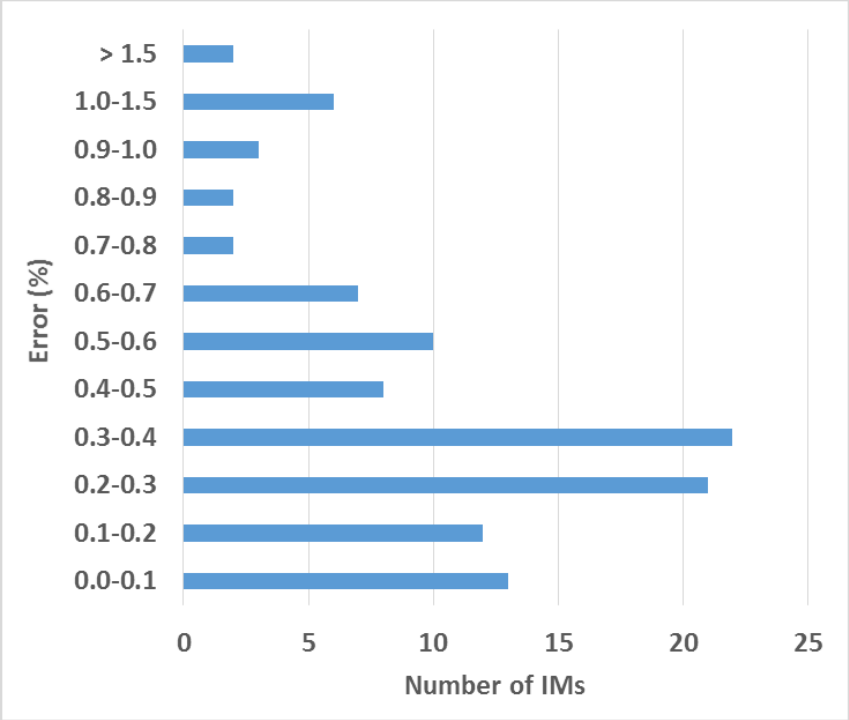

Fig. 4-4: Accuracy of the proposed formula.

The most important point of the Fig. 4-4 is that for 76 IMs or more than 70% of the IMs, the error is less than 0.5% which is considered an acceptable error in efficiency estimation calculations. For the remaining 32 IMs, the errors of 17 IMs are in the range of 0.5% to 0.7% and only for 15 IMs or around 14% of the IMs the error is larger than 0.7%.

The error shown in Fig. 4-4 is in terms of the output power while for efficiency estimation, input power is used in the denominator of the efficiency equation. It means that if the errors are evaluated in terms of the input power, it will show higher accuracy for the proposed formula and a larger number of the IMs will be in an acceptable range.

Equation (4-6) which is proposed in [81] considers the mechanical loss as 1.2% of the input power, this reveals that for only 51 IMs or around 46% of the IMs, the error remains less than 0.5%. Therefore, the new proposed formula provides a better accuracy for 4-pole, 60 Hz IMs.

4.4 Loss Calculation Using FEA

Efficiency is defined as the ratio of the output power to the input power. IEEE Std-112 method A [2] proposes that the efficiency is calculated by the loading test and measuring the input and output powers. Although, this can be virtually done in FEA software, the results are not

reliable. The challenges to include the core loss and mechanical loss in the power flow calculation of the FEA is the main reason that makes the FEA estimated efficiency results unreliable. However, FEA is helpful to estimate the resistive and core losses. These losses in addition to the mechanical and stray load losses can be used for efficiency estimation of an IM. In this section, the methods and formulas for this purpose are discussed in detail.

Although using 3D FEA can result in more accurate estimation than the 2D model, the required simulation time is very long and computers with high performance are necessary. Therefore, the 2D model is employed to remedy this concern.

4.4.1 Stator Resistive Loss

Using a time variation of each stator phase current from FEA solution, the stator resistive loss of an IM can be calculated as follows:

$$P_{SCL} = \frac{1}{T}\int_0^T \left(\sum_{m=1}^{3} R_s I_{sm}^2\right) dt \tag{4-9}$$

where m is the number of the phase, R_s is the stator phase resistance and I_{sm} is the phase current. The stator and rotor resistive losses are considered the largest part of the machine losses especially for small machines. An accurate estimation of R_s plays an important role for accurate loss results. In 2D FEM, the end winding resistance which is a significant part of the total resistance is ignored, therefore the end winding resistance is added to the model as an external resistance. For a coil with a_p number of parallel paths, total conductor length of l_c and cross-sectional area of the conductor A_c, the resistance can be calculated as follows [78].

$$R_S = \frac{l_c}{\sigma_c a_p A_c} \tag{4-10}$$

where σ_c is the conductivity of the conductor material. An accurate estimation of the winding length in an electrical machine is very difficult. This is more difficult in case of machines with distributed windings such as IMs. Based on the empirical equations for low-voltage machines with round enameled wires, the average length l_{av} of a coil turn in meters can be calculated as follows [78]:

$$l_{av} = 2l + 2.4W + 0.1 \tag{4-11}$$

where *l* is the stator stack length and *W* is the average coil span, both in meters. For larger machines where the prefabricated windings are utilized, the following formulas can be used based on their rated voltage:

$$l_{av} = 2l + 2.8W + 0.4 \tag{4-12}$$

$$l_{av} = 2l + 2.9W + 0.3 \quad when \;\; U_{rated} = 6 \dots 11\ kV \tag{4-13}$$

In (4-11) to (4-13), it can be assumed that the second and third terms of the equations provide the end winding length.

4.4.2 Rotor Resistive Loss

Rotor resistive loss can be calculated in the same manner as the stator. Since the frequency of the rotor current is smaller than the supply frequency, enough rotor bar current cycles should be considered. Hence, the FEA simulation file should be run for a longer time to get acceptable results. Furthermore, at low loads this problem gets worse. To avoid this concern, using the airgap power calculation is the simplest way to calculate the rotor resistive loss. Since the mechanical and stray load loss are not included in the FEA model, the output power of the machine can be considered as converted power (P_{conv}). The airgap calculated power and consequently the rotor resistive loss can be calculated as follows:

$$P_{ag} = \frac{P_{conv}}{1 - s} \tag{4-14}$$

$$P_{RCL} = s\, P_{ag} \tag{4-15}$$

where *s* is the slip. In the same manner of the stator resistance, the end ring resistance should be added to the model.

4.4.3 Core Loss (P_{fe})

The core loss of an IM comprises hysteresis loss and eddy current losses. Hysteresis loss is due to the residual flux in magnetic materials. It depends on the hysteresis loop area and frequency of the machine. The currents which are induced by variable flux of the machine inside the core material is called eddy currents and the corresponding loss which turns into heat is called eddy current loss [71]. Due to the lamination technique used to increase the electrical resistivity of the

core materials, the eddy current loss is usually less than the hysteresis in particular for normal frequency (50 and 60 Hz) machines. The total core loss can be estimated by [82]:

$$P_{fe} = K_h f B^n + K_e f^2 B^2 \quad (4\text{-}16)$$

Where K_h and K_e are the hysteresis and eddy current losses coefficients extracted from experimental data, n is a Steinmetz constant normally equal to 1.6, f is the frequency and B is the flux density. From FEA, the core loss can be calculated. However, the calculated loss is always less than the measured value. The mechanical stress during the manufacturing process of the machine can change the magnetic properties of the machine core and increase the core loss. Cutting and punching the core steel sheets are the main mechanical stress which are applied to the machines.

Punching can reduce the permeability of the materials especially at lower flux density [83], [84] and increase the core loss up to 10% as stated in [84, 85] and up to 20% as stated in [86]. Among cutting methods, a core loss increase of 10% in [85], 30% in [87, 88], and 50% in [89] are reported for Guillotine shear as a mechanical cutting method. Laser cutting is commonly used in electrical machines. For CO_2 lasers, higher losses compared to mechanical cutting are reported in [86, 89, 90], while for high flux density, losses in mechanical cut are higher than the ones in laser cut [91]. Nd:YAG Laser also increases the loss [84]. In [92], it is shown that an increase of the core loss is decreased by increasing the strip width. Therefore for small machines, the increase of the loss is expected to be greater than in larger machines.

As a conclusion, a 20-30% increase in the core loss seems to be a reasonable value to consider the cutting and punching effects. Hence it is applied to the core loss calculated using FEA results.

4.4.4 Stray Load Loss

According to the IEEE Std. 112-2004, "the stray load loss is that portion of the total loss in the electrical machine not accounted for by the sum of the resistive loss, core loss and mechanical loss" [2]. Since the origin of the P_{SLL} is very complicated, defining the specific methodology or formula to estimate the P_{SLL} using FEA is difficult.

In [93], stray load loss of induction motor is estimated using 2D and 3D FEA and the total stray load loss is defined as a summation of the copper stray loss and iron stray loss. The difference between the total copper loss and the loss caused by the fundamental current waveform is considered as copper stray loss. The iron stray loss is defined as the difference between total iron loss and the loss caused by the fundamental waveform of the magnetic field.

In [70] it is claimed that these losses are mainly due to the harmonics generated by the windings, slots and airgap and leads to an increase in the core loss and high frequency loss in the rotor bars at loaded condition compared to no-load condition. In [94], this is used to estimate the stray load loss using the FEA and results are validated for a 10-hp IM. The results show that the calculated value is less than the measured one. Therefore, there is no accepted methodology to determine the P_{SLL} using FEA. In this chapter, similar to the rest of the thesis, empirical results are used to determine P_{SLL} which are presented in section 2.3.4.

4.4.5 Mechanical Loss

This is discussed in section 4.3.

4.5 Equivalent Circuit Using FEA

IEEE Std-112 Method F/F1 proposes to use the equivalent circuit to estimate the efficiency of an IM. A conventional equivalent circuit of an IM is shown earlier in Fig. 2-2. In this figure, R_1 and X_1 are the stator resistance and the leakage reactance, R_2 and X_2 are the rotor resistance and the leakage reactance. X_m is the magnetizing reactance and R_{fe} is the representative of the core losses. s is the slip. P_{in} and P_{out} are the input and the output powers.

A common way to determine these parameters is to perform DC, no-load and locked rotor tests. These tests can be implemented in the FEA. However, before implementing the tests, there are some problems which should be taken into account.

As mentioned in section 4.4, 2D FEA is used in this chapter. Therefore, the resistance and leakage reactance of end winding of stator and rotor end rings should be added to the model. In particular, the resistance of the stator end winding and rotor end rings contribute to the copper loss of the machine and directly affect the efficiency of the machine. In this chapter, MotorSolve/Infolytica FEA software is used to determine the end winding and ring parameters and are added to the model as external resistance and inductance to the rotor and stator electrical

circuits. Fig. 4-5 shows the end winding resistance and leakage inductance added to the stator winding as an external circuit. It should be noticed that the stator windings are connected in delta.

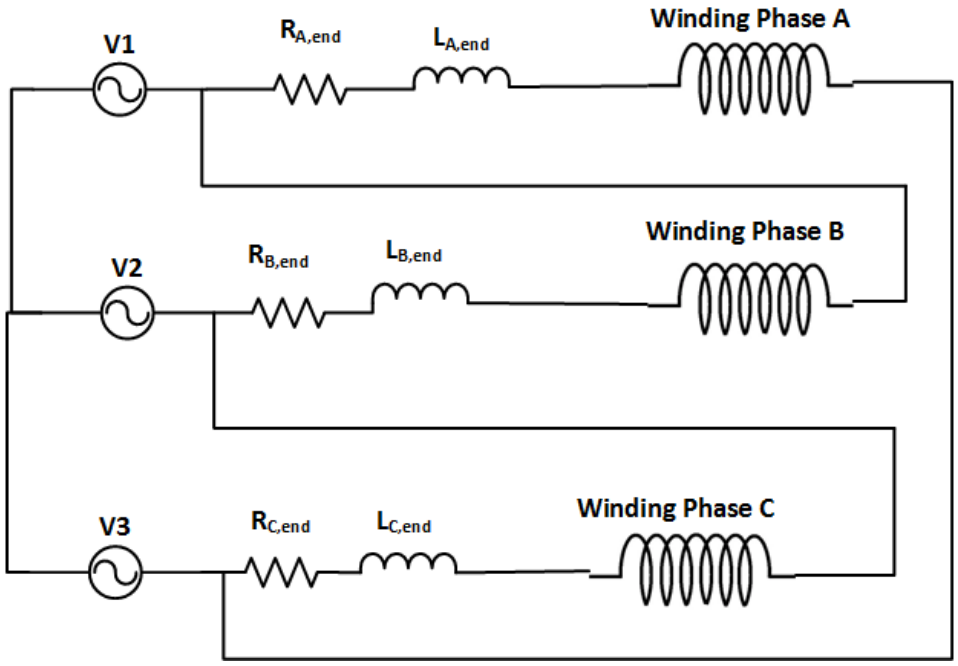

Fig. 4-5: Stator end winding resistance and leakage inductance added as external circuit to FEA.

The total stator resistance can be estimated by implementing the DC test in FEA.

4.5.1 Locked Rotor Test

By implementing the locked-rotor test in the FEA software, the rotor equivalent resistance and rotor and stator inductances can be estimated. The locked rotor test should be performed at the rated current and maximum 25% of rated frequency. This is mainly to reduce the skin effect in rotor bars which normally work at a slip frequency (up to 5% of the rated frequency). However, to improve the results, it is recommended to perform the locked rotor test at three different frequencies all at rated current: one at the rated frequency, one approximately around 50% of the rated frequency and the last one at the maximum 25% of the rated frequency. Then, the values of rotor resistance and total leakage reactance are calculated at each frequency and the developed curves of the values versus the frequency are used to determine the rotor resistance and leakage reactance of the rotor at any reduced desired frequency.

To run the FEA at rated current, there are two options. First, supply the circuit by voltage source and achieve the required voltage by trial and error to generate the rated current. Second,

supply the circuit by a current source and apply a current equals to rated current as shown in [95]. The locked rotor test is simulated in FEA by letting the machine speed equals to zero.

The total reactance which is the summation of the stator and rotor leakage reactances can be calculated as follows:

$$X_{eq} = \frac{Q_{in,L}}{3I_{1L}^2} \tag{4-17}$$

I_{1L} is the locked rotor phase current which should be equal to the rated current, $Q_{in,L}$ is the input reactive power which can be calculated as follows:

$$Q_{in,L} = \sqrt{3I_{1L}^2 V_{1L}^2 - P_{in,L}^2} \tag{4-18}$$

$Q_{in,L}$ and V_{1L} are the input power and the phase voltage at locked rotor condition.

To separate the stator and rotor reactances, NEMA design can be used to determine the ratio X_1/X_2 [22]. It is shown that in the transient condition such as start-up transient, these ratios are not valid anymore. Because in this situation, leakage reactances vary due to saturation of the core and in particular stator and rotor teeth [96]. Since the variation of the stator and rotor leakage reactances is not identical, this ratio is not valid for all currents [95]. But for the objective of this thesis which is the efficiency estimation of the machine at different loads, only the values of reactances at rated conditions are estimated and assumed to be constant at other loads. The rotor resistance can be estimated from the locked rotor test and pervious information about the stator resistance obtained from the DC test.

$$R_1 + R_2 = \frac{P_{in,L}}{3I_{1L}^2} \tag{4-19}$$

4.5.2 No load test

Based on the both IEEE Std-112 and IEC60034-2-1, the no load test is used to determine the mechanical loss (friction and windage losses) and core loss of an IM. As mentioned in section 4.3, this test is performed at different voltages to distinguish between the core loss and mechanical loss. Then, the core loss and total input reactive power at rated load are used to determine R_{fe} and X_m.

However, the mechanical loss is not included in FEA. Therefore, machine model in FEA is only run at no load condition with rated voltage.

The voltage across R_{fe} and X_m at no load is calculated as follows:

$$V_2 = V_1 - (R_1 + jX1)I_{1,0} < \theta_{1,0} \tag{4-20}$$

where $I_{1,0}$ and $\theta_{1,0}$ are the no load current amplitude and angle. X_m can be estimated using the total reactive power at no load.

$$X_m = \frac{3V_2^2}{Q_{in,0} - 3X_1 I_{1,0}^2} \tag{4-21}$$

Since the core loss is not included in the power flow of FEA, the input power cannot be used to estimate R_{fe}. Therefore, the method described in the section 4.4.3 is used to determine the core loss as follows.

$$R_{fe} = \frac{3V_2^2}{P_{fe}} \tag{4-22}$$

4.6 Results

To study both methods, a 5-hp IM is investigated with specifications in Table 4-2.

Table 4-2: IM's specifications.

Output Power	Rated Voltage	Rated Current	Rated Speed	Poles	Efficiency	Insulation Class	NEMA Design
5	220	16	1730	4	86	B	C

To analyze the machine, MagNet/Infolytica FEA software [97] is used to implement the 2D FEA model. To increase the accuracy of the model, the end winding and end ring resistances and inductances are determined by the MotorSolve/Infolytica FEA software [98] and are coupled to the model as an external circuit. The three-phase voltage source is connected to the external circuit to drive the machine.

The model is run under the loaded, no-load and locked rotor conditions. Although the stator resistance can be calculated from FEA, a DC test is also conducted to determine the stator resistance and verify the software results. Fig. 4-6 shows a flux distribution of the IM.

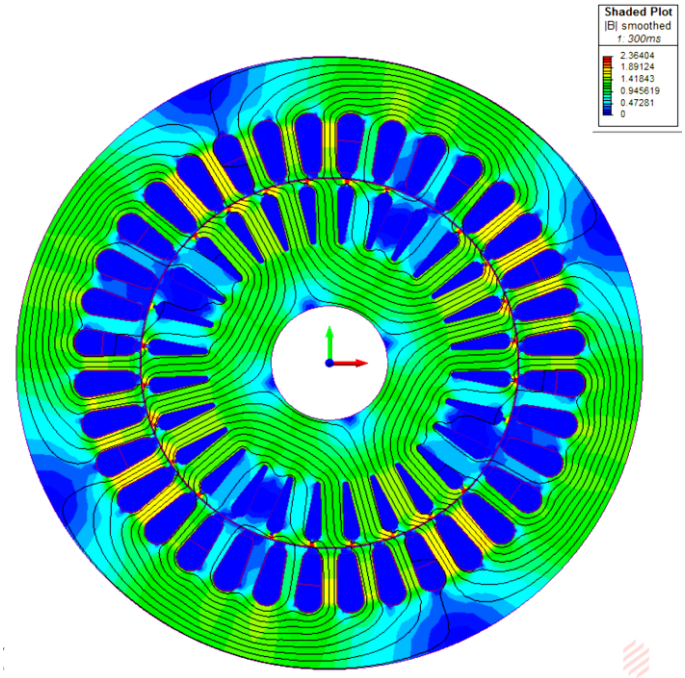

Fig. 4-6: Flux distribution of the machine.

An experimental set-up is implemented to verify the results. The set-up is shown in Fig. 4-7 which includes a dynamometer coupled to the IM. Efficiency of the machine at different loads is measured based on method A (direct measurement) of the IEEE Std-112. For this purpose, a torque transducer is mounted on the shaft to measure the shaft torque and consequently the output power is calculated using rotor speed. A high resolution power analyzer is utilized to measure the input power supplied by the source to the motor. A variable resistive load is connected to the dynamometer for estimating the efficiency at different loads.

In addition to the loading test, the no-load and locked rotor tests are conducted to extract the equivalent circuit parameters and determine the core loss and mechanical loss based on the procedures described in IEEE Std-112. Then method F of IEEE Std-112 is applied to the estimated parameters to evaluate the efficiency of the machine at different loads. Finally, Method B of IEEE Std-112 is used to determine the stray load loss of the machine.

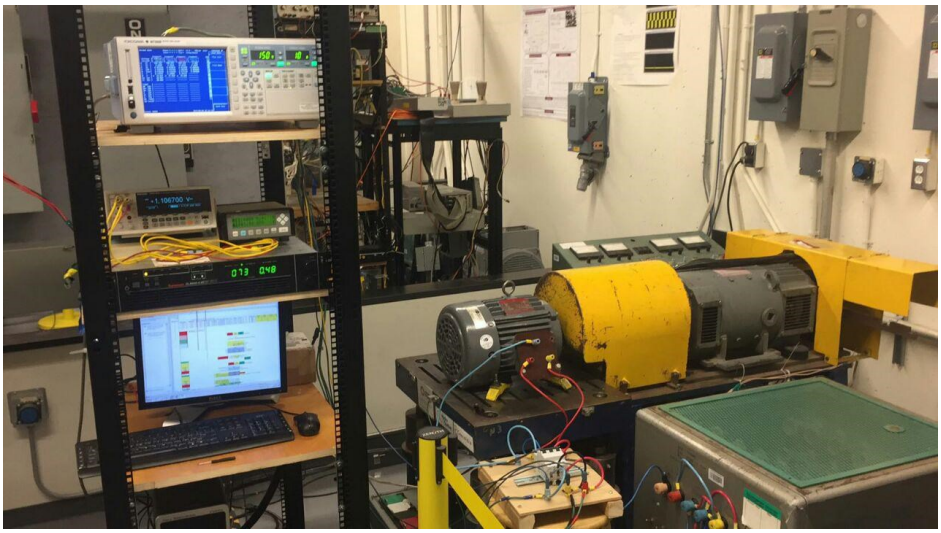

Fig. 4-7: Experimental setup.

4.6.1 Loss Calculation Results

Table 4-3 shows the estimated efficiency from FEA.

Table 4-3: Estimated efficiency using FEA.

Load (%)	Measured	FEA	Error
100	88.39	87.96	-0.43
75	89.44	88.74	-0.7
50	89.01	87.85	-1.16
25	84.39	82.55	-1.84

The results show that the estimated values from FEA are less than the measured values. To investigate the sources of error, loss components are studied individually. Performing the no-load test, core loss and P_{FW} are determined as 31.35 W and 99.24 W respectively. The estimated P_{FW} using (4-8) is 34.69 which again proves the accuracy of the new proposed formula for P_{FW} estimation. However, the estimated core loss considering an increase of 25% due to the cutting and punching effects is 85.82 W which is less than the measured value. The measured P_{SLL} from method B of IEEE Std-112 is 51.06 W and the assumed value is 45.62 according to [99]. So, there are small errors in these losses. As a result, it can be expected that the error in the estimated

efficiency is mainly originated from the resistive loss calculation. Table 4-4 shows the estimated and measured values of the resistive loss at different loads.

Table 4-4: Estimated and measured resistive losses.

	P_{SCL} (W)		P_{RCL} (W)	
Load (%)	Exp.	FEA	Exp.	FEA
100	196.99	227.38	111.14	114.89
75	126.82	151.16	56.81	60.47
50	84.16	103.31	23	25.76
25	59.73	74.37	5.66	6.42

Referring to Table 4-4, although the estimated rotor resistive loss at different loads are close to the measured ones, the estimated stator resistive losses are larger than the measured ones. The reason for this error arise from the current inaccuracy. As an example, the measured stator line current at the full load is 14.08 A while the obtained line current from FEA is 15.08 A which increases the estimated stator loss by the factor of the stator resistance values. Note that neither the measured value nor FEA value of the stator current are not same as the rated current.

4.6.2 Equivalent Circuit Results

To apply method F1 of IEEE Std-112 for efficiency estimation, the equivalent circuit parameters are extracted using FEA. The estimated equivalent circuit parameters from FEA are compared with the measured one and the results are listed in Table 4-5.

Table 4-5: Equivalent circuit parameters.

Load (%)	**FEA**	**Measurement**
R_1 (Ω)	0.884	0.882
X_1 (Ω)	2.254	2.046
R_{fe} (Ω)	1553.6	1346.1
X_m (Ω)	49	51.32
R_2 (Ω)	0.822	0.838

These results are achieved by implementing the DC, no-load and locked rotor tests in FEA software. There are other proposed methods for accurate estimation of the parameters and in particular leakage reactance of the machine which is not in the scope of this chapter.

Applying method F1 of IEEE Std-112 to the values in Table 4-5 results in the efficiency values shown in Table 4-6. These results are compared to the results of Method A of IEEE Std-112 (direct measurement).

Table 4-6: Efficiency estimation using equivalent circuit.

Load (%)	Method A	FEA	Error
100	88.39	88.01	-0.38
75	89.44	89.27	-0.17
50	89.01	88.69	-0.32
25	84.39	83.58	-0.81

As expected, due to the errors in FEA estimated parameters shown in Table 4-6, the estimated efficiency has errors and these errors are increased by load reduction. However, this error is less than all errors shown in Table 4-3 for direct loss calculations. This improvement in the estimated efficiency is because the estimated stator current has less error compared to the FEA result. In this case the full load current is 14.8 A which is lower than 15.08 A that is estimated from FEA.

4.6.3 Discussion on the Results and Model

Several points on building the model and results are valuable to be mentioned.

Estimating the stator winding resistance either using the software or empirical equations does not result in an accurate outcome. For the tested IM, the estimated R_1 using the MotorSolve/Infolytica and empirical equations are 1.2 Ω and 1.05 Ω respectively, while the actual R_1 is 0.882 Ω. This is due to the unconventional stator windings distribution. It is well known that higher R_1 leads in a lower estimated efficiency. Therefore, R_1 is set equal to the actual value to study the model accuracy. This problem is not serious for R_2 due to the structure of the rotor bars and end rings.

Using approaches presented in sections 4.4 and 4.5 requires some knowledge about the temperature of the IM under load. Prediction of the temperature of the machine at loading conditions is a complicated and difficult problem due to the several factors affecting the thermal behavior of the machine. The cooling system, thermal properties of the material, shape of structure and amount of the losses are some of these factors [57, 58]. However this subject is not in the scope of the chapter. Therefore, using the insulation class of the machine or some database can be helpful to determine the temperature.

Applying the load in FEA is different from method F1 of IEEE std-112. In method F1, the output power is defined as a load. It means that for the tested IM, the output power is set to be 5 hp and then input power at this condition is calculated based on the equivalent circuit equations in an iterative manner. However, the load in FEA is defined as a torque value and the output power is calculated using the load torque and the estimated speed using the solution. Therefore, by trial and error, the required load torque is determined to obtain the desired output power. Furthermore, running the machine with a current source is not acceptable because the rated current of the machine is 16 A while the estimated current from FEA and measured values at full load are 15.08 and 14.08 respectively.

Based on the FEA results, the core loss increases with load. Fig. 4-8 shows the estimated core loss using FEA vs. the load. The increase of the core loss is considered part of stray load loss. Therefore, the estimated core loss at no load condition is used for both efficiency estimation using the loss calculation and for core loss resistance determination.

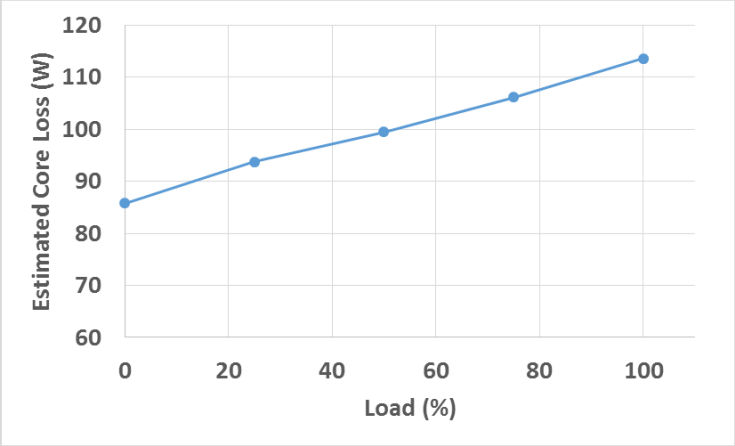

Fig. 4-8: The estimated core loss at different loads.

Among the estimated parameters, X_m has a significant effect on the efficiency in particular at low loads. Although X_m may not directly contribute to losses, it affects the efficiency especially at low loads. X_m values are normally much smaller than R_{fe} (see Table 4-5) and in some of applications of the equivalent circuit of the machine such as designing a control system, R_{fe} is neglected. Therefore, X_m is the dominant part of the equivalent circuit at low loads. It determines the no-load current of the machine. The no-load current passes through the stator resistance no matter how much the load is and its value can directly affect the stator resistive loss. As a result, the precise estimation of X_m is crucial for efficiency results. The study of parameters also showed that the accuracy of the estimated X_1 and X_2 affects mainly the full load efficiency and accuracy of low loads efficiency does not depend on their accuracy.

4.7 Summary

This chapter addressed the efficiency estimation of IM using FEA. for this purpose, two approaches were studied and some points were provided to improve the accuracy of the results. The first approach was based on the loss calculation using FEA solutions and empirical formulas. In the second method, method F1 of IEEE Std-112 was applied to the parameters of the equivalent circuit parameters extracted from FEA. It was shown that, although the magnetizing reactance did not directly contribute to the losses, it affected the other losses in particular at low loads. Furthermore, a new and simple formula based on the machine rated power was proposed to estimate the mechanical loss of IMs with 4 pole and totally enclosed, fan cooled (TEFC) system operating at 60 Hz. This formula was obtained after testing more than 100 IMs in the power range of 1-500 hp.

Chapter 5: Drive-Fed Induction Machine Efficiency

5.1 Introduction

Nowadays, adjustable-speed drives (ASDs) are used extensively in the industry. Despite their prominent capabilities and features in controlling the speed and torque of the electrical machines, these ASDs reduce the efficiency of the machine compared to the direct-fed operation mode. This reduction is due to additional losses generated by harmonics in output voltage and current content of ASDs. Due to the complex nature of these losses, accurate calculation of these losses is very difficult. This chapter intends to present a simple and straightforward way to predict an induction machine (IM) efficiency in a drive-fed mode by using its results in the direct-fed mode. For this purpose, four different IMs are tested in three modes: the direct-fed, scaler drive-fed and direct torque control (DTC) drive-fed IM. The results are then compared. Furthermore, a simple method is proposed to predict the efficiency of a drive-fed IM by using the direct-fed mode results.

5.2 Effect of Time Harmonics on Efficiency

The advances in power electronics devices result in a rapid development of power converters to produce the desired voltage and frequency for any drive system. These converters are widely used in adjustable-speed drives (ASD) for IMs, and today, industrial drives are commercially available in the market. This has led to an increase in the applications of IMs in the industry. Although ASDs offer speed and torque control, they increase losses and reduce machine efficiency [100]. This reduction in efficiency depends on the control strategy adopted by the industrial drive and its voltage generation strategy, as well as machine structure and design. The origin of these losses is the harmonics generated by the ASDs and they are sometimes called harmonic losses [101].

There are two methodologies reported in the literature in order to measure the harmonic losses. In [102] the difference between the input power values for drive-fed and direct-fed modes at fundamentally-equal voltage and torque conditions is referred to the harmonic losses. On the

other hand, they are estimated as reported in [103] by calculating the difference between the total input power and the simultaneously measured fundamental input power at Drive-fed mode.

Harmonic losses consist of several losses in the machine which are difficult to measure or separate due to their complex nature. The first part of the harmonic losses is due to the skin effect in the stator and rotor conductors. The effective resistance of the conductors increases at higher frequencies by reducing the effective cross-section are of the conductors. At higher frequencies, current tends to flow through the outer surface of the conductors therefore, this phenomenon is severe in conductors with larger cross-sections. In an IM, the cross-section of the stator winding wire is much smaller than the rotor bars and hence, the skin effect is significant in the rotor bars. Furthermore, in large machines, the multiple wires rather than one single wire are used to increase the fill factor of the slots which helps in reducing the skin effect.

The equations to include the skin effect in the rotor resistance have been provided in [104] this can normally be done based on the rotor bar shapes. In [105, 106], it is reported that the rotor resistance varies with square root of the harmonic order. In [107], it is shown that the rotor bar resistance varies with square root of the harmonic order, however, the end ring resistance does not experience the same changes. The work in [108] adopts another strategy and instead of providing a formula for the rotor resistance variation, it suggests considering the variation of the total machine resistance with harmonic order in power of 0.6

Core loss comprises the hysteresis and eddy current losses. Voltage harmonics of ASDs can deteriorate the flux waveforms of the machine. The flux pulsation generates extra hysteresis and eddy current losses [109, 110]. A precise prediction of iron loss in case of drive-fed IMs is very difficult due to the complex nature of distribution characteristics of the stator and rotor iron loss. Furthermore, it become more complicated when the ferromagnetic material saturation, crystal orientation, and manufacturing process are considered [111]. In [112] it is shown that while the additional core loss due to harmonics in the 6-step voltage source inverter is negligible, in a PWM inverter, it is significant and cannot be neglected. At harmonic frequencies, the end-leakage and skew-leakage fluxes which normally contribute to stray load loss may contribute to harmonic core losses [113, 114].

Spatial harmonics are available in IMs directly fed from a sine wave supply. Time-harmonic currents can also excite the spatial harmonics and create space-harmonic magneto-motive force (mmf) losses. These losses can be called as high-frequency stray load losses [113].

In [101], four IMs from one manufacturer with different power ratings and four 7.5 kW IMs made by different manufacturers are tested to find a relationship between the stray load loss and harmonic losses caused by a PWM inverter. This paper claims that the harmonic losses are always less than the stray load loss, but there is no strict correlation between them. However, it can be expected to increase the harmonic losses for machine with higher ratings.

The accurate prediction of the machine efficiency in drive-fed condition is difficult. This chapter provides a simple and straightforward method to predict the drive-fed IM efficiency by answering this question: "Does the direct-fed efficiency test give any information above the drive-fed efficiency test?" For this purpose four IMs are tested in three modes; the direct-fed, scaler control drive-fed and direct torque control (DTC) drive-fed. Among 4 IMs, two IMs are designed for direct-fed applications and other two IMs are designed for Pulse Width Modulation (PWM) applications. All the additional losses due to harmonics are categorized based on conventional types of the losses presented in IEEE Std-112: stator and rotor resistive losses, core loss, friction and windage losses and stray load loss. In other words, the variation of these losses in drive-fed mode is studied based on the measurement methodology described in IEEE Std-112 for direct-fed mode. Furthermore, the fundamental equivalent circuit parameters are used to estimate the losses and their accuracy is studied.

5.3 Control Strategy

In this chapter, the ABB drive ACS800 is used to drive four IMs. Both the scalar and direct torque controls are implemented on this drive. ABB industrial variable speed drives are designed for industrial applications, especially for applications in process industries such as pulp & paper, metals, mining, cement, chemical, and oil and gas. These drives are highly flexible AC drives that can be configured to meet the precise needs of industrial applications.

The complete drives cover a wide range of powers and voltages, including industrial voltages up to 690 V and can be used for applications requiring high overload abilities. The heart of the drive is DTC that provides accurate static and dynamic speed and torque control, high starting

torque and long motor cables. Basically, the drive is composed of a rectifier, DC link and filter, and an inverter. All are in one package and can be installed without any additional cabinet or enclosure. Furthermore, the internal fan is used for cooling. Some of specifications of this drive are presented in Table 5-1. The drive operates with variable switching frequency scheme and the average value is 3 kHz.

Table 5-1: Specifications of ABB drive ACS800-U11-0020-5 [115].

Parameter	*K*ρ (W s^2/m^4)
Input Voltage	3-phase, 380 to 480 (500) V
Input Current	27 (29) A
Input Frequency	48 to 63 Hz
Fundamental Power Factor Connection	0.98 (at nominal load)
Output Voltage	3-phase, 0 to input voltage
Output Current	29 (31) A
Output Frequency	0 to 300 Hz
Frequency Resolution	0.01 Hz
Switching Frequency	3 kHz (average)
Efficiency	98% at nominal power level

Fig. 5-1 shows the output current and voltage of a drive in DTC mode supplying to a 7.5 hp squirrel-cage induction motor at full load.

Fig. 5-2(a) shows the harmonic content of the output voltage. The spectra range up to a harmonic order of 1000 have been shown in Fig. 5-2(b). Note that the fundamental harmonic has been removed from the figure and other components are shown in terms of percentage of the fundamental magnitude. It is obvious that drive uses variable switching frequency scheme. Because of the fixed switching frequency scheme, the harmonics related to switching frequency should be dominant in the harmonic content.

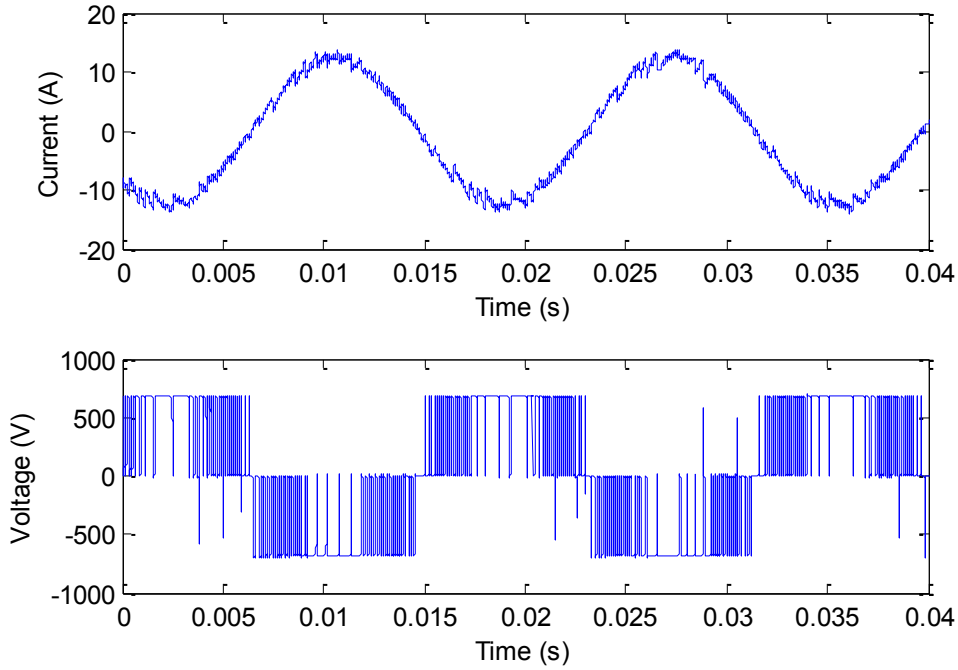

Fig. 5-1: Output current and voltage waveforms of DTC drive supplying a 7.5 hp IM at full load.

In this section, a brief introduction on scalar control and DTC is provided. However, the detailed discussion of these control strategies is not within the scope of this thesis.

5.3.1 Scalar Control

V/f scheme control is one of the well-known scalar control techniques that is commonly used in industrial AC drives and suitable for low performance applications such as pumps and fans. Scalar control is based on the steady-state model of the motor and does not depend on the machine's parameters. Therefore, this control scheme has been used in industry due to its robustness and simplicity [116].

In scalar control, the machine speed is controlled by changing the operating frequency which also affects the torque while the stator voltage magnitude is controlled to maintain constant airgap flux. To achieve these objectives, the ratio of voltage magnitude to frequency is kept constant. For low-speed operation where the frequency of operation is low, the voltage drop along the stator winding is significant which results in limitation on the generated stator flux. Therefore, to compensate the possible stator flux reduction and maintain the stator flux near to the nominal

value, a boost voltage is added to the reference amplitude of the phase voltage at lower frequencies [117, 118].

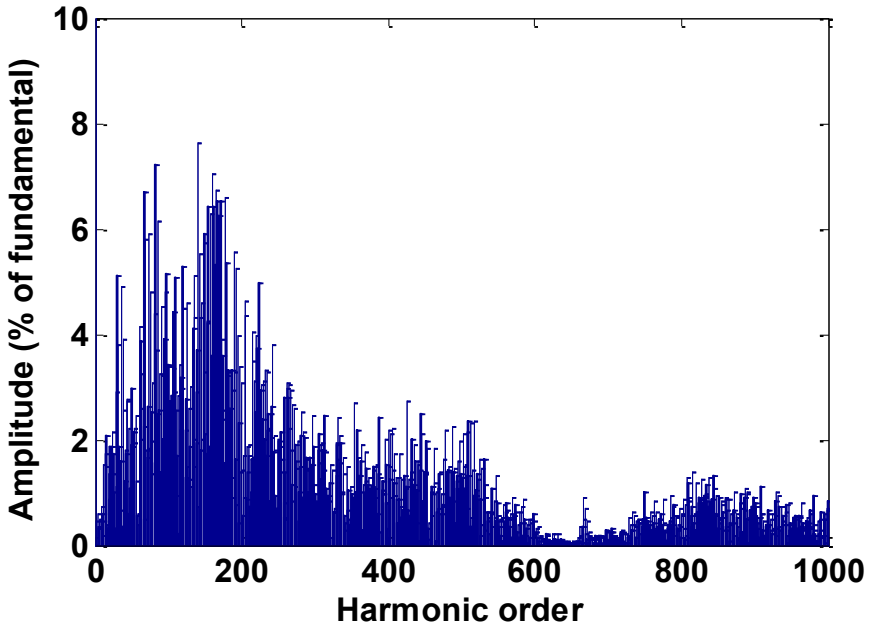

(a)

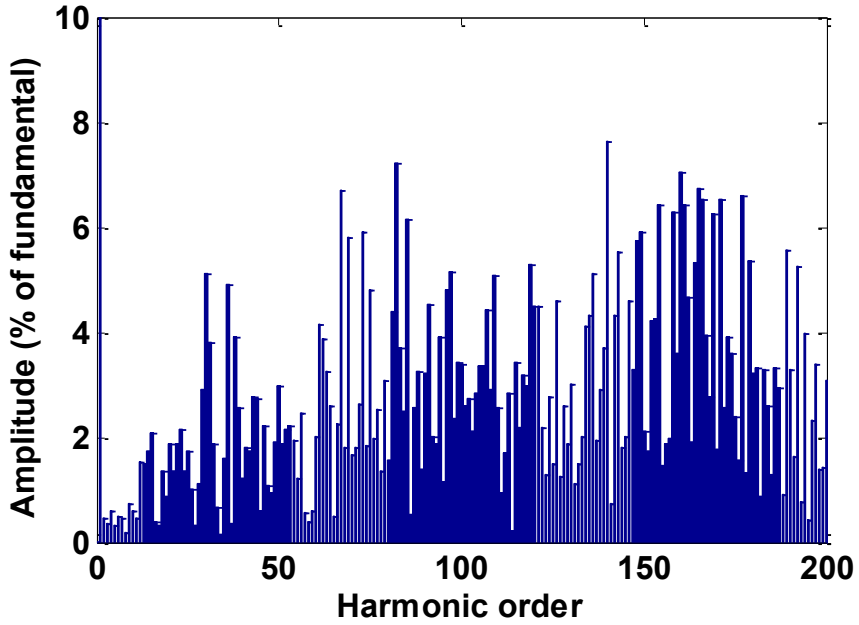

(b)

Fig. 5-2: Harmonic spectrum for the output voltage of DTC drive supplying a 7.5 hp IM at full load (a) Harmonic contents up to 1000th order, (b) Zoom-in spectrum.

In this scheme, the coupling of the motor's equation is neglected. For example, the variation of both the voltage and frequency simultaneously affect the flux and electromagnetic torque of the motor. In other words both torque and flux are functions of voltage or current and frequency. Therefore, the method is only suitable for adjustable-speed applications in which the accurate speed or position control similar to a servo system is not required. Moreover, the instantaneous torque control cannot be achieved by scalar control methods and suffers from poor transient response and poor controllability [119, 120].

5.3.2 Direct Torque Control

Direct torque control (DTC) was introduced in Japan by Takahashi and Nagochi [121] and also in Germany by Depenbrock [122] and first marketed by ABB. Fast dynamic response, possible sensorless operation and robustness to disturbances are the main advantages of DTC compared to scaler control. However, unlike scalar control, DTC requires high performance controllers such as digital signal processing (DSP) for its implementation [123].

DTC method strongly relies on the stator variables. In fact, the stator voltage is used to estimate the stator flux and the electromagnetic torque of the machine is estimated using the stator voltage and current. Therefore changing the stator voltage results in a rapid change of the stator flux. Since the rotor flux changes slowly, this will change the angle between the stator and rotor fluxes and as a results the torque will vary [123, 124].

The conventional DTC utilizes two hysteresis controllers. A two-level hysteresis controller is commonly utilized to control the stator flux, while a three-level hysteresis controller is used to control the torque. High steady state torque ripple is the main drawback of the conventional DTC [125].

In the modified DTC, the hysteresis controllers are replaced by PI controllers. Three PI controllers are used to control the speed, torque and flux. In this scheme, when the reference is determined by the user, the calculated speed error is supplied to the speed controller which gives the torque reference value. The difference between the torque reference and actual torque plus the difference between the calculated stator flux reference and actual flux are considered as the torque and stator flux errors which are respectively given to the corresponding PI controllers. The output

of these two controllers is used to determine the switching signals for a voltage source inverter driven by a sinusoidal pulse-width modulation (SPWM) [126, 127].

5.4 Experimental Setup

To study the effect of drive on the losses, four IMs are tested which their specifications are listed in Table 5-2.

Table 5-2: Motor Specifications.

Motor	M1	M2	M3	M4
Power (hp)	7.5	7.5	5	3
Rated Voltage (V)	460	460	460	460
Rated Current (A)	8.85	11	8	4.4
Frequency (Hz)	60	60	60	60
Winding Configuration	D	D	D	Y
Rated Speed (rpm)	1755	1755	1730	1740
NEMA Design	B	B	B	B
Poles	4	4	4	4

Among these motors, Motor M2 and M3 are designed for direct-fed applications and Motor M1 and M4 are designed for PWM applications. Many if the motor manufacturers offer three-phase, general-purpose, premium efficiency motors that feature “inverter-friendly” insulation systems. These machines are designed by including more iron and copper materials than those used in conventional electric motors. In particular, increasing the mass and cross section of the copper coils can increase the efficiency by reducing the resistance of the windings. Furthermore, thanks to the new technologies, the fill factor in the slots are increased which helps increasing the conductor size in the same slot area. Other characteristics of these motors to ensure higher efficiency are:

- Thinner laminations of improved steel properties
- Reduced air gap
- Optimized cooling fan designs
- Special & improved bearings

Moreover, the motors designed for PWM application should be able to withstand the voltage spike produced by the inverter.

All the conducted tests are based on IEEE Std. 112. To measure the input power, voltage, and current at the terminals of IMs, a digital Yokogawa WT3000 Precision Power Analyzer is employed. As the load, a resistor bank is connected to the 13-kW dynamometer coupled to IM. The load is controlled by the field circuit of the dynamometer. A torque transducer mounted on the IM's shaft and a multichannel signal conditioner are utilized to measure the shaft torque and speed. A programmable power supply is used to generate the sin wave in the direct-fed condition and an industrial ABB drive is used to supply the IM in drive-fed mode. This setup and the ABB drive are shown in Fig. 5-3. A block diagram of the experimental setup is also presented in Fig. 5-4.

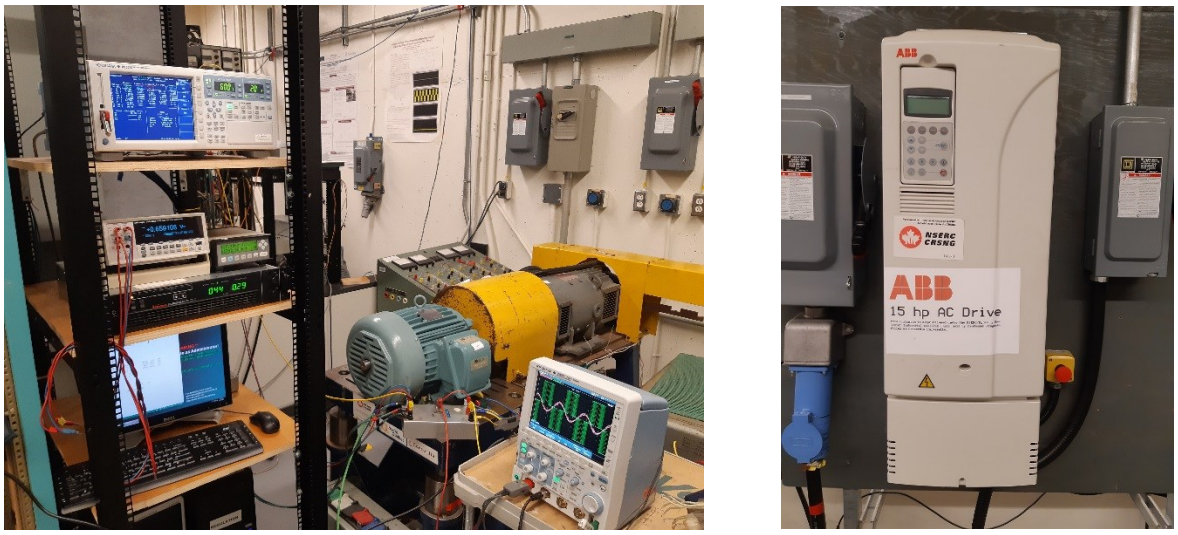

Fig. 5-3: Experimental Setup and ABB Drive.

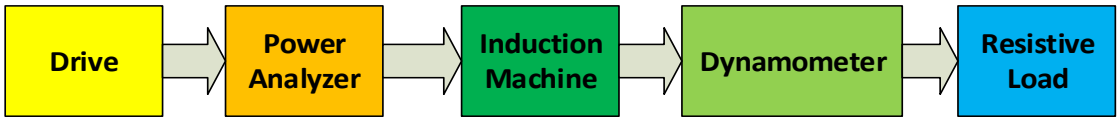

Fig. 5-4: Block diagram of the experimental setup..

This industrial drive can operate in two modes: DTC and scalar control. For both control techniques the load torque on the induction machine is maintained constant. However, with DTC alone the IM speed is also controlled.

In the next sections, the no-load and loading tests are performed in direct-fed and drive-fed modes and the results are compared.

5.5 No-Load Losses

IEEE Std-112 and IEC 600034-2 suggest to determine the core loss (P_{fe}) and friction and windage loss (P_{FW}) by conducting the no-load test. In this process, it is assumed that there is no stray load loss at no-load and the rotor resistive loss is negligible due to a rotor speed close to the synchronous speed. Therefore, when stator resistive loss (P_{SCL}) is subtracted from the input power, the result will be the summation of P_{fe} and P_{FW}. This summation is sometimes called the constant losses of IM and assumed as a load-independent. By loading the machine, the rotor speed decreases and P_{FW} slightly reduces, however the increase of P_{fe} with load compensates this reduction. Furthermore, the increase of P_{fe} with load is normally larger than the reduction of P_{FW}. These extra losses are considered part of the stray load loss (P_{SLL}) [94]. To segregate P_{FW} and P_{core}, their summation is measured at no-load at different voltages starting from the rated value to down by proper steps and then plotted versus squared voltage. Five or six points are normally sufficient for this purpose. By linear regression analysis of the last three points, the intersection of the line with zero voltage axis gives the P_{FW}.

Harmonics generated by ASDs may change the no load losses. For comparison purposes, the no load test is conducted for all IMs listed in Table 5-2 as described in IEEE Std-112. Then the machine is driven in a scalar control mode. The reason for using only the scalar control mode is the fact that the machine speed is not controlled by the drive and also only the rated voltage and frequency are applied to the motor, while in DTC mode, the speed of the machine should be determined by the user.

Table 5-3 shows the no-load test results for direct-fed and drive-fed modes. According to the results, there is a negligible change in P_{SCL}. By subtracting P_{SCL} from the no-load input power, an increase of the other losses (summation of P_{FW} and P_{fe}) can be observed. Assuming that P_{FW} is constant for both conditions the direct-fed and drive-fed modes and by neglecting the P_{RCL}, this increase can be assigned to P_{fe}. Constant P_{FW} is a valid assumption because the speed at both conditions is almost the same and the P_{FW} is independent of harmonics. Furthermore, based on IEEE Std-112, P_{SLL} is considered load-dependent and zero at no-load, therefore, all no-load extra

losses except for P_{SCL} variation in case of drive-fed are assigned as additional core losses due to harmonics.

Table 5-3: No-load test results.

	Machine	M1	M2	M3	M4
	P_{FW}	47.73	57.21	32.63	26.63
Direct-fed	P_{SCL}	20.17	27.57	35.02	29.02
	P_{fe}	98.3	234.42	82.85	110.91
Drive-fed	P_{SCL}	20.51	26.78	34.11	29.02
	P_{fe}	132.56	265.81	103.36	132.83
Comparison	P_{fe} increase (%)	34.85	13.39	24.76	19.76
	P_{fe} increase (W)	34.26	31.39	20.51	21.92

The comparison between the two scenarios shows that different core losses increase for each IM. For example, motors M1 and M2 with 7.5 hp rated power have 98.3 W and 234.42 W core loss in direct-fed mode, while they experience 34.26 W and 31.39 W core loss increase respectively in drive-fed mode. This is respectively equal to 34.85% and 13.39% increase of the core loss in drive-fed mode. For motor M4 with 3 hp, this increase is 21.92 W (19.76%) compared to 20.51 W (24.76%) for motor M3 (5 hp). This clearly shows that it is not possible to predict the increase in the core loss only based on the machine rated power and it cannot be expected to same percentage of P_{fe} increase for all machines.

To find a relationship between the core loss increase and machine parameters, the conventional equivalent circuit parameters of each machine are extracted from the no-load and locked rotor tests based on IEEE Std-112. They are shown in Table 5-4.

Table 5-4: Equivalent circuit parameters.

	M1	M2	M3	M4
R_1 (Ω)	2.475	1.5776	3.3976	1.88
X_1 (Ω)	6.354	6.265	9.942	3.642
X_m (Ω)	268.54	183.95	233.62	114.81
R_{fe} (Ω)	6177.2	2542.88	6311.66	1782.47
R_2 (Ω)	2.278	2.247	4.474	1.391

To calculate X_2, the ratio of X_1/X_2 is determined based on the machine NEMA design. To analyze a drive-fed IM, the harmonic equivalent circuit rather than conventional equivalent circuit is required. In this paper, it is assumed that the harmonic analysis has the same configuration as conventional one. It is shown in Fig. 5-5.

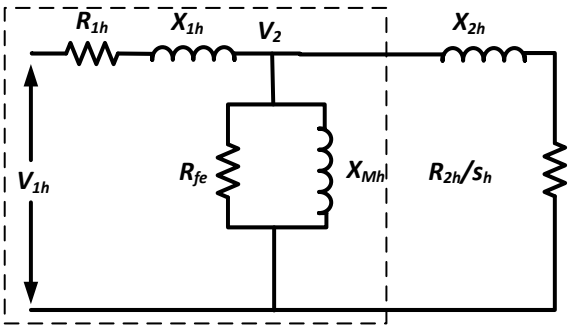

Fig. 5-5: Harmonic equivalent circuit.

In the harmonic equivalent circuit, it is assumed that R_{fe} is constant at all harmonics. Furthermore, the skin effect of stator resistance (R_1) can be neglected for IMs with small and medium rated powers ($R_{1h} = R_1$), because the cross-section of the stator conductors is small and for larger cross-sections, multiple wires rather than single wire are utilized. Although the initial goal of using multiple wires is to increase the fill factor of slots and ease placing the coils in the slots, however reduction of skin effect at higher harmonics can be considered as an additional advantage.

The leakage and magnetizing inductances, can be expressed as follows:

$$X_{1h} = h\, X_1 \tag{5-1}$$

$$X_{Mh} = h\, X_M \tag{5-2}$$

where the h is the order of harmonic. In this section, only the no-load test is studied, hence the rotor part of the equivalent circuit is not discussed. To predict the core loss at no-load, the rotor part of the equivalent circuit is removed from the calculation. The drive output voltage harmonic is measured at no-load and applied to the circuit and the dissipated power on R_{fe} is calculated. Table 5-5 shows the estimated P_{fe} from the equivalent circuit.

Table 5-5: Estimated and measured P_{fe}.

Machine	M1	M2	M3	M4
Estimated P_{fe} (W)	121.1	260.43	104.24	124.85
Measured P_{fe} (W)	132.56	265.81	103.36	132.83

To calculate these values, only the harmonics of order 6n ± 1 have been used. The reason for this has been clearly mentioned in [108]. According to the results, the predicted values are sufficiently close to the measured values.

5.6 Load Test and Stray Load Loss

IEEE Std-112 Method A suggests to conduct the load test to determine the efficiency of an IM by direct measurement of the input and output powers. In addition, using the P_{FW} and P_{fe} from the no-load test, Method B of IEEE Std-112 can be applied to segregate the losses and determine the P_{RCL} and P_{SLL}. Fig. 5-6 shows the measured efficiency for the four IMs using method A in three modes: Direct-fed, DTC drive-fed and Scalar Control drive-fed IMs.

To make a fair comparison, the following measures are adapted:

- Based on the procedure described in IEEE Std-112, before recording the required data, the IMs should be run for a long time to reach the thermal stability. In chapter 3 and ref. [128], it is shown that, at constant load, the machine efficiency reduces after start due to heating. Therefore, reaching thermal stability is essential for all three modes before recording data.
- The efficiency is measured at 25, 50, 75 and 100% of the rated output power. In all three modes, the output power rather than shaft torque is kept constant during experiment.
- In direct-fed and scalar drive-fed modes, there is no speed control and the speed is measured at the corresponding load value.
- In scalar control drive-fed mode, the frequency of the output voltage is adjusted to the rated value at all loads.
- In DTC fed-mode, the machine speed is controlled by the drive and set to the corresponding measured speed in direct-fed mode.

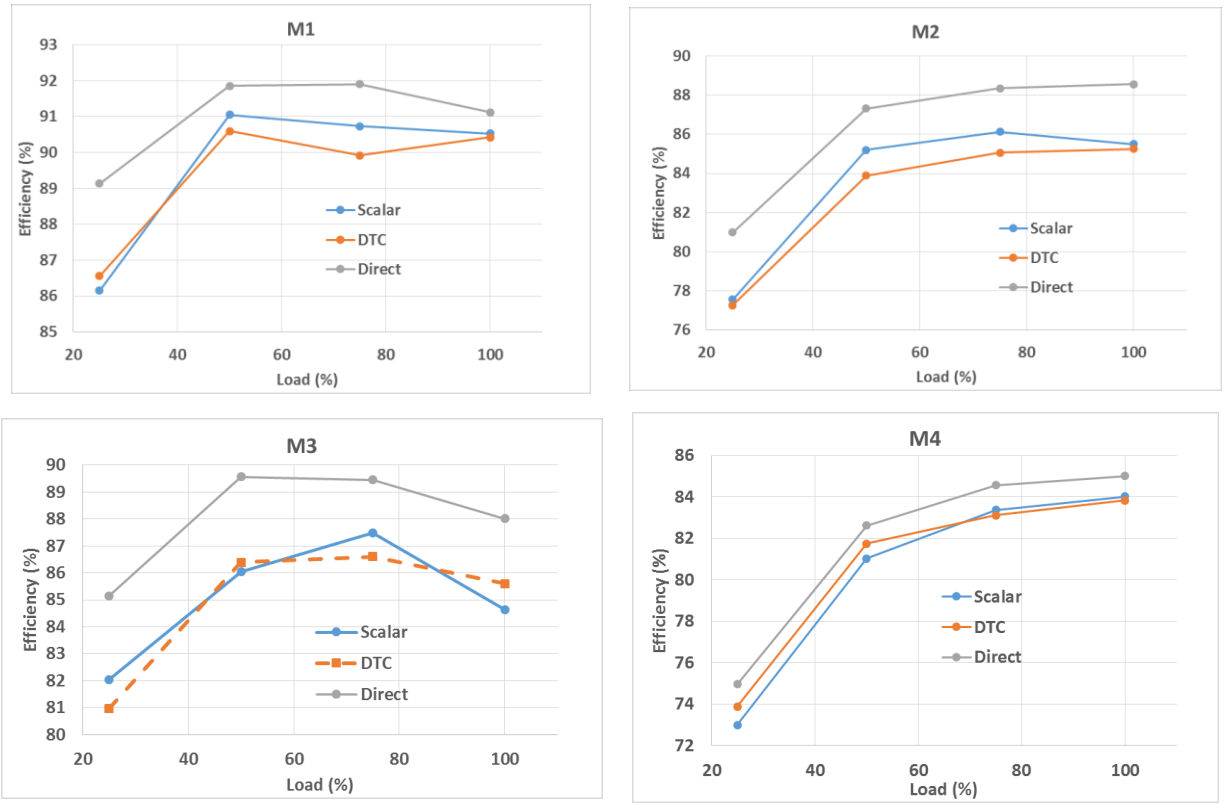

Fig. 5-6: Measured efficiency using Method A of IEEE Std-112.

According to Fig. 5-6, the efficiency of the IMs is reduced in the drive-fed mode compared to the direct-fed mode. In general, it can be expected that at high loads, the measured efficiency at DTC-fed mode is less than scaler drive-fed mode, but this is not valid for lower loads. The reduction of the efficiency for IMs in drive-mode conditions is already proven in previous literatures, however the interesting point of these experiments is the amount of efficiency reduction for each motor. Fig. 5-7 shows the amount of efficiency reduction in each mode.

According to Fig. 5-7, motors M2 and M3 suffer 2.5 to 4% efficiency reduction, while it is less than 2% for motors M1 and M4. In particular for the rated load, motors M2 and M3 experience more than 2.5% efficiency reduction while this reduction for motors M1 and M4 is around 1% . This is an important advantage since most of the IMs work close to the full load condition.

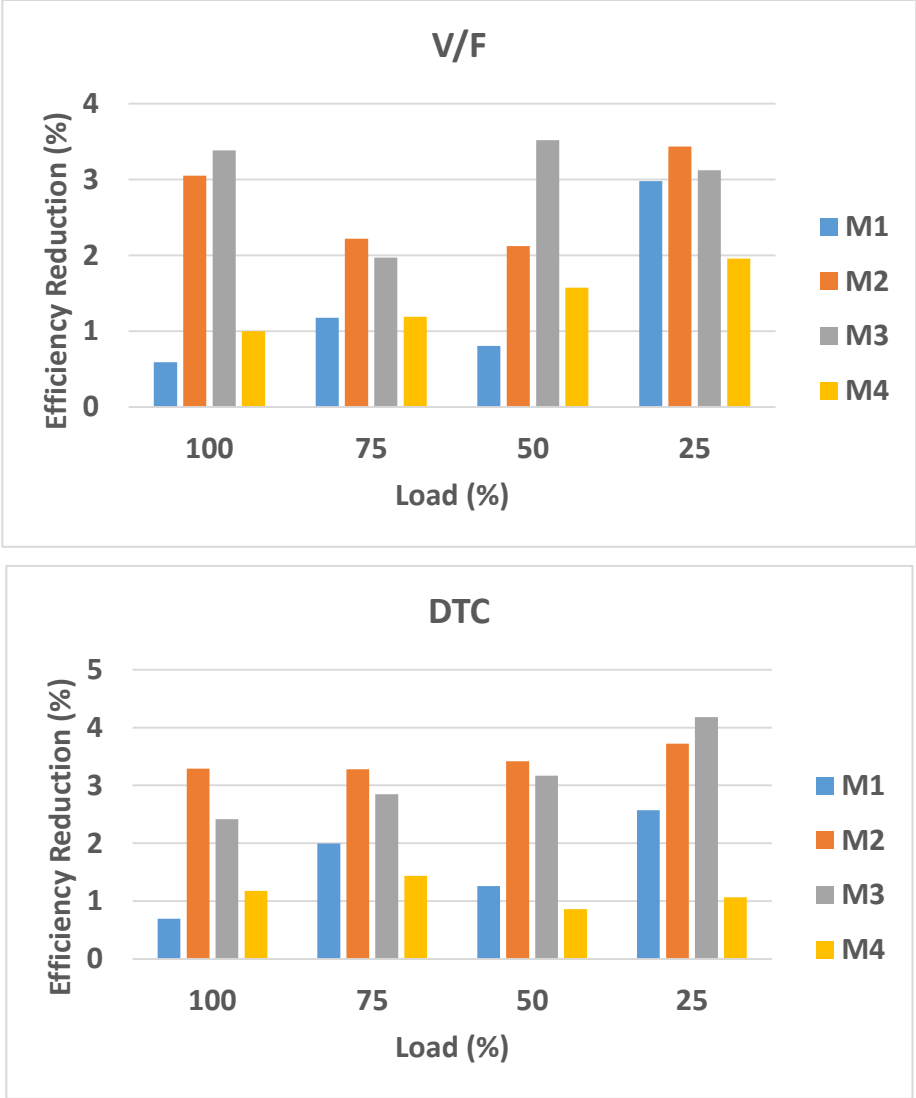

Fig. 5-7: Efficiency reduction in DTC and scaler drive (V/F) modes.

To study the effect of drives on the losses, the form B2 Method B of IEEE Std-112 is used to segregate the losses at full load condition and the results are presented in Table 5-6. For this purpose, the measured P_{fe} in the direct-fed no load is used in direct-fed load test and the measured P_{fe} in drive-fed no load is used in both DTC and scalar drive-fed load tests.

First, P_{SCL} is determined by using the measured input current and stator resistances at load condition. The results show that the variation of P_{SCL} is small and raised by about 5 to 10% of the direct-fed mode for scalar mode and less than 5% of direct-fed mode for DTC mode.

Table 5-6: Loss segregation results at rated load.

Motor	M1			M2			M3			M4		
Losses (W)	P_{SCL}	P_{RCL}	P_{SLL}	P_{SCL}	P_{RCL}	P_{SLL}	P_{SCL}	P_{RCL}	P_{SLL}	P_{SCL}	P_{RCL}	P_{SLL}
Direct-fed	215.6	123.58	62.54	164.67	143.8	127	178.34	127.8	73.93	120.25	54.79	83
Scalar	225	131.3	61	178.73	161	286	192.5	145	200	128.27	60	80.4
DTC	220	123.3	74	173.38	150.41	320	184.95	132	175	121.92	56.26	94.31

Furthermore, P_{RCL} variations are also negligible. In form B2 of IEEE Std-112, the electromagnetic power and slip are used to calculate P_{RCL}. For this purpose, the electromagnetic power is obtained by subtracting the measured P_{SCL} at the corresponding load and measured P_{fe} at no-load. Based on Table 5-6, P_{RCL} in DTC drive-fed mode is higher than direct-fed mode while in scaler drive-fed mode, it is higher than DTC drive-fed mode. The reason for this is that in scalar mode, the speed of the machine is less than that of the DTC. Moreover, for DTC drive-fed and direct-fed modes in which the speed is equal, the electromagnetic power is higher in drive-fed mode due to additional input loss to compensate extra losses.

To estimate P_{SLL}, indirect measurement is used which is based on the original definition of P_{SLL} provided by IEEE Std-112. It means that the P_{SLL} is estimated by subtracting all pervious losses (P_{SCL}, P_{RCL}, P_{fe} and P_{FW}) from the total losses achieved from the input and output powers difference. According to the results, P_{SLL} increases by 10-20% for motors M1 and M4 while this value is more than 100% for motors M2 and M3.

5.7 Discussion of Results

In terms of efficiency and loss variation, the following conclusion can be made for this work:

- The efficiency reduction of IM can be expected in case of the drive-fed mode operation compared to the direct-fed mode operation.
- For the same drive system, the amount of efficiency reduction depends on the machine design (Motor M1 and M2).
- IMs designed for PWM application experience a smaller amount of efficiency reduction compared to IMs designed for direct-fed application.
- Application of drive affects both load-independent and load-dependent losses.

- Drive-fed no load test can be utilized to determine the effect of drive on independent loss.
- Since P_{FW} is not affected by the drive, the increase in core loss by drive can be extracted from the difference of no-load test losses at direct-fed and drive-fed modes.
- Drive fed core loss can be predicted by applying the drive output voltage harmonic content to the harmonic equivalent circuit of the IM at no load condition by neglecting the rotor part.
- Machine designer experts can reduce the effect of drive by reducing the core loss value in the machine.
- All three load-dependent losses may increase by using the drive.
- P_{SCL} in drive-fed mode increases by 5-10% of the P_{SCL} in the direct-fed mode. By neglecting the skin effect, the slight rise in the machine's temperature and current in the drive-fed mode compared to direct-fed mode are the main reasons for this increase.
- P_{RCL} in drive-fed mode increases by 5-10% of the P_{RCL} in the direct-fed mode.
- P_{SLL} increase in drive-fed mode operation compared to direct-fed mode operation. This increase is around 10-20% for the PWM designed IMs, and more than 100% for direct-fed designed IMs.

5.8 Summary

In this chapter, the effects of an ASD on IM losses were studied to predict the drive-fed IM efficiency using the direct-fed results. Four IMs were tested in three modes: the direct-fed mode, scalar control mode and DTC mode. Among the IMs, two were designed for direct-fed applications and two IMs were designed for PWM applications. Based on the results, the efficiency reduction of IM could be expected in case of drive fed mode operation compared to direct-fed mode operation. For the same drive system, the amount of efficiency reduction depends on machine design. IMs designed for PWM application experienced a smaller amount of efficiency reduction compared to IMs designed for direct-fed application. Regardless of the machine design, in drive-fed mode, the core loss of the machine increased and could be predicted by applying drive output voltage harmonic content to the harmonic equivalent circuit of the IM at no load condition by neglecting the rotor part. P_{SCL} and P_{RCL} in drive-fed mode increased by 5-10% of the corresponding

values in direct-fed mode. P_{SLL} increased around 10-20% for the PWM designed IMs, and more than 100% for direct-fed designed IMs.

Chapter 6: Conclusions and Future Works

6.1 Conclusion

In chapter 1, the importance of the efficiency estimation of IMs was addressed and two international standards and five categories of the proposed methods in the literature were described. The advantages and drawbacks of each one in terms of capability to apply for in-situ application were presented. The objectives of this research work were presented which is to study the methods for in-situ efficiency determination of IMs.

In chapter 2, optimization-based algorithms as efficiency estimation methods with minimum intrusiveness were discussed in detail and a brief review of previous works was presented. The optimization-based algorithms could estimate the equivalent circuit parameters using the loading data of the machine and determine the efficiency by applying method F1 of IEEE Std-112. In terms of the efficiency and equivalent circuit parameters estimation, this chapter covered three subjects. First, the non-intrusive methods and techniques to determine the five parameters (R_1, X_2, s, P_{FW}, P_{SLL}) were discussed. This could reduce the number of variables of the problem which was important when only data of one operating point were used as input data of the algorithms. Then, a range determination of the remaining unknown parameters of the equivalent circuit (X_1, X_m, R_{fe}, R_2) was proposed. The proposed method was based on the machine nameplate data and empirical data of the no-load current of more than 100 IMs. The determined range could narrow the search space for the evolutionary algorithm and force it to look for the correct answer in a small search space. Therefore, this increased the probability of converging to a correct answer. Finally a genetic algorithm (GA) based efficiency estimation algorithm was proposed to evaluate the efficiency of working IMs using only data of one operating point. The proposed algorithm utilized two consecutive GAs to improve the accuracy of the results. The proposed algorithm was used to determine the efficiency at three conditions. In the first condition, the range of parameters was determined manually, but the output power term was added to the objective function of the problem to force the algorithm to the correct answer. In the second condition, the proposed range determination method was included in the algorithm, but the output power term was removed from

the objective function. In the last condition, both the parameter range determination and output power term in the objective function were included in the GA based proposed algorithm. The results show that using the output power could give better accuracy, but it resulted in a higher deviation in the estimated parameters. Applying the proposed range determination method without utilizing the output power in the objective function led to a better parameter estimation with the cost of lower accuracy. This was useful for in-situ applications where the output power was generally unknown. Using the output power in the objective function plus the proposed range determination showed results with higher accuracy. Moreover, it was proven that using the measured values of the friction and windage losses rather than the assumed values in the algorithm could improve the accuracy of the results. Furthermore, the modified equivalent circuit of the IM which included the friction and windage losses and stray load loss was utilized to improve the accuracy of the results. It was shown that, this strategy could slightly improve the accuracy of the results only if the output power term would have been used in the objective function. For in-situ applications where the output power was not available, the technique could cause high error due to the increase in the number of variables.

Chapter 3 dealt with two problems. First, the proposed parameter range determination method in chapter 2 was improved by using the operating data of the machine. The new proposed method was more effective than the previous method in terms of providing the smaller search space for evolutionary algorithms. The second problem was the long time requirement to reach the thermal stability of the electrical machines. In this chapter, it was shown that the temperature rise of the machine increased the losses in particular the resistive losses and reduced the efficiency of the machine. In other words, at a certain output power, by increasing the temperature of the machine, the input power of the machine increased in order to compensate the additional losses due to heating which resulted in an efficiency reduction. As a result, to have proper data for efficiency estimation purpose, it was necessary to record the data at thermally stable condition which might take several hours. To overcome this problem, a particle swarm optimization (PSO) based efficiency estimation algorithm was proposed in this chapter. The proposed algorithm utilized the data of the full load operation of the machine 30 minutes after start to estimate the equivalent circuit parameters. Then, two approaches were proposed to predict the temperature of the machine at a thermally stable condition. The first approach was based on the machine insulation class determined by the nameplate data. The second approach was based on the trend of

temperature rise during the first 30 minutes of the machine operation after start. For this purpose, during 30 minutes interval, the temperature rise of the machine was recorded every 10 minutes and by using a curve fitting tool, the full load temperature rise of the machine at thermally stable condition was predicted. The comparison between the estimated and experimental results showed that the proposed algorithm was successful to determine the equivalent circuit parameters. In terms of the estimated efficiencies, the second approach provided better results compared to the first approach. It was proven that a better prediction of the temperature resulted in a better estimation of the rotor speed and efficiency. Moreover, a very simple and straightforward approximation was used to evaluate the temperature of the machine at partial loads. This could be implemented by assuming a direct linear relationship between the machine losses and the temperature. This might not give accurate results of partial load temperature, but it provided more acceptable results compared to the condition that the full load temperature was considered for all loads.

In chapter 4, the challenges and difficulties of using two-dimensional (2D) finite element analysis (FEA) to estimate the efficiency of IMs were addressed. Two methodologies were adopted. The first methodology was based on the direct calculation of the machine losses from FEA results. For this purpose, the FEA model should be run at any desired load to estimate the losses and efficiency at that load. By reviewing the literature on the effect of cutting and punching the lamination on core loss variation, it was recommended to consider 20-30% increase for the estimated core loss using FEA to improve the accuracy of the results. In the second methodology, first, the equivalent circuit parameters of the machine were extracted by implementing the DC, no-load and locked rotor tests of the machine in FEA model. Method F1 of IEEE Std-112 was then applied to the estimated parameters to predict the efficiency at any desired loads. To achieve the results with an acceptable accuracy, it was mandatory to add the stator end winding and rotor end rings inductances and resistances to the 2D FEA model. In particular, due to the significant effect of the stator resistive losses on the efficiency of the machine, accurate estimation of the stator end winding resistance was essential. Moreover, although the magnetizing reactance did not directly contribute to the losses, it affected however other losses particularly at lower loads. Since, the mechanical loss (known in this thesis as the total of friction and windage losses) was not included in the FEA model, a simple formula based on the rated power of the machine was proposed to estimate the mechanical loss of the IMs with 4-pole and TEFC system operating at 60 Hz. This formula was obtained after testing more than 100 IMs in the power range of 1-500 hp.

In chapter 5, the effects of an industrial drive on various IMs were studied. Scalar control and direct torque control (DTC) which were known as two common control schemes were implemented in this work by using adjustable-speed drives (ASDs) from ABB. Four IMs were tested and among them, two IMs were designed for direct-fed applications and other two machines were designed for PWM applications. Based on the presented results, regardless of the IM type and control scheme, ASDs reduced the efficiency of the machine. However, the efficiency reduction for PWM designed IMs was less than the ones for direct-fed designed IMs. The core loss of the machine increased in case of the drive-fed condition and varied for each IM. The loss could however be predicted by applying the harmonic content of the output voltage of ASD to the no-load harmonic equivalent circuit. In the harmonic equivalent circuit at no-load, the rotor part of the circuit was removed. In drive-fed condition, the stator and rotor resistive losses were increased to about 5-10% compared to those losses in the direct-fed condition. In terms of stray load loss, there was a big difference between the drive- and direct-fed cases. The stray load loss increased to around 10-20% for the PWM designed IMs, while this increase was more than 100% for direct-fed designed IMs.

6.2 Proposed Future Works

In this section, based on the knowledge and experience achieved during this research work, the following subjects can be considered as future works.

6.2.1 Harmonic equivalent circuit model

Under direct-fed condition, the equivalent circuit parameters change due to the presence of harmonics. Although this subject has been addressed in the literature, the provided equivalent circuit methods lack the acceptable accuracy for efficiency estimation purpose. Furthermore, since different control schemes have different characteristics, it is essential to develop a comprehensive harmonic equivalent circuit which can be applied to the IMs regardless of the type of control scheme.

6.2.2 Prototyping a non-intrusive IM efficiency estimation tool for in-situ application

Several research works have been conducted to estimate the efficiency of the working induction machine, however implementing the proposed methods and prototyping the tools for

commercialization purposes have not received enough attention. Thus, it would be highly advantageous to prototype and build an industrial version of this tool.

6.2.3 Investigating the effect of torque ripple on the estimated output torque and efficiency

Increased torque ripple is one of the inevitable effects of harmonics on the machine performance. Presence of torque ripple causes fluctuations in the output and input powers. More torque ripple means more fluctuation for the measured torque and power. This can introduce some difficulties for measurement of the efficiency. So it is suggested to study the effect of torque ripple on the accuracy of measured efficiency and provide some solutions to overcome this problem and improve the accuracy of the results.

6.2.4 Design an embedded efficiency estimation for drive-fed application

Some of the ASDs need currents and/or voltages and speed measurements for their performance. Furthermore, a lot of research works have provided online temperature measurement and parameter estimation. This provides a good opportunity to develop an online efficiency estimation module inside the drives. On the other hand, the generated harmonics by ASDs introduce some difficulties to estimate the efficiency of the machine. It would be beneficial to investigate the possible methods to implement a method inside the drives to estimate the efficiency of the machine.

6.2.5 Stray load loss estimation using FEA

Stray load loss analysis with FEA is very difficult due to the fact that it originates from different sources. Although using the empirical results has been suggested by IEEE Std-112 and IEC 600034-2 Standards, it is evident that using them is not accurate for all machines. Since the FEA simulations have a detailed machine model including electrical, magnetic and geometric features, it can help in this regard.

References

[1] Xenergy, "United States Industrial Electric Motor Systems Market Opportunities Assessment," prepared for Oak Ridge Nat. Lab. and DOE's Office of Ind. Technol., Office of Energy Efficiency and Renewable Ey, U. S. Department of Energy, Washington D.C., 1998.

[2] "IEEE Standard Test Procedure for Polyphase Induction Motors and Generators," IEEE Std 112-2004, IEEE Power Engineering Society, New York, NY, 2004.

[3] "Rotating Electrical Machines - Part 2-1: Standard Methods for Determining Losses and Efficiency from Tests (Excluding Machines for Traction Vehicles). IEC 60034-2-1 (2007)," IEC, Geneva, Switzerland, 2007.

[4] "IEEE Recommended Practice for Testing Insulation Resistance of Rotating Machinery," IEEE Std 43-2000, New York, March 2000.

[5] "IEEE Standard Test Code for Resistance Measurement," IEEE Std 118-1978, New York, May 1978.

[6] "IEEE Recommended Practice for General Principles of Temperature Measurement as Applied to Electrical Apparatus," IEEE Std 119-1974, New York, 1975.

[7] "IEEE Master Test Guide for Electrical Measurements in Power Circuits," ANSI/IEEE Std 120-1989, 1989.

[8] E. B. Agamloh, "An evaluation of induction machine stray load loss from collated test results," *IEEE Trans. Ind. Appl,* vol. 46, no. 6, p. 2311–2318, Nov./Dec. 2010.

[9] P. Pillay, M. Al-Badri, P. Angers, and C. Desai, "A New Stray-Load Loss Formula for Small and Medium-Sized Induction Motors," *IEEE Trans. Energy Convers.,* vol. 31, no. 3, pp. 1221-1227, Sep. 2016.

[10] W. Cao, "Comparison of IEEE 112 and new IEC standard 60034-2-1," *IEEE Transactions on Energy Conversion,* vol. 24, no. 3, pp. 802-808, September 2009.

[11] J. S. Hsu, J. D. Kueck, M. Olszewski, D. A. Casada, P. J. Otaduy, and L. M. Tolbert, "Comparison of induction motor field efficiency evaluation methods," *IEEE Transaction on Industry Applications,* vol. 34, no. 1, p. 117–125, Feb. 1998.

[12] J. D. Kueck, "Development of a method for estimating motor efficiency and analyzing motor condition," in *Conference Record of 1998 Annual Pulp and Paper Industry Technical Conference*, Portland, ME, USA, 1998.

[13] B. Lu, T. Habetler, and R. Harley, "A survey of efficiency-estimation methods for in-service induction motors," *IEEE Transactions on Industry Applications,* vol. 42, no. 4, pp. 924-933, 2006.

[14] S. J. Chapman, Electric Machinery Fundamentals, Mc Graw Hill, 2004.

[15] [Online]. Available: http://circuitglobe.com/applications-of-induction-motor.html.

[16] F. Ferreira and A. T. de Almeida, "Considerations on in-field induction motor load estimation methods," in *IEEE International Conference on Electrical Machines*, 2008.

[17] J. R. Holmquist, J. A. Rooks and M. E. Richter, "Practical approach for determining motor efficiency in the field using calculated and measured values," *IEEE Transactions on Industry Applications,* vol. 40, no. 1, pp. 242-248, Jan.-Feb. 2004.

[18] "In-Plant Electric Motor Loading and Efficiency," Ontario Hydro.

[19] A. Dell'Aquila, L. Salvatore and M. Savino, "A New Test Method For Determination Of Induction Motor Efficiency," *IEEE Transactions on Power Apparatus and Systems,* Vols. PAS-103, no. 10, pp. 2961-2973, Oct. 1984.

[20] J. R. Willis, G. J. Brock and J. S. Edmonds, "Derivation of induction motor models from standstill frequency response tests," *IEEE Transactions on Energy Conversion,* vol. 4, no. 4, pp. 608-615, Dec. 1989.

[21] J. D. Kueck, M. Olszewski, D. A. Casada, J. Hsu, P. J. Otaduy, and L. M. Tolbert, "Assessment of methods for estimating motor efficiency and load under field conditions," Oak Ridge Nat. Lab., Oak Ridge, TN, Oak Ridge National Laboratory Rep., ORNL/ TM-13165, 1996.

[22] "Motors and Generators," NEMA MG1-2003 Standard, 2003.

[23] Y. El-Ibiary, "An accurate low-cost method for determining electric motors' efficiency for the purpose of plant energy management," *IEEE Transaction on Industry Applications,* vol. 39, no. 4, pp. 1205- 1210, Aug. 2003.

[24] R. Babau, I. Boldea, T. J. E. Miller and N. Muntean, "Complete Parameter Identification of Large Induction Machines From No-Load Acceleration–Deceleration Tests," *IEEE Transactions on Industrial Electronics,* vol. 54, no. 4, pp. 1962-1972, Aug. 2007.

[25] J. P. Bacher and F. Waldhart, "Determination of three phase induction machine efficiency from start up data," in *18th International Conference on Electrical Machines*, Vilamoura, 2008.

[26] L. A. Pereira, L. F. A. Pereira, S. Haffner, P. Sogari and M. Perin, "Estimation of parameters of induction machines from no-load starting without speed acquisition," in *IEEE International Electric Machines and Drives Conference (IEMDC)*, Miami, FL,, 2017.

[27] J. S. Hsu, B. P. Scoggins, "Field test of motor efficiency and load changes through air-gap torque," *EEE Transaction on Energy Conversion,* vol. 10, no. 3, pp. 477-483, Sep. 1995..

[28] J. S. Hsu and P. L. Sorenson, "Field assessment of induction motor efficiency through air-gap torque," *IEEE Transaction on Energy Conversion,* vol. 11, no. 3, pp. 489-494, Sep. 1996.

[29] Bin Lu, T. G. Habetler, and R. G. Harley, "A nonintrusive and in-service motor-efficiency estimation method using air-gap torque with considerations of condition monitoring," *IEEE Transaction on Industry Applications,* vol. 44, no. 6, pp. 1666-1674, Dec. 2008.

[30] P. Pillay, V. Levin, P. Otaduy and J. Kueck, "In - Situ Induction otor Efficiency Determination Using the Genetic Algorithm," *IEEE Transactions on Energy Conversion,* vol. 31, no. 4, pp. 326-333, December 1998.

[31] A. G. Siraki and P. Pillay,, "Comparison of Two Methods for Full-Load In Situ Induction Motor Efficiency Estimation From Field Testing in the Presence of Over/Undervoltages and Unbalanced Supplies," *IEEE Transactions on Industry Applications,* vol. 48, no. 6, pp. 1911-1921, Nov.-Dec. 2012.

[32] A. G. Siraki and P. Pillay, "An In Situ Efficiency Estimation Technique for Induction Machines Working With Unbalanced Supplies," *IEEE Transactions on Energy Conversion,* vol. 27, no. 1, pp. 85-95, March 2012.

[33] A. G. Siraki, P. Pillay and P. Angers, "Full Load Efficiency Estimation of Refurbished Induction Machines From No-Load Testing," *IEEE Transactions on Energy Conversion,* vol. 28, no. 2, pp. 317-326, June 2013.

[34] M. Al-Badri, P. Pillay, and P. Angers, "A Novel In Situ Efficiency Estimation Algorithm for Three-Phase IM Using GA, IEEE Method F1 Calculations, and Pretested Motor Data," *IEEE Trans. Energy Convers.,* vol. 30, no. 3, pp. 1092-1102, Sep. 2015.

[35] M. Al-Badri, P. Pillay and P. Angers, "A Novel Technique for In Situ Efficiency Estimation of Three-Phase IM Operating With Unbalanced Voltages," *IEEE Transactions on Industry Applications,* vol. 52, no. 4, pp. 2843-2855, July-Aug. 2016.

[36] Bin Lu, Thomas G. Habetler, and Ronald G. Harley, "A Nonintrusive Efficiency Estimation Method for In-Service Motor Testing using a Modified Induction Motor Equivalent Circuit," in *37th IEEE Power Electronics Specialists Conference*, 2006.

[37] B. Lu, W. Qiao, T. G. Habetler and R. G. Harley, "Solving Induction Motor Equivalent Circuit using Numerical Methods for an In-Service and Nonintrusive Motor Efficiency Estimation Method," Shanghai, 5th International Conference on Power Electronics and Motion Control , IPEMC 2006.

[38] V. P. Sakthivel, R. Bhuvaneswari and S. Subramanian, "Non-intrusive efficiency estimation method for energy auditing and management of in-service induction motor using bacterial foraging algorithm," *IET Electric Power Applications,* vol. 4, no. 8, pp. 579-590, September 2010.

[39] V. P. Sakthivel, R. Bhuvaneswari and S. Subramanian, "An accurate and economical approach for induction motor field efficiency estimation using bacterial foraging algorithm," *Elsevier, Measurement,* vol. 44, no. 4, pp. 674-684, May 2011.

[40] V. P. Sakthivel, R. Bhuvaneswari and S. Subramanian, "Bacterial foraging algorithm application for induction motor field efficiency estimation under unbalanced voltages," *Elsevier, Measuremen,* vol. 46, no. 7, pp. 2232-2237, August 2013.

[41] P. Sen, Principles of Electric Machines and Power Electronics, 2nd ed., John Wiley & Sons,, 1997.

[42] S. Corino, E. Romero, and L. Mantilla, "How the efficiency of induction motor is measured?," in *International Conference on Renewable Energy and Power Quality (ICREPQ)*, Santander, 2008.

[43] P. Cochran, Polyphase Induction Motors, Analysis: Design, and Application, CRC Press, May 17, 1989.

[44] L. Sang-Bin and T. G. Habetler, "An online stator winding resistance estimation technique for temperature monitoring of line-connected induction machines," *IEEE Transactions on Industry Applications,* vol. 39, no. 3, pp. 685-694, May-June 2003.

[45] K. D. Hurst and T. G. Habetler, "A comparison of spectrum estimation techniques for sensorless speed detection in induction machines," *IEEE Transactions on Industry Applications,* vol. 33, no. 4, pp. 898-905, Jul/Aug 1997.

[46] K. D. Hurst and T. G. Habetler, "Sensorless speed measurement using current harmonic spectral estimation in induction machine drives," *IEEE Transactions on Power Electronics,* vol. 11, no. 1, pp. 66-73, Jan 1996.

[47] A. I. de Almeida, F. J. T. E. Ferreira, J. F. Busch, and P. Angers, "Comparative analysis of IEEE 112-B and IEC 34–2 efficiency testing standards using stray load losses in low-voltage three-phase, cage inductionmotors," *IEEE Trans. Ind. Appl,* vol. 38, no. 2, pp. 608-614, Mar./Apr. 2002.

[48] A. Boglietti, A. Cavagnino, M. Lazzari, and M. Pastorelli, "International standards for the induction motor efficiency evaluation: A critical analysis of the stray-load loss determination," *IEEE Trans. Ind. Appl.,* vol. 40, no. 5, p. 1294–1301, Sept./Oct. 2004.

[49] "Rotating Electrical Machines—Part 2: Methods for Determining Losses and Efficiency of Electrical Machinery From Tests (Excluding Machines for Traction Vehicles) With Amendments 1: 1995 and 2: 1996," IEC Std 60 034-2, 1972.

[50] M. Al-Badri, P. Pillay, and P. Angers, "A Novel Algorithm for Estimating Refurbished Three-Phase Induction Motors Efficiency Using Only No-Load Tests," *IEEE Trans. Energy Convers.,* vol. 30, no. 2, pp. 615-625, June 2015.

[51] K. Venkatesan and J. Lindsay, "Comparitive study of losses in voltage and current source inverted fed induction motors," *IEEE Transactions on Industry Applications,* Vols. IA-18, no. 3, pp. 240-246, 1982.

[52] R. L. Haupt and S. E. Haupt, Practical Genetic Algorithms, 2nd ed., Hoboken, NJ, USA: Wiley, 2004.

[53] J. Faiz and M. Ghasemi Bijan, "Estimation of induction machine inductances using three-dimensional magnetic equivalent circuit," *IET Electric Power Applications,* vol. 9, no. 2, pp. 117-127, February 2015.

[54] M. Chirindo, M. A. Khan and P. S. Barendse, "Considerations for Nonintrusive Efficiency Estimation of Inverter-Fed Induction Motors," *IEEE Transactions on Industrial Electronics,* vol. 63, no. 2, pp. 741-749, Feb. 2016.

[55] A. M. N. Lima, C. B. Jacobina and E. B. de Souza Filho, "Nonlinear parameter estimation of steady-state induction machine models," *IEEE Transactions on Industrial Electronics,* vol. 44, no. 3, pp. 390-397, Jun. 1997.

[56] M. Al-Badri, P. Pillay and P. Angers, "Induction machine rapid performance tests," in *IEEE Energy Conversion Congress and Exposition (ECCE),*, Cincinnati, OH, 2017.

[57] L. Alberti and N. Bianchi, "A Coupled Thermal–Electromagnetic Analysis for a Rapid and Accurate Prediction of IM Performance," *IEEE Transactions on Industrial Electronics,* vol. 55, no. 10, pp. 3575-3582, Oct. 2008.

[58] C. Kral, A. Haumer and T. Bauml, "Thermal Model and Behavior of a Totally-Enclosed-Water-Cooled Squirrel-Cage Induction Machine for Traction Applications," *IEEE Transactions on Industrial Electronics,* vol. 55, no. 10, pp. 3555-3565, Oct. 2008.

[59] T. A. Jankowski et al., "Development and Validation of a Thermal Model for Electric Induction Motors," *IEEE Transactions on Industrial Electronics,* vol. 57, no. 12, pp. 4043-4054, Dec. 2010.

[60] N. Jaljal, J. F. Trigeol and P. Lagonotte, "Reduced Thermal Model of an Induction Machine for Real-Time Thermal Monitoring," *IEEE Transactions on Industrial Electronics,* vol. 55, no. 10, pp. 3535-3542, Oct. 2008.

[61] M. Ghasemi Bijan, M. Al-Badri, P. Pillay and P. Angers, "Induction Machine Parameter Range Constraints in Genetic Algorithm Based Efficiency Estimation Techniques," in *IEEE International Electric Machines & Drives Conference (IEMDC)*, Miami, FL, USA, May 2017.

[62] R. C. Eberhart and J. Kennedy, "A new optimizer using particle swarm theory," in *6th Int. Symp. Micromachine Human Sci.*, Nagoya, Japan, 1995.

[63] Kwang Y. Lee, Mohamed A. El-Sharkawi, "Chapter 4 Fundamentals of Particle Swarm Optimization Techniques," in *Modern Heuristic Optimization Techniques: Theory and Applications to Power Systems*, Wiley-IEEE Press, January 2008.

[64] J. H. Lee, J. Y. Song, D. W. Kim, J. W. Kim, Y. J. Kim and S. Y. Jung, "Particle Swarm Optimization Algorithm With Intelligent Particle Number Control for Optimal Design of Electric Machines," *IEEE Transactions on Industrial Electronics,* vol. 65, no. 2, pp. 1791-1798, Feb. 2018.

[65] A. P. Engelbrecht, "Particle Swarm Optimization: Global Best or Local Best?," in *2013 BRICS Congress on Computational Intelligence and 11th Brazilian Congress on Computational Intelligence, Ipojuca*, Recife, Brazil, 2013.

[66] Y. Shi and R. Eberhart, "A modified particle swarm optimizer," in *Proceedings of IEEE International Conference on Evolutionary Computation (ICEC'98)*, Anchorage, 1998.

[67] Y. Shi and R. Eberhart, "Parameter selection in particle swarm optimization.," in *Proceedings of the 1998 Annual Conference on Evolutionary Programming*, San Diego, 1988.

[68] H. Yoshida, K. Kawata, Y. Fukuyama, S. Takayama and Y. Nakanishi, "A particle swarm optimization for reactive power and voltage control considering voltage security assessment," *IEEE Transactions on Power Systems ,* vol. 15, no. 4, p. 1232–1239, November 2000.

[69] S. Naka, T. Genji, T. Yura, and Y. Fukuyama, "A hybrid particle swarm optimization for distribution state estimation," *IEEE Transactions on Power Systems,* vol. 18, no. 1, p. 60–68, February 2003.

[70] C. I. McClay and S. Williamson, "The variation of cage motor losses with skew," *IEEE Transactions on Industry Applications,* vol. 36, no. 6, pp. 1563-1570, Nov/Dec 2000.

[71] P. C. Sen, "Principles of Electric Machines & Power Electronics", 2nd ed., John Wiley & Sons, 1999.

[72] J Faiz, M Ghasemi Bijan, B Mahdi Ebrahimi, "Modeling and Diagnosing Eccentricity Fault Using Three-dimensional Magnetic Equivalent Circuit Model of Three-phase Squirrel-cage Induction Motor," *Electric Power Components and Systems,* vol. 43, no. 11, pp. 1246-1256, June 2015.

[73] J. Faiz, M. Keravand, M. Ghasemi-Bijan, S. M.Â.Cruz and M. Bandar-Abadib, "Impacts of rotor inter-turn short circuit fault upon performance of wound rotor induction machines," *Electric Power Systems Research,* vol. 135, pp. 48-58, June 2016.

[74] J. Faiz, B. M. Ebrahimi, B. Akin and H. A. Toliyat, "Comprehensive Eccentricity Fault Diagnosis in induction motors using finite element," *IEEE Transactions on Magnetics,* vol. 45, no. 3, pp. 1764-1767, March 2009.

[75] J. Bacher, F. Waldhart and A. Muetze, "3-D FEM Calculation of Electromagnetic Properties of Single-Phase Induction Machines," *IEEE Transactions on Energy Conversion,* vol. 30, no. 1, pp. 142-149, March 2015.

[76] "Rotating Electrical Machines - Part 2-1: Standard Methods for Determining Losses and Efficiency from Tests (Excluding Machines for Traction Vehicles)," IEC 60034-2-1 (2007), Geneva, Switzerland, 2007.

[77] E. B. Agamloh, "An evaluation of induction machine stray load loss from collated test results," *IEEE Trans. Ind. Appl,* vol. 46, no. 6, p. 2311–2318, Nov./Dec. 2010.

[78] Juha Pyrhonen, Tapani Jokinen and Valeria Hrabovcova, Design of Rotating Electrical Machines, 2nd Edition, Wiley & Sons, Ltd., 2013.

[79] SKF, "General catalogue from SKF. Catalogue 4000/IV E," 1994.

[80] L. Veg, J. Laksar and J. Sobra, "Verification of actual mechanical losses on the rotor of induction machine," in *IEEE Conference on Energy Conversion (CENCON)*, Kuala Lumpur, 2017.

[81] M. Al-Badri, P. Pillay and P. Angers, "A Novel In Situ Efficiency Estimation Algorithm for Three-Phase IM Using GA, IEEE Method F1 Calculations and Pre-Tested Motor Data," *Energy Conversion, IEEE Transactions on,* vol. 30, no. 3, pp. 1092-1102, Sept. 2015.

[82] M. Ibrahim and P. Pillay, "Core Loss Prediction in Electrical Machine Laminations Considering Skin Effect and Minor Hysteresis Loops," *IEEE Transactions on Industry Applications,* vol. 49, no. 5, pp. 2061-2068, Sept.-Oct. 2013.

[83] W. M. Arshad, T. Ryckebush, A. Broddefalk, F. Magnussen, H. Lendenmann and M. Lindenmo, "Characterization of electrical steel grades for direct application to electrical machine design tools," *Journal of Magnetism and Magnetic Materials,* vol. 320, no. 20, pp. 2538-2541, October 2008.

[84] M. Emura, F.J.G. Landgraf, W. Ross and J.R. Barreta, "The influence of cutting technique on the magnetic properties of electrical steels," *Journal of Magnetism and Magnetic Materials,* Vols. 254-255, pp. 358-360, January 2003.

[85] W. M. Arshad, T. Ryckebush, F. Magnussen, H. Lendenmann, "Incorporating lamination processing and component manufacturing in electrical machine design tools," in *IEEE Industry Applications Annual Meeting*, New Orleans, LA, 2007.

[86] H. Naumoski, B. Riedmüller,A. Minkow and U. Herr, "Investigation of the influence of different cutting procedures on the global and local magnetic properties of non-oriented electrical steel," *Journal of Magnetism and Magnetic Materials,* vol. 392, pp. 126-133, October 2015.

[87] P. Baudouin, M. De Wulf, L. Kestens and Y. Houbaert, "The effect of the guillotine clearance on the magnetic properties of electrical steels," *Journal of Magnetism and Magnetic Materials,* vol. 256, no. 1-3, pp. 32-40, January 2003.

[88] A.J. Moses, N. Derebasi, G. Loisos and A. Schoppa, "Aspects of the cut-edge effect stress on the power loss and fux density distribution in electrical steel sheets," *Journal of Magnetism and Magnetic Materials,* Vols. 215-216, pp. 690-692, June 2000.

[89] M. Hofmann, H. Naumoski, U. Herr and H. Herzog, "Magnetic Properties of Electrical Steel Sheets in Respect of Cutting: Micromagnetic Analysis and Macromagnetic Modeling," *IEEE Transaction on Magnetics,* vol. 52, no. 2, pp. 1-14, Feb. 2016.

[90] S. Steentjes, G. von Pfingsten and K. Hameyer, "An Application-Oriented Approach for Consideration of Material Degradation Effects Due to Cutting on Iron Losses and Magnetizability," *IEEE Transactions on Magnetics,* vol. 50, no. 11, pp. 1-4, Nov. 2014.

[91] P. Baudouin, A. Belhadj, F. Breaban, A. Deffontaine and Y. Houbaert, "Effects of laser and mechanical cutting modes on the magnetic properties of low and medium Si content nonoriented electrical steels," *IEEE Transactions on Magnetics,* vol. 38, no. 5, pp. 3213-3215, Sep. 2002.

[92] Y. Liu, S. K. Kashif and A. M. Sohail, "Engineering considerations on additional iron losses due to rotational fields and sheet cutting," in *18th International Conference on Electrical Machines*, Vilamoura, 2008.

[93] S. L. Ho, W. N. Fu and H. C. Wong, "Estimation of Stray Losses of Skewed Rotor Induction Motors Using Coupled 2D and 3-D Time Stepping Finite Element Methods," *IEEE Transactions On Magnetics,* vol. 34, no. 5, pp. 3102-3105, September 1998.

[94] K. Yamazaki and Y. Haruishi, "Stray load loss analysis of induction motor-comparison of measurement due to IEEE standard 112 and direct calculation by finite-element method," *IEEE Transactions on Industry Applications,* vol. 40, no. 2, pp. 543-549, March-April 2004.

[95] M. A. Masadeh, K. S. Amitkumar and P. Pillay, "Power Electronic Converter-Based Induction Motor Emulator Including Main and Leakage Flux Saturation," *IEEE Transactions on Transportation Electrification,* vol. 4, no. 2, pp. 483-493, June 2018.

[96] A. Tessarolo, S. Mohamadian and M. Bortolozzi, "A New Method for Determining the Leakage Inductances of a Nine-Phase Synchronous Machine From No-Load and Short-Circuit Tests," *IEEE Transactions on Energy Conversion,* vol. 30, no. 4, pp. 1515-1527, Dec. 2015.

[97] Mentor, a Siemens Business, *MagNet 7.8, 2D/3D Electromagnetic Field Simulation Software,* Wilsonville, OR, USA, 2018.

[98] Mentor, a Siemens Business, *MotorSolve 6.0.1, Electric Machine Design Software,* Wilsonville, OR, USA, 2018.

[99] P. Pillay, M. Al-Badri, P. Angers and C. Desai, "A New Stray-Load Loss Formula for Small and Medium-Sized Induction Motors," *IEEE Transactions on Energy Conversion,* vol. 31, no. 3, pp. 1221-1227, Sept. 2016.

[100] Lassi Aarniovuori, Paavo Rasilo, Markku Niemela and Juha J. Pyrhonen, "Analysis of 37-kW Converter-Fed Induction Motor Losses," *IEEE Transactions on Industrial Electronics,* vol. 63, no. 9, pp. 5357 - 5365, Sept. 2016.

[101] W. Cao, K. J. Bradley, J. C. Clare and P. W. Wheeler, "Comparison of Stray Load and Inverter-Induced Harmonic Losses in Induction Motors Using Calorimetric and Harmonic Injection Method," *IEEE Transactions on Industry Applications,* vol. 46, no. 1, pp. 249-255, Jan.-Feb. 2010.

[102] K. Bradley, W. Cao, J. C. Clare, and P. Wheeler, "Predicting inverter-induced harmonic loss by improved harmonic injection," *IEEE Transactions on Power Electronics,* vol. 23, no. 5, p. 2619–2624, Sep. 2008.

[103] E. Nicol Hildebrand and H. Roehrdanz, "Losses in three-phase induction machines fed by PWM converter," *IEEE Transactions on Energy Conversion,* vol. 16, no. 3, p. 228–233, Sep. 2001.

[104] F. G. G. de Buck, P. Giustelinck and D. de Backer, "A Simple but Reliable Loss Model for Inverter-Supplied Induction Motors," *IEEE Transactions on Industry Applications,* Vols. IA-20, no. 1, pp. 190-202, Jan. 1984.

[105] Maamoun, A. M. A. Mahmoud, A. F. Kheireldin and M. A. Saleh, "The harmonic effects in an induction motor fed from a cycloconverter," in *Fourth International Conference on Power Electronics and Variable-Speed Drives*, London, UK, 1990.

[106] I. T. Force, "The Effects of Power System Harmonics on Power System Equipment and Loads," *IEEE Transactions on Power Apparatus and Systems,* Vols. PAS-104, no. 9, pp. 2555-2563, Sept. 1985.

[107] S. Mukherjee, G. E. Adams and R. G. Hoft, "FEM analysis of inverter-induction motor rotor conduction losses," *IEEE Transactions on Energy Conversion,* vol. 4, no. 4, pp. 671-680, Dec. 1989..

[108] P. G. Cummings, "Estimating Effect of System Harmonics on Losses and Temperature Rise of Squirrel-Cage Motors," *IEEE Transactions on Industry Applications,* Vols. IA-22, no. 6, pp. 1121-1126, Nov. 1986.

[109] L. T. Mthombeni and P. Pillay, "Core losses in motor laminations exposed to high-frequency or nonsinusoidal excitation," *IEEE Transactions on Industry Applications,* vol. 40, no. 5, pp. 1325-1332, Sept.-Oct. 2004.

[110] E. Dlala and A. Arkkio, "A General Model for Investigating the Effects of the Frequency Converter on the Magnetic Iron Losses of a Squirrel-Cage Induction Motor," *IEEE Transactions on Magnetics,* vol. 45, no. 9, pp. 3303-3315, Sept. 2009.

[111] Z. Haisen, Z. Dongdong, W. Yilong, Z. Yang and X. Guorui, "Piecewise Variable Parameter Loss Model of Laminated Steel and Its Application in Fine Analysis of Iron Loss of Inverter-Fed Induction Motors," *IEEE Transactions on Industry Applications,* vol. 54, no. 1, pp. 832-840, Jan.-Feb. 2018.

[112] A. Boglietti, P. Ferraris, M. Lazzari and F. Profumo, "Iron losses in magnetic materials with six-step and PWM inverter supply (induction motors)," *IEEE Transactions on Magnetics,* vol. 27, no. 6, pp. 5334-5336, Nov. 1991.

[113] B. J. Chalmers and B. R. Sarkar, "Induction-motor losses due to nonsinusoidal supply waveforms," *Proceedings of the Institution of Electrical Engineers,* vol. 115, no. 12, pp. 1777-1782, Dec. 1968.

[114] Hamid Bentarzi, Yacine Kerouch, Larbi Refoufi and Nikos Mastorakis, "Additional losses modeling in PWM inverter fed induction motor including skin effects," in *Proceedings of the 11th WSEAS international conference on Automatic control, modelling and simulation*, Istanbul, Turkey, May 2009.

[115] [Online]. Available: https://new.abb.com/drives/low-voltage-ac/industrial-drives/industrial-acs800-series/acs800-single-drives/acs800-11.

[116] S. R. Prakash Reddy and U. Loganathan, "Improving the Dynamic Response of Scalar Control of Induction Machine Drive Using Phase Angle Control," in *IECON 2018 - 44th Annual Conference of the IEEE Industrial Electronics Society*, Washington, DC, 2018.

[117] A. Smith, S. Gadoue, M. Armstrong and J. Finch, "Improved method for the scalar control of induction motor drives," *IET Electric Power Applications,* vol. 7, no. 6, pp. 487-498, July 2013.

[118] Z. Zhang, Y. Liu and A. M. Bazzi, "An improved high-performance open-loop V/f control method for induction machines," in *IEEE Applied Power Electronics Conference and Exposition (APEC)*, Tampa, FL, 2017.

[119] B. K. Bose, "Scalar Decoupled Control of Induction Motor," *IEEE Transactions on Industry Applications,* Vols. IA-20, no. 1, pp. 216-225, Jan. 1984.

[120] B. K. Bose, Modern Power Electronics and AC Drives, 2002.

[121] I. Takahashi and Noguchi, "A New Quick-Response and High-Efficiency Control Strategy of an Induction Motor," *IEEE Transactions on Industry Applications,* Vols. IA-22, no. 5, pp. 820-827, Sept. 1986.

[122] M. Depenbrock, "Direct self-control (DSC) of inverter-fed induction machine," *IEEE Transactions on Power Electronics,* vol. 3, no. 4, pp. 420-429, Oct. 1988.

[123] N. R. N. Idris, C. L. Toh and M. E. Elbuluk, "A New Torque and Flux Controller for Direct Torque Control of Induction Machines," *IEEE Transactions on Industry Applications,* vol. 42, no. 6, pp. 1358-1366, Nov.-dec. 2006.

[124] Z. Sorchini and P. T. Krein, "Formal Derivation of Direct Torque Control for Induction Machines," *IEEE Transactions on Power Electronics,* vol. 21, no. 5, pp. 1428-1436, Sept. 2006.

[125] T. G. Habetler, F. Profumo, M. Pastorelli and L. M. Tolbert, "Direct torque control of induction machines using space vector modulation," *IEEE Transactions on Industry Applications,* vol. 28, no. 5, pp. 1045-1053, Sept.-Oct. 1992.

[126] Yen-Shin Lai and Jian-Ho Chen, "A new approach to direct torque control of induction motor drives for constant inverter switching frequency and torque ripple reduction," *IEEE Transactions on Energy Conversion,* vol. 16, no. 3, pp. 220-227, Sept. 2001.

[127] Z. Shang, "Simulation and Experiment for Induction Motor Control," Master of of Applied Science, University of Windsor, Windsor, Ontario, 2011.

[128] M. Ghasemi Bijan and P. Pillay, "Efficiency Estimation of the Induction Machine by Particle Swarm Optimization Using Rapid Test Data With Range Constraints," *IEEE Transactions on Industrial Electronics,* vol. 66, no. 8, pp. 5883-5894, Aug. 2019.